is made between the thermodynamical equilibrium pressure, the kinetic pressure, and their relation to the transition pressure. At their low pressure phase, the resistance invariance of the mercury chalcogenides, up to their transition pressures, indicated that these materials belong to the special class of the zero gap semiconductors-semimetals. However, at their high pressure phase, these materials are normal semiconductors. It is observed that one can influence the up- and downstroke transition pressure of the pressure induced polymorphic phase transition by nucleations to minimize the width of the transition hysteresis. The systematic dependance of the activation volumes upon various nucleation concentrations has been demonstrated, as well as the direct dependance of the rate of reaction on the nucleation concentration. Due to the simplicity of the pressure induced polymorphic phase transition, the determined activation volumes can be considered to represent the true activation volumes characterizing the transition state. However, in the case of liquids, mainly due to the presence of a foreign medium such as the solvent, the arrangement results in a more complex system. Therefore, the quantitative analysis of the experimental data based on the heterogeneous nucleation model was readily possible in the solids.

TO MY PARENTS

AND MY WIFE

ACKNOWLEDGEMENTS

The author wishes to express his gratitude to Professor B.A. Lombos for suggesting the problem and for his guidance through the course of this investigation.

He is indebted to Dr. B.C. Pant and Dr. W. Hwang for the many fruitful discussions on the subject. Thanks are also due to Mrs. A. Margittai for her assistance in part of the experimental work.

It is a great pleasure and honour for the author to thank Professor V. Ramachandran and Professor M.N.S. Swamy for going through the manuscript.

Some suggestions given by Dr. E. Whalley, the external examiner, for the improvement of the thesis are gratefully acknowledged.

The author deeply acknowledges the patience, sacrifices and encouragement offered by his wife, Christine Mona, during the entire period of the study and for her diligent work in typing the manuscript.

Special gratitude and appreciation are due to Dean J.C. Callaghan for arranging financial assistance from his N.R.C. Grant No. A 2154.

TABLE OF CONTENTS

LIST OF TABLES

LIST OF FIGURES

LIST OF IMPORTANT ABBREVIATIONS AND SYMBOLS

B_1	Compressibility of phase I
B_2	Compressibility of phase II
B_L	Liquid compressibility
D_1	Density of phase I
D_2	Density of phase II
E_c	Conduction band energy
E_v	Valence band energy
G	Kane's momentum matrix element
h	Planck's constant
$\hbar$	$h/2$
k	Boltzmann's constant
K	A momentum vector space in the reciprocal lattice
$\Delta\ell$	Base plate displacement
m_I	Sample mass of the outset of upstroke transition
m_{II}	Sample mass at the end of the transition
m_e^*	Electron effective mass
m_h^*	Hole effective mass
n'	Number of moles
N	Concentration of growth nuclei in a sample
N_o	Concentration of growth nuclei in non-nucleated samples
N'	Number of nuclei along the sample length L

N''	Number of nuclei on a cross-sectional surface ZW
P_k	Nucleation dependent kinetic pressure
P_t	Outset of upstroke transition pressure
P_t'	Pressure at which transition is completed
P_{th}	Nucleation independent thermodynamical equilibrium pressure
ΔP	Total pressure change
ΔP_t	The difference in transition pressure between non-nucleated and nucleated samples
r'	Transition rate constant
R	Gas constant
R_o	Resistance at atmospheric pressure
R_H	Hall coefficient
ΔR	Change of resistance
V_1	Sample volume at atmospheric pressure
V_I	Sample volume at the outset of upstroke transition pressure
V_{II}	Sample volume in phase II at the end of transition
$V(t)$	Total volume of the sample at time t
$V_1(t)$	Volume of phase I at time t
$V_2(t)$	Volume of phase II at time t
V_L	Liquid volume
V_m	Molecular volume
$V^\#$	Transition state volume
$\Delta V^\#$	Activation volume

ΔV	Total volume change due to transition
$\Delta V(t)$	Partial volume change at time t
ΔVR	Total volume reduction of the large sample
ρ_1	Resistivity of phase I
ρ_2	Resistivity of phase II

CHAPTER I

INTRODUCTION

In the past few decades, high pressure research has been extensively studied experimentally and theoretically by many investigators [1,2]. A large number of different materials have been examined under high pressure [3]. However, the majority of those studies were focused on thermodynamic relations, e.g. pressure, volume and temperature (P,V,T), describing the state of a system on the materials. In the case of solids, the importance of pressure as an experimental variable stemmed from the fact that it enables one to change the interatomic distances and hence provides valuable information often unobtainable by using temperature as the experimental variable [4].

Hydrostatic pressures above 40 kilobars (kbar) are considered a specialized field and are usually defined as very high pressures. Conventional high pressures, on the other hand, are those pressures ranging anywhere from 1 to 40 kbar [5].

Many solids are found to have more than one stable phase at different pressures, e.g. ice, bismuth, thallium, barium and mercury chalcogenides [3]. Transitions between these phases are usually detected by observing abrupt changes in volume, resistance or both, as a function of pressure. Various techniques have been developed for

measuring such changes for a wide range of pressures as well as temperatures. A combination of volume and resistance variation measurements can be useful in clarifying obscure situations in phase transitions. These situations arise from minor volume changes and major resistance changes.

The study of pressure-volume relation and the phase transition of solids at high pressures will facilitate the understanding of the structure and composition of the earth's core and mantle [6] . It is possible to attain a wide range of temperature and the appropriate range of pressures assumed to be in the earth's interior, notably between the core and mantle, where the pressure reaches only 10 kbar [5]. Therefore, the analyses of the kinetics and the reaction mechanism of the pressure induced polymorphic phase transition can be very useful in understanding some of the earth's physical phenomena such as earthquakes [6] .

In spite of the voluminous literature on the high pressure research, only few investigations have been published on the kinetics of the chalcogenides related to the pressure induced polymorphic phase transition [7-9] . However, more systematic research work is required to understand the kinetic mechanisms of the solid-solid polymorphic phase transition under pressure, particularly in mercury chalcogenides.

Semimetals or zero gap semiconductors (see p.21) can provide an important application in material science.

By alloying one of these materials with a semiconductor of a larger energy gap, a new semiconductor alloy with a close to zero energy gap can be obtained. This alloy is extremely useful in producing very high frequency (infrared region) diode detectors.

Mercury chalcogenides are semimetals or zero energy gap semiconductors [10,11] at atmospheric pressure and wide energy gap semiconductors [12] at high pressure, i.e. after transition. Such properties encourage the study of this class of materials.

The compressions of mercury chalcogenides were measured for the first time by Bridgman in 1940 [13]. He noticed a sharp volume change, corresponding to phase transitions at 7,650 kg/cm^2 in the case of mercury selenide (HgSe), and similarly at 12,800 kg/cm^2 for mercury telluride (HgTe). Bridgman correctly speculated that the polymorphic phase transitions in both, HgSe and HgTe, changed from the zinc-blende structure to the hexagonal cinnabar structure. A large resistance change, by several orders of magnitude, accompanying the polymorphic phase transition in HgSe was detected at 7.5 kbar, as reported by Kafalas et al. in 1962 [12]. The increase in resistance at transition was attributed to the change of the material's state from a semimetal to a semiconductor. Furthermore, upon decreasing the pressure, a pronounced hysteresis in the phase transition was noticed (see Figure 4.1). Kafalas et al. retained the

high pressure phase of HgSe by cooling their high pressure cell with liquid nitrogen while the sample was pressurized in excess of 13 kbar. Such cooling prevented the sample's electrical resistance from increasing upon reducing the pressure to one atmosphere. Then, by means of the X-ray diffraction technique, they were able to conclude that the HgSe compound before transition, i.e. the low pressure phase (phase I), has the zinc-blende structure; and after transition, i.e. the high pressure phase (phase II), has the hexagonal structure. The latter corresponds to the red HgS hexagonal structure. It was also confirmed by Mariano et al.[14] that the low and high pressure phases of HgSe are the zinc-blende and the hexagonal cinnabar structures, respectively. The upstroke and the downstroke transition pressures, which define the widths of transition hystereses for HgSe, HgTe and their alloys, were measured [7,8] using both volume and resistance measurement techniques (see Chapter VI). In their investigation of HgSe, Lacam et al. [8] further reported that the relative volume change produced by the pressure induced phase transition is 8.2% of the original volume. The resistance change, however, is in the order of 10^4 times the original value. The dependence of the transition pressure on HgSe-HgTe alloy composition was also reported [15]. Polymorphic phase transitions for some group II-VI compounds at high pressures and various temperatures were investigated by Jayaraman et al. [16]. They reported that the solid-solid transitions in HgSe

and HgTe were sluggish, but to a lesser degree at temperatures higher than room temperature. However, they added that the total hystereses in these solid-solid transitions decreased with increasing temperature. The decrease of the hystereses was further attributed to the speeding up of nucleation and growth processes (see p. 43)

The kinetics of the pressure induced polymorphic phase transition of the chalcogenides were reviewed by Onodera [9] . He indicated that the presence of impurities in the substances showed importance in determining the nature of the kinetics of transitions. He further indicated that a change in electrical resistance of several orders of magnitude at the transition is due to a change of band structure. This in turn is due to a change in the crystal structure. The data analysis of Onodera was based on the assumption that a fraction of the material transformed at any instant during transition, from one phase to another, was proportional to its resistance change. Such an assumption has been modified in this work, based on the experimental results of the simultaneous measurements and the analyses of the volume and resistance variations during the pressure induced polymorphic phase transitions in HgSe.

Most of the earlier high pressure measurements, particularly those above the conventional limit, have been restricted to pressure-volume [3] relation. Those measurements, obtained by the conventional indirect volumetric measurement technique, provided very

important data on the compressibilities and phase transformations of many substances. On the other hand, the direct resistance measurement technique is structure sensitive, especially in semiconductors. Therefore, this technique is not only useful to measure the solid-solid polymorphic phase transformation, but can also provide information on the material's electronic structure variation as a function of pressure.

The purpose of this investigation is to examine and analyze the kinetic aspects of the solid-solid pressure induced polymorphic phase transitions. The method of the investigation to be employed is a direct high sensitive technique due to the large resistance variation of HgSe. Thus, HgSe has been selected because of the following changes accompanying its transition at a relatively low pressure below 10 kbar:

1) Electronic structure, from a semimetal or a zero gap semiconductor to a large energy gap semiconductor.
2) Crystal structure, from the zinc-blende to the hexagonal cinnabar.
3) Volume reduction by more than 8 %.
4) Resistance increase by a factor of 10^4.

Furthermore, the research set out is to identify the thermodynamical equilibrium pressure and to explain eventually the existance of the transition hysteresis

between the two phases. This is in addition to the possible analysis of the band structure variations related to the energy gap of HgSe under pressure.

A detailed study of heterogeneous nucleation and the mechanism of the solid-solid pressure induced polymorphic phase transition in mercury selenide is presented in this thesis. Based on the experimental results obtained, the study is analyzed.

Chapter II gives the band structures of HgSe and HgTe, together with the influence of pressure on the band structures of these and other related materials. It also presents the general principles of the kinetic theory of the solid-solid polymorphic phase transition.

Chapter III discusses material preparations, equipments used, including the high pressure apparatus, and the experimental procedures. It also describes the two measurement techniques employed to measure the volume and the resistance variations of the samples under pressure.

Chapter IV presents the experimental results obtained from both, the volumetric and the resistance measurement techniques. The important data of the empirical influence of heterogeneous nucleations (see p. 70) on transition pressures are also described.

A heterogeneous model that follows the experimental data very closely is proposed in Chapter V. This model is used to characterize the kinetics of the pressure induced solid-solid polymorphic phase transition according to the absolute rate theory developed by Evans and Polanyi [17] . Moreover, the reaction kinetics, with respect to the thermodynamics driving forces (pressure and temperature) in relation to the polymorphic phase transition are discussed.

The analysis of the experimental results found in Chapter IV is given in Chapter VI. This is in addition to the kinetic data obtained by using the model of Chapter V. Also, a clear distinction is outlined between thermodynamic and kinetic pressures and their relation to transition pressure.

Chapter VII incorporates the summary and conclusions of the present investigation.

CHAPTER II

GENERAL REVIEW

2.1 INTRODUCTION

The influence of hydrostatic pressures on the energy band structure of a solid can provide vital information on the characteristics and the type of that solid (metal, semiconductor, insulator or others). It is the purpose of this chapter to present this effect for mercury chalcogenides as well as for some other related semiconductors. Consequently, a general review on the energy band structures of these materials at one atmospheric and at higher pressures will be discussed.

Furthermore, since the pressure induced polymorphic phase transition changes the energy band structure of a solid which can be followed by the resistance measurement technique, the last portion of this chapter discusses in general the heterogeneous kinetics theory and the mechanism of phase transformation.

2.2 ENERGY BAND STRUCTURES OF SOLIDS

The crystal structure of a solid determines to a great extent the energy band configuration. Therefore, based on a particular energy band configuration, the electrical properties and hence the classification of the solid can be determined accurately.

Most of the important semiconductors are of diamond or zinc-blende structures, characterized by tetrahedral coordination, i.e. each atom is surrounded by four equidistant nearest neighbours which lie at the corners of a tetrahedron. The diamond and the zinc-blende structures can be considered as two interpenetrating face-centered cubic lattices [18,p.9]. In the diamond structure such as in silicon (Si), all the atoms are Si, while in the zinc-blende structure such as in gallium arsenide (GaAs), one of the sublattices is Ga and the other is As.

2.2.1 The Brillouin Zone and K-Space

The band structure of a crystalline solid, i.e. the energy-momentum (E-K) relationship, is normally obtained by the solution of the Schroedinger equation of an appropriate one electron problem. K is a momentum vector space in the reciprocal lattice, where a vector in the reciprocal lattice is related to another vector in the direct lattice by the Kronecker delta times the factor 2π. The Schroedinger equation is given by

$$\left[-\frac{\hbar^2}{2m}\nabla^2 + W(r)\right]\psi_K(r) = E_K\,\psi_K(r)$$

with the general solution [19]

$$\psi_K(r) = e^{iK\cdot r}u_K(r)$$

where $\hbar=h/2\pi$, and h is a universal atomic constant (Planck's constant), W(r) is the potential energy of the particle, m is its mass, $\psi_K(r)$ is the wave function with the wave propagation vector K, E_K is the energy of the system and $U_K(r)$ is a periodic function in r (r is a vector in the direct lattice), corresponding to a perfectly free electron of momentum $\hbar K$ (de Broglie's relation).

Since the direct lattice is periodic, the reciprocal lattice is also periodic and hence the reciprocal lattice is composed of many repeated unit cells. Each unit cell repeats the energy states of a neighbouring one, therefore, one unit cell (reduced zone) in the reciprocal lattice is all that is needed to specify the energy states of the whole lattice. This reduced zone in the reciprocal lattice is known as the Brillouin zone [18,p.241] . Thus, a plot of the energy E as a function of the wave vector K, can specify uniquely the energy band structure of a solid.

The Brillouin zone for diamond and zinc-blende structures which is the same as that of the face-centered cube, is given in Figure 2.1-A. Similarly, the Brillouin zone for the wurtzite structure is given in Figure 2.1-B. The most important symmetry points and symmetry lines are indicated in these figures. The particular interests to the present discussion are the center of the zone (Γ) where K=(000), the zone edge (L) intersecting the axis (Λ) where K=(111), and the zone edge (X) intersecting the axis (Δ)

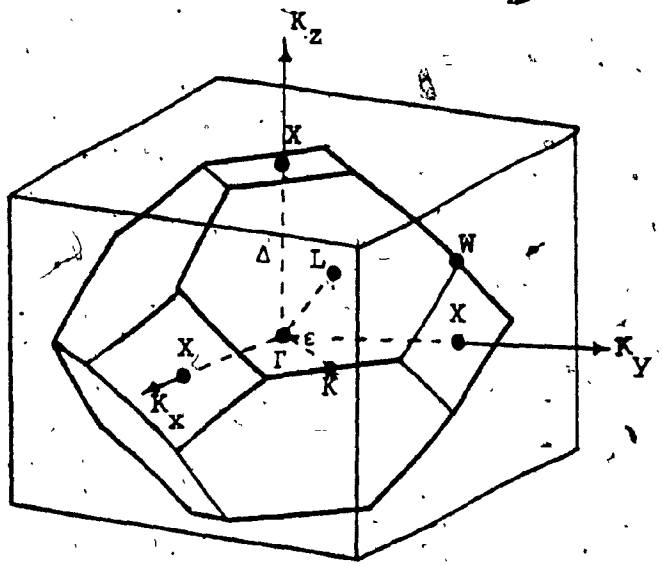

Fig. 2.1-(A) - Brillouin zone for diamond and zinc-blende lattices.

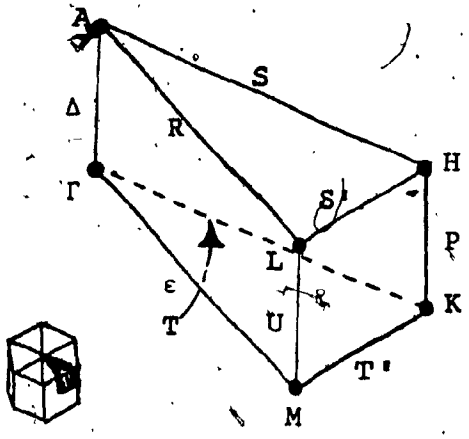

Fig. 2.1-(B) - Brillouin zone for a wurtzite lattice.

where K=(100). It is to be noted hereafter that (Γ), (L) or (Λ) and (X) or (Δ) will be used to represent K=(000), K=(111) and K=(100) symmetries, respectively.

2.2.2 The Energy Gap

In the case of non-metallic crystals, particularly semiconductors, it is desirable to explain the expression "the width of the forbidden band or the energy gap E_g". It is defined as a region in the reduced zone at which no allowed energy states can be maintained and is given by

$$E_g = E_c(K_c) - E_v(K_v) \qquad (2.1)$$

K_c is a point in the reduced zone where the lowest conduction band reaches its minimum energy value. K_v is a point in the reduced zone where the highest valence band attains its maximum energy value. If the minimum energy separation E_g between the lowest conduction band E_c and the highest valence band E_v is located at a particular value of K, as in HgSe, HgTe and other crystals, then the electronic transition is classified as a "direct gap transition". In this case $K_v=K_c$ or dK=0 and the energy gap E_g is given by

$$E_g = E_c(K) - E_v(K) \qquad (2.2)$$

On the other hand, if $K_v \neq K_c$ or the minimum gap exists between different values of K, as in silicon, germanium

and other crystals, then these are called "indirect gap transition" materials. Figure 2.2 compares the basic difference between direct and indirect transitions relative to K-space from the center of the Brillouin zone. The solid arrow (a) where dK=0 indicates a direct transition case with E_{g_1} as its energy gap, while the dotted arrow (b) exhibits an indirect transition case with E_{g_2} as its energy gap.

2.3 PRESSURE AS A SOLID STATE PARAMETER

The influence of pressure on the band structures of solids has been shown by means of quantum mechanical treatment [20] . Therefore, when hydrostatic pressures are applied to crystals, the energy band configuration changes. This will be discussed below for some important semiconductors. However, when the crystal structure changes under pressure, i.e. undergoes phase transition, it is accompanied by a modification of the electronic configuration of the solid. As a function of pressure and at a given temperature, the displacement of the conduction band relative to the valence band is measured and expressed by its pressure coefficient $(\partial E_g/\partial P)_T$. This coefficient can be obtained for example [21] by using the following relation :

$$\left(\frac{\partial E_g}{\partial P}\right)_T = \left(\frac{\partial E_g}{\partial V}\right)_T \left(\frac{\partial V}{\partial P}\right)_T \qquad (2.3)$$

where V is volume and P is pressure.

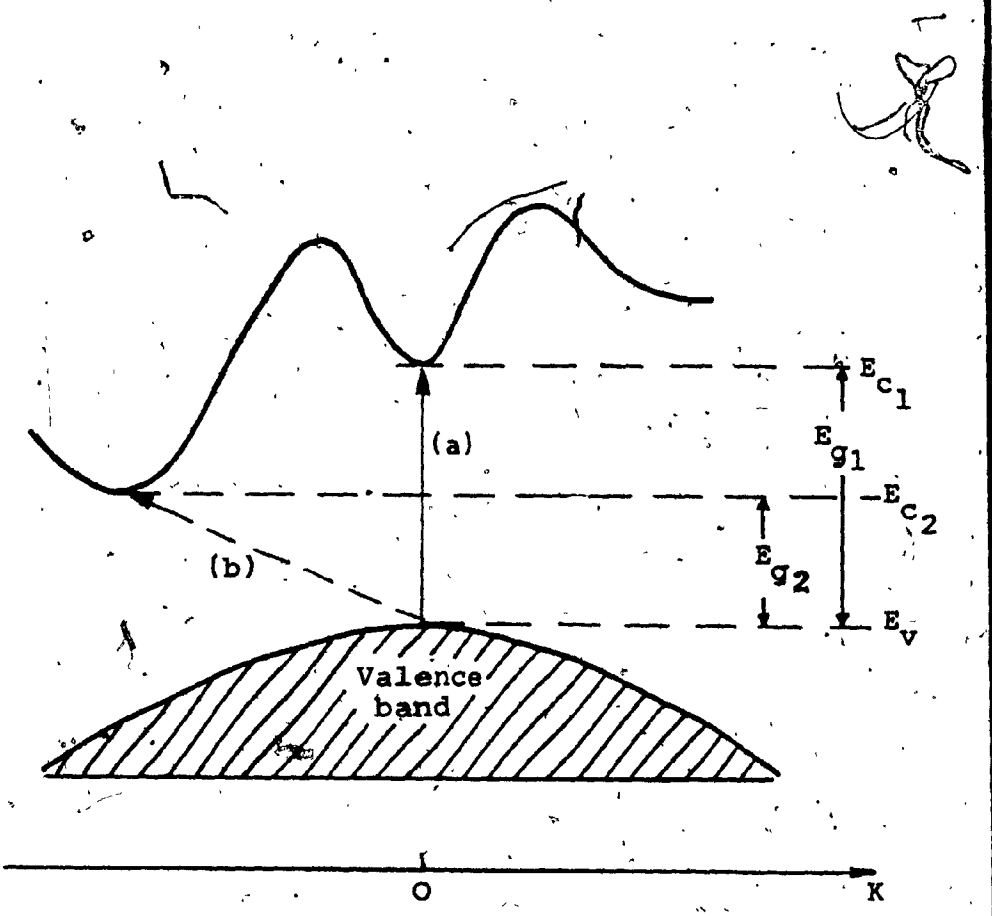

Fig. 2.2 - Electronic transitions in band structures.
(a) indicates a direct transition, E_{g_1}.
(b) indicates an indirect transition E_{g_2} [19].

The value of $\left(\frac{\partial E_g}{\partial V}\right)_T$ can be evaluated directly from band calculation by changing the lattice constant, whereas the value of $\left(\frac{\partial V}{\partial P}\right)_T$ can be estimated from the measured compressibility of the solid. Hence, the basis for any association of the pressure coefficient with the energy gap between the valence band maximum and a particular symmetry of the conduction band minimum is primarily experimental. Therefore, it is important to demonstrate the influence of pressure on the band structure and hence, on the transport properties of some semiconductors including mercury chalcogenides.

The earliest experiments to examine the effect of pressure on the resistivity of germanium (Ge) were performed by Bridgman [22]. He concluded that the resistance is single valued in pressure with no hysteresis, starting with a linear increase, followed by a rapidly accelerating rise of resistance at higher pressures, as given in Figure 2.3 . Later investigators [23,24] have interpreted that the resistance change to the accelerating rise is due to the increasing importance of a new set of states, having different pressure coefficients from those at low pressures. Table 2.1 lists these pressure coefficients for Ge as well as for some other semiconductors including HgSe and HgTe. A positive pressure coefficient for a particular symmetry indicates that the conduction band at that symmetry moves away from the valence band maxima, i.e. the energy gap E_g opens up, and conversely

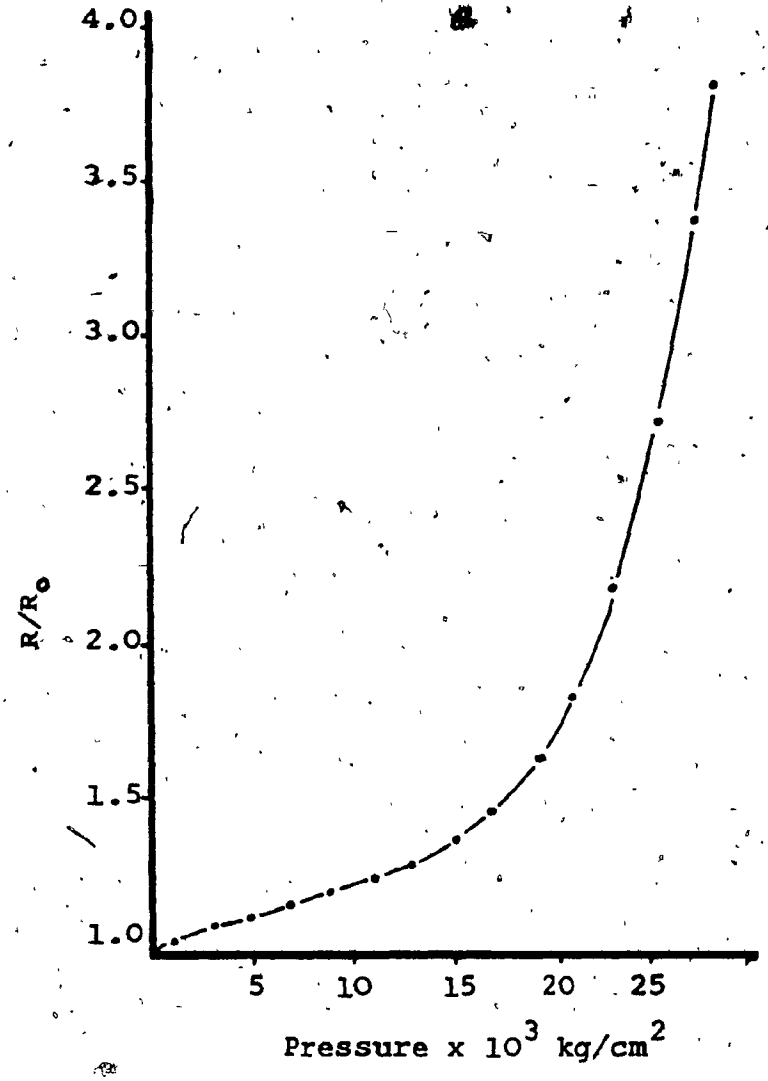

Fig. 2.3 – The relative resistance of a specimen of n-type Ge at room temperature as a function of pressure [22].

Table 2.1

Properties of some semiconductors including zero gap materials

Compound	Energy Gap (ev)	Conduction Band Minima	$(\partial E_g / \partial P)_T$ ev/atm.	References
Ge	0.66 (300°K)	L_1	5×10^{-6}	[23 - 25]
	0.803 (300°K)	Γ_2'	12×10^{-6}	[25]
	0.85 (300°K)	Δ_1	0 to -2×10^{-6} -1.2×10^{-6}	[25] [28]
Si	1.21 (0°K)	Δ_1	-1.5 to -2.0×10^{-6}	[27 - 28]
Sn[1]	0.09 (0° - 300°K)	L_1	5×10^{-6}	[25, 29]
	- 0.3 ev (0° - 150°K)	Γ_8'	-12×10^{-6}	[29]
GaAs	≈1.8 (300°K)	L_1	9.4×10^{-6}	[28]
	1.5 (300°K)	Γ_1'	9.4×10^{-6} 12.0×10^{-6}	[28, 30] [25]
	> 2.0 (300°K)	Δ_1	-8.7×10^{-6} a -1.4×10^{-6}	[28] [25, 30]
GaP	≈2.4 (300°K)	L_1	1.8×10^{-6}	[28]
	≈2.6 (300°K)	Γ_1	1.8×10^{-6}	[28]
	2.3 (300°K) 2.2 (300°K)	Δ_1	-1.7×10^{-6} b -1.8×10^{-6}	[28] [25]
HgTe[2]	- 0.3 (4.2°K)	Γ_8		[11]
	- 0.19 ± 0.04 (300°K)	Γ_8	-14.5×10^{-6}	[55]
	- 0.175 (300°K) - 0.137 (340°K)	Γ_8	-14×10^{-6}	[57]
HgSe	- 0.24 (4.2°K)	Γ_8		[45]
	- 0.15 (300°K)	Γ_8		[44]

a - between 60 - 130 kbar
b - between 20 - 50 kbar
1 - the thermal gap $E_t = 0$ at all temperatures and pressures [29]
2 - the thermal gap $E_t = 0$ at all temperatures and pressures [11, 33, 35, 44, 45, 55 - 57]

a negative pressure coefficient indicates the opposite effect. Note that Ge is an indirect transition semiconductor with the conduction band minima located at L_1 at one atmospheric pressure. Paul [25] has pointed out that the transition direction shifts with pressure near 50,000 kg/cm^2 from (L_1) to (Δ_1). This arises because as a function of pressure the Ge gap opens up, i.e. the conduction band at (L_1) moves upward away from the valence band maxima at (Γ'_{25}), up to a pressure of 50,000 kg/cm^2. Above such a pressure, a new conduction band appears to be the lowest conduction band at (Δ_1) due to its negative pressure coefficient. Thus, above the mentioned pressure, the (Δ_1) conduction band is the closest to the valence band, changing the transition for the energy gap from (L_1) to (Δ_1).

It is of importance to know that Ge undergoes a phase transition at very high pressure. Empirically, it is detected at pressures near 120-125 kbar by a sharp resistance decrease [26], which indicates a solid-solid phase transformation, apparently to a metallic state. However, in the case of mercury chalcogenides, the opposite phenomenon is observed. For example, in the present investigation a sharp resistance increase is detected above 9 kbar for HgSe, indicating a solid-solid phase transformation from a semimetal or a very narrow gap semiconductor to a larger gap semiconductor.

The lowest conduction band in Si is located at (Δ_1) with an energy gap $E_{\Delta_1} - E_{\Gamma'_{25}}$ = 1.1 ev at 300°K and hence it is an indirect transition semiconductor. The influence of 30,000 kg/cm^2 of hydrostatic pressure on Si, as reported by Bridgman [22], decreases its resistance to about one half of the initial value. The first pressure coefficient measurement for (Δ_1) in Si, which was determined by Paul and Pearson [27], is given in Table 2.1. This was followed by pressure measurements up to 140,000 kg/cm^2 without noticing any sign for transition [28]. However, at higher pressures, near 195-200 kbar, a sharp resistance decrease, depicting a phase transition, was observed for Si by Minomura and Drickamer [26]. They estimated that the resistivity of the high pressure phase was in the order of 10^{-4} Ω-cm. This is nearly the same order of magnitude measured for mercury chalcogenides at the low pressure phase [11]. The solid-solid phase transition, which was found in Si, is another example of phase transformation under pressure from a semiconducting state to a metallic state.

Measurements on the band structure of gray tin (α-Sn) at atmospheric and elevated pressures indicated a complexity that was not quite explained before the introduction of the inverted band model by Groves and Paul [29]. The essential feature of this model is the location of (Γ_8) valence band [(Γ'_{25}) single group representation] and

(Γ_6) conduction band [(Γ_2') single group representation]. Figure 2.4-A and 2.4-B display the normal and the inverted band structures about K=O, respectively. In the inverted band model at K=O, i.e. at the center of the Brillouin zone, the normal diamond or zinc-blende conduction band (Γ_6) becomes the light-hole valence band, separated from the heavy-hole valence band (Γ_8) by the energy gap $E_g = E\Gamma_6 - E\Gamma_8$. Furthermore, the light-hole valence band (Γ_8) becomes the conduction band. Thus, it is observed that in the inverted band model, $E\Gamma_8 > E\Gamma_6$, contrary to that of the normal band one where $E\Gamma_6 > E\Gamma_8$. Since dK=O, Sn is a direct gap material. In this model, the sign of the energy gap $E_g = E\Gamma_6 - E\Gamma_8$ is negative due to its ($\Gamma_6 - \Gamma_8$) band inversion, contrary to the sign of the energy gap $E_g = E\Gamma_6 - E\Gamma_8$ of a normal band structure which is positive. However, it is to be noted that in the inverted band structure, above the light-hole valence band level (Γ_6), the heavy-hole or the highest valence band level (Γ_8), slightly overlaps the conduction band level (Γ_8) at K=O. This energy overlap or the thermal energy gap E_t is so small (nearly zero ev) and, hence, the expression "zero-gap semiconductor" was developed [29]. In addition to the conduction band at (Γ_8), Groves and Paul observed a second conduction band minimum, contributing to the transport properties of Sn, which is located at (L_6) [(L_1) single group representation], slightly (0.09 ev) above the level of (Γ_8) minima. They noted that the thermal zero gap E_t is fixed at all temperatures and hydrostatic

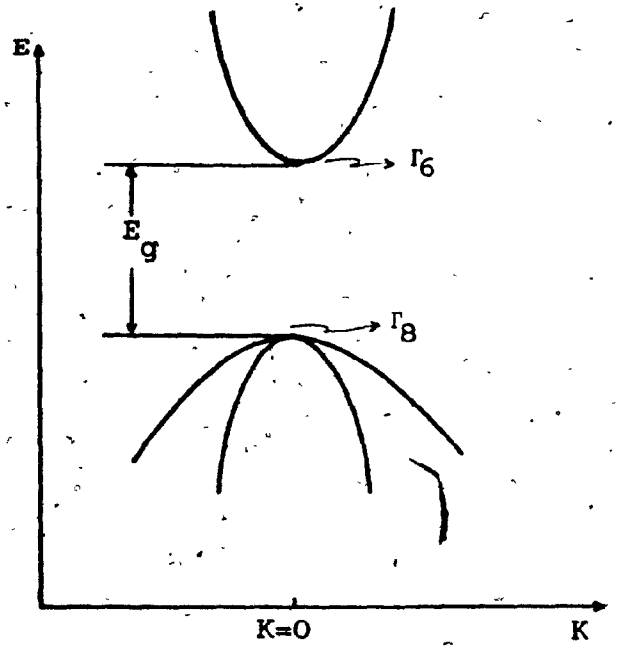

Fig. 2.4-(A) - The normal band structure

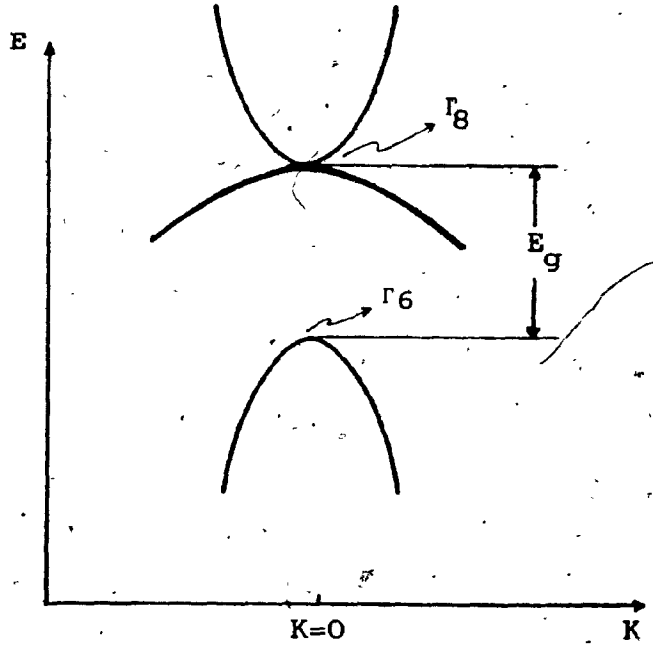

Fig. 2.4-(B) - The inverted band structure

pressures. The same model with some modifications was used for mercury chalcogenides and will be discussed later.

GaAs is a direct transition semiconductor with a second conduction band minimum found at (X_1), about 0.5 ev above the (Γ_1) minima [30]. However, as a function of pressure, the conduction band minima at (Γ_1) moves upward, while the second conduction band minimum at (X_1) moves downward [Table 2.1], resulting in a shift in the transition at high pressure to an indirect gap semiconductor. A phase transition was detected at 240-250 kbar by Minomura and Drickamer [26] with a large resistance drop to several orders of magnitude. They concluded that this phase transition changes GaAs from the semiconducting to a close-packed metallic state.

The lowest conduction band minimum in gallium phosphide (GaP) has been identified by Edwards et al. [28] to be located at (Γ_1) and hence is an indirect transition semiconductor. Two conduction band minima were reported [31], the lowest at (Δ_1) and the next higher at (Γ_1). It was indicated [28] that for GaP a change occurs in the selection rule for the energy gap from (Δ_1) to (Γ_1) at pressures between 20-25 kbar. It was published only recently that a pressure induced polymorphic phase transition from a semi-conductor to a metal in GaP was detected by an abrupt resistance change (a decrease to more than five orders of magnitude) in the vicinity of 500 kbar [32]. This is a

very high pressure compared to the transition pressures of HgSe above 9 kbar and HgTe above 15 kbar [8]. For such a pressure, mercury chalcogenides may perhaps encounter more than one phase transition. However, this can only be verified by experiments.

2.4 ENERGY BAND STRUCTURE OF MERCURY CHALCOGENIDES AT ATMOSPHERIC PRESSURE

Mercury chalcogenides consist of mercury sulfide (HgS), HgSe and HgTe. Only limited information on mercury sulfide (HgS) is available in the literatures and hence it is ignored for the rest of this Chapter. HgSe and HgTe, on the other hand, belong to the family of materials known as zero gap semiconductors or, alternatively, zero overlap semimetals [33] . The band structures for HgSe and HgTe at all pressures, up to their transition pressure, are very similar to the one previously discussed for Sn, namely the inverted band structure [33] . However, at pressures above their transition pressures, HgSe and HgTe change their band order to the normal band structure [15] of Figure 2.4-A.

The first major step towards the understanding of the band structure of HgSe was reported by Harman and Strauss in 1961 [34] . These investigators carried out an analysis of the Hall coefficient versus temperature data for HgSe and $HgSe_{0.5}$ $Te_{0.5}$ between 70° and 350°K, based on the

assumptions of one non-parabolic conduction band, one parabolic valence band and the Fermi-Dirac statistics. They were not able to explain their data on the basis of a simple two-band model, however, they found good agreement with their experiments by adopting a band model in which the conduction and valence bands overlap as in Figure 2.5. The energy gap E_g was defined in this model as

$$E_g = E_c - E_{v_2} \qquad (2.4)$$

where E_c is the lowest energy level of the conduction band and E_{v_2} is the energy level of the valence band v_2 as in the normal two-band model. The overlap or the thermal energy gap E_t, on the other hand, was defined as

$$E_t = E_c - E_{v_1} \qquad (2.5)$$

where E_{v_1} is the energy level of the valence band v_1. They estimated the thermal gap E_t for HgSe and $HgSe_{0.5}Te_{0.5}$ to be -0.07 ev, whereas the energy gap E_g to be 0.1 ev for HgSe and 0.2 ev for the alloy. They further concluded that these materials are semimetals rather than semiconductors. However, since the valence band deeply overlapped the conduction band, this model was not generally accepted as a semimetallic model for HgSe because of its inconsistency with other III-V and II-VI compounds of the zinc-blende family [35].

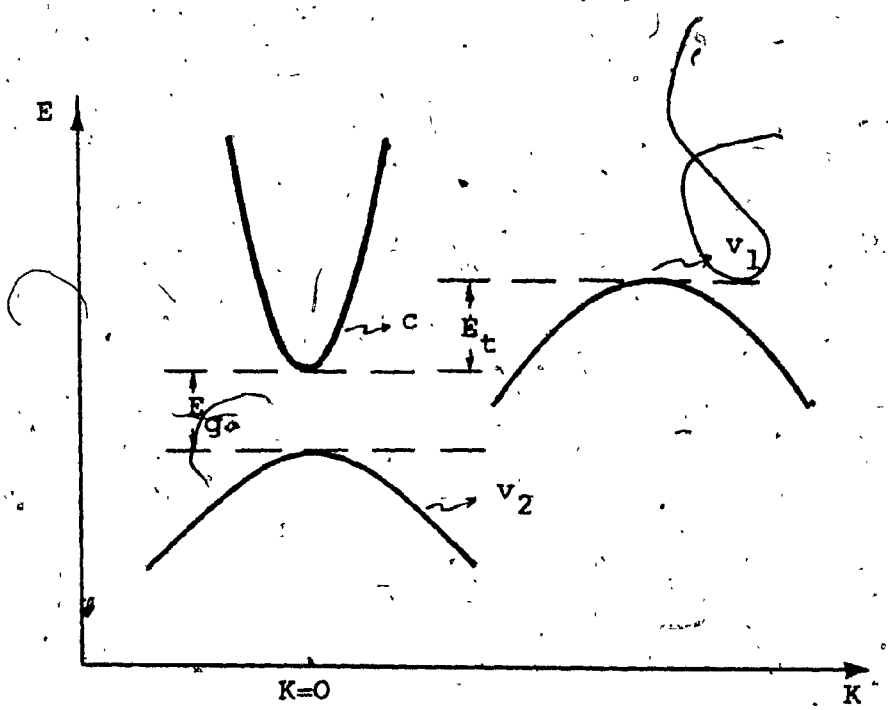

Fig. 2.5 - Schematic E(K) diagram for the band model employed for HgSe and $HgSe_{0.5}\ Te_{0.5}$ by Harman and Strauss [34].

Early measurements related to the band structure of HgTe were reported in 1958 [36,37,38]. These researchers carried out their measurements based on the assumptions of one parabolic conduction band, one parabolic valence band, classical statistics and carrier mobilities changing with temperature as $T^{-3/2}$. The analysis of their electrical resistivity and Hall coefficient versus temperature measurements yielded the result that HgTe is a very small energy gap (i.e. $E_g \simeq 0.02$ ev) semiconductor.

An extension of the inverted band structure was later applied to HgTe by Harman et al. [39], as illustrated in Figure 2.6, where the conduction band (Γ_6) of III-V compounds (see Figure 2.7) is inverted to be the light-hole valence band (Γ_6). Furthermore, the light-hole valence band (Γ_8) and the heavy-hole valence band (Γ_8) have become the conduction band (Γ_8) and a heavy-hole-like valence band, respectively. The energy gap $E_g = E_{\Gamma_6} - E_{\Gamma_8}$ is found to be -0.14 ev, while the overlap or thermal gap E_t is -0.02 ev; both values are quoted at room temperature, and hence Harman et al. classified this material as a semimetal.

The lowest conduction band of HgSe has been verified to be centered at K=0 and is non-parabolic [40,41]. Using Kane's theory (see p.36), the band parameter values $G=7.1\times10^{-8}$ ev-cm, $|E_g| = 0.24$ ev [41], and $G=7.6\times10^{-8}$ ev-cm,

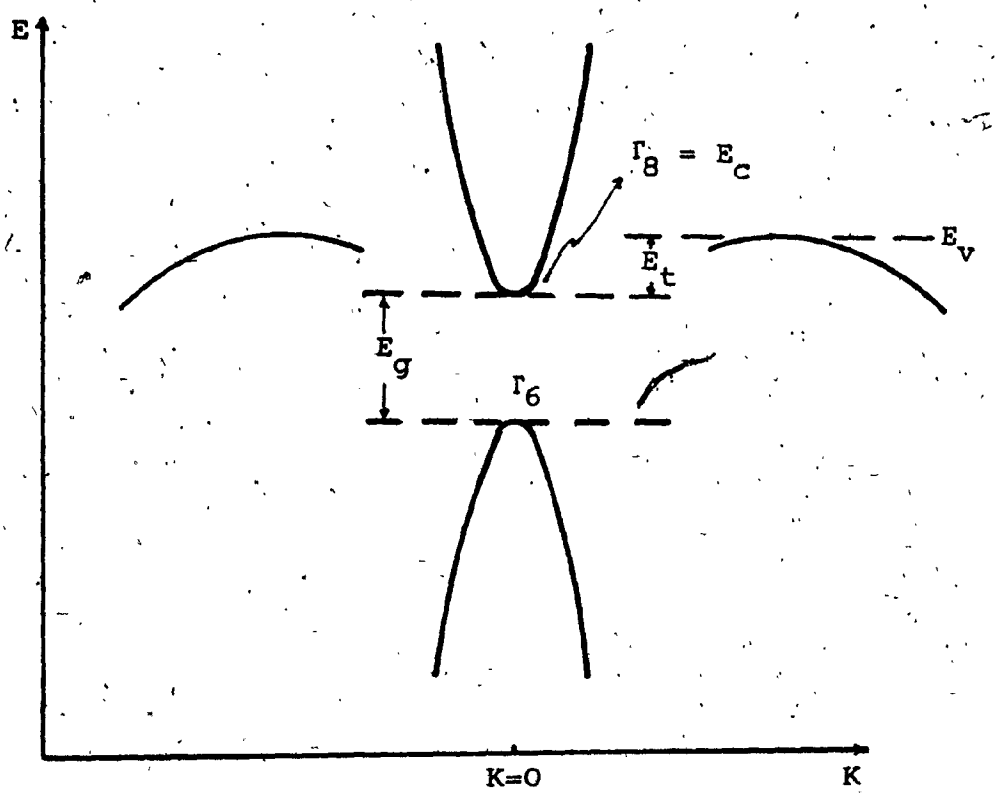

Fig. 2.6 - Schematic E(K) diagram for the band model utilized for HgTe by Harman et al. [39].

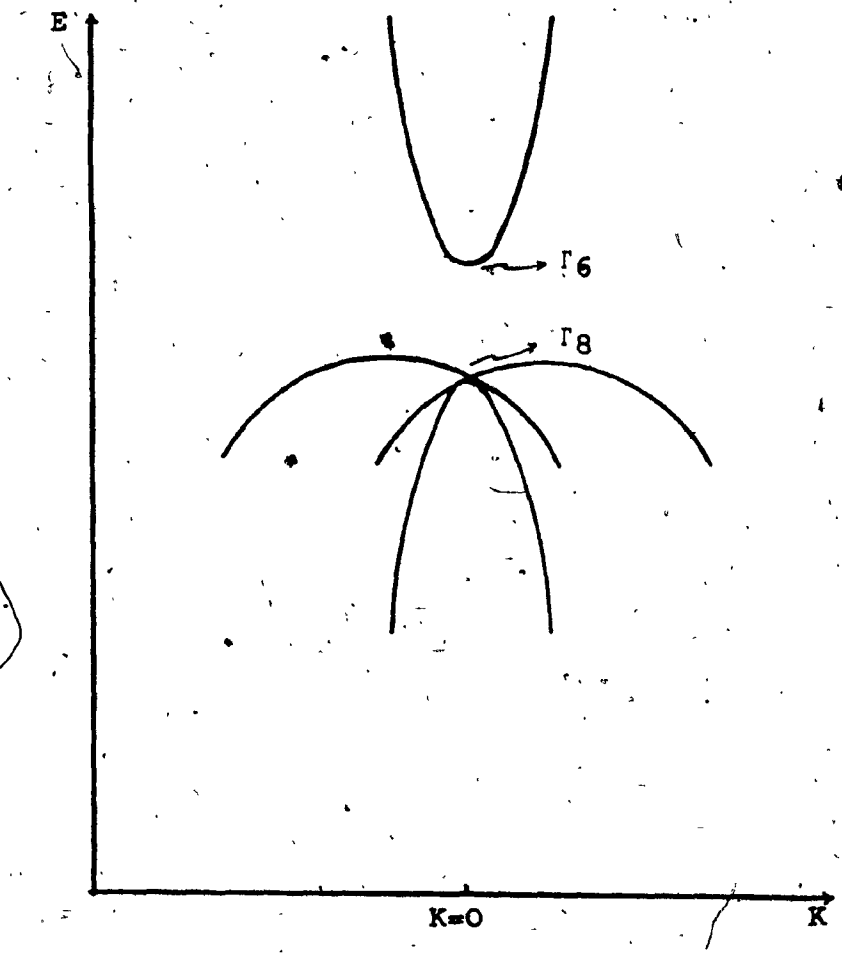

Fig. 2.7 - Schematic E(K) diagram for III-V compounds as in InSb [51].

$|E_g| = 0.22$ ev, at room temperature, and the pair of values $G=7.2\times10^{-8}$ ev-cm, $|E_g| = 0.061$ ev at $4.2^{\circ}K$, were reported [35]. G is Kane's momentum matrix element. Theoretically, both (Γ_6) symmetry, as for example in indium antimonide (InSb), or (Γ_8) symmetry, as in Sn or HgTe, can represent the conduction band at K=0 [42]. However, a number of investigators [42-46] emphasized (Γ_8) as the correct choice, i.e. the inverted band structure, for the band symmetry of HgSe. It is noticed from the results of Lehoczky et al. [35] that the absolute value of the energy gap $|E_g|$ decreases as a function of temperature, as stated earlier. Furthermore, they estimated that the valence band overlap of the conduction band or the thermal gap E_t is -0.00504 ev and does not change with temperature. They concluded that HgSe is a zero gap semiconductor.

The value of $E_g = E\Gamma_6 - E\Gamma_8$, employing the inverted band model, was measured by Pidgeon and Groves [47] at $1.5^{\circ}K$ and $77^{\circ}K$ to yield -0.303 ev and -0.26 ev, respectively. Recently, Lombos et al. [11] reported the Hall effect measurements for the alloys of $HgTe_{1-x}Se_x$, using the inverted band structure, as illustrated in Figure 2.8. The thermal gap or the band overlap between the heavy-hole valence band v_1 and the conduction band (Γ_8) was defined as $E_t = E_c - E_{v_1}$, while the energy gap was defined as $E_g = E\Gamma_6 - E\Gamma_8$. Lombos et al. indicated that their experimental data fitted the inverted band model in the case of HgTe,

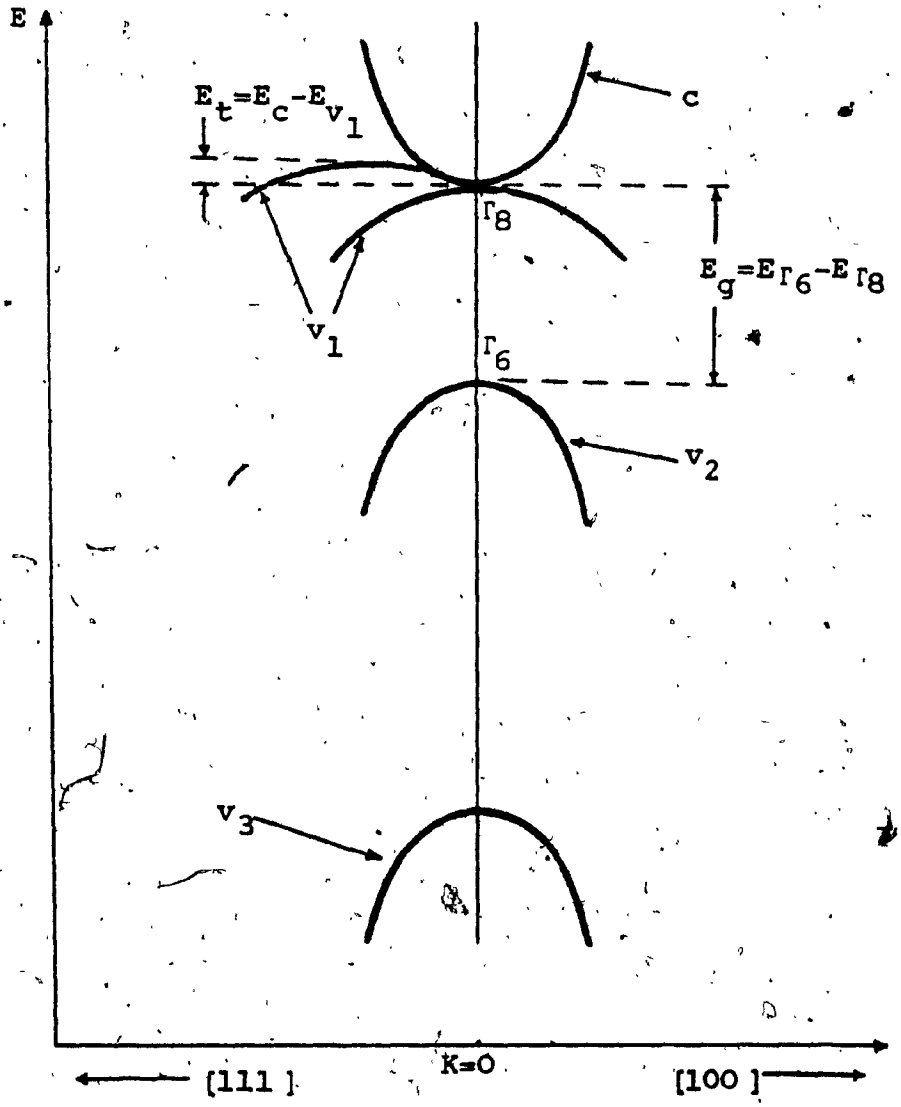

Fig.(2.8) - Energy (E) versus wave vector (K) schematic diagram for the inverted band model used for the analysis of the electrical properties of the mercury chalcogenides by Lombos et al. [11].

with an estimated $E_t < 10^{-3}$ ev and $E_g = -0.3$ ev at 4.2°K. For HgSe and the alloys, however, their analysis indicated that E_g as well as E_t were very close to zero and thus, might be considered zero gap semiconductors.

2.5 TRANSPORT PROPERTIES OF MERCURY CHALCOGENIDES AT ATMOSPHERIC PRESSURE

The band structure of a crystal is an important factor in determining the transport properties of a material. The edges of the bottom of the conduction band minima and the top of the valence band maxima of a particular band structure can determine for example the effective mass (a measure of the curvature of the energy band), the mobility (an average drift velocity of an electron in a material with an applied electric field) and any warping due to degeneracy or non-parabolicity.

Using the Hall coefficient measurements, an early value for the electron effective mass m_e^* of 0.03 m (m is the free electron mass) for HgTe at room temperature was measured by the Rodots in 1959 [48]. Harman in 1960 [49] obtained from Seebeck measurements for HgSe a value of 0.04 m for m_e^*. It has to be mentioned, however, that in these early analyses of the measurements, a parabolic conduction band was assumed. The first experimental analysis with the Hall effect measurement on the transport

properties of HgSe-HgTe solid solutions, based on a non-parabolic conduction band, was reported by Rodot et al. in 1961 [50]. In the light of the experimental analysis with the alloy composition of $HgTe_{1-x}$ Se_x, they noted that for the Se-rich samples the Hall coefficient R_H varied only little with temperature, while for the Te-rich samples R_H was a temperature dependent. They concluded that the former is an n-type, while the latter may be a p-type at very low temperatures. The results of their transport parameters (i.e. carrier concentrations, mobilities and effective masses), along with the results of other reporters on similar parameters are summarized in Table 2.2 .

In the case of HgSe, only n-type crystals with carrier concentrations in the range of 3.60×10^{16} cm^{-3} to 2×10^{19} cm^{-3} have been reported [35,45]. The electron concentration n and the Hall mobility μ_H variation between 4.2° and $300^{\circ}K$ were measured by Lehoczky et al. [35]. They indicated that for low concentration samples, i.e. $n=10^{16}$ cm^{-3}, an intrinsic behaviour (strongly changing with temperature) appeared between 20° and $300^{\circ}K$, while a departure from this intrinsic behaviour became more pronounced as the donor concentration approached the middle of the 10^{17} cm^{-3} range. Furthermore, they measured and found that samples with electron concentrations above 10^{18} cm^{-3} were almost independent of temperature within the indicated range. Their Hall mobility measurements showed that μ_H practically does not change

Table 2.2

Transport parameters of HgTe and HgSe at one atmospheric pressure and various temperatures

Material	Temperature T (^{o}K)	Concentration n (cm^{-3})	Hall Mobility μ_H ($cm^2 v^{-1} sec^{-1}$)	Electron Effective Mass Ratio $\frac{m^*_e}{m}$	Remarks	Ref.
HgTe	4.2	2.1×10^{15}	6.5×10^5			[51]
		2.5×10^{15}	5.5×10^5	0.036	$G = 8.3 \times 10^{-8}$ ev-cm	[54]
	77	5.9×10^{17}	0.81×10^4		$b = \frac{\mu_e}{\mu_h} = 70$	[50]
		0.612×10^{17}	0.612×10^4		$\mu_h = 51\ cm^2 v^{-1} sec^{-1}$	[58]
			2.5×10^4		at $T = 143^{o}$K	[38]
	293 - 300	5.9×10^{17}	1.37×10^4			[50]
		6.4×10^{16}		0.023		[39]
		2.4×10^{17}		0.029	$m^*_h/m = 0.3$	[39]
		4.3×10^{17}		0.038		[39]
		5.95×10^{18}		0.075		[39]
			1.7×10^4			[38]
	373	7.3×10^{17}	0.99×10^4			[50]
HgSe	77	2.6×10^{18}	2.07×10^4	0.044		[50]
				0.007	$m^*_h/m = 0.17$; $G = 9 \times 10^{-8}$ ev-cm	[34]
	293 - 300	2.25×10^{18}	0.73×10^4			[50]
		2.5×10^{18}		0.050 ± 0.003	$G = 8 \times 10^{-8}$ ev-cm	[40]
				0.007		[34]
	373	2.25×10^{18}	0.43×10^4	0.044		[50]

G = Kane's momentum matrix element [52]
m^*_h = hole effective mass
μ_e = electron mobility
μ_h = hole mobility

with temperatures up to near 50°K; it linearly decreases as a function of temperature to almost one order of magnitude (at 300°K) of its low temperature value for samples with n in the range of 10^{16} to 10^{18} cm^{-3}. These mobility data yielded good agreement with their microscopic theory treatment of electrical conduction in the zero gap semiconductor.

HgTe single crystals can be grown as p-type or n-type with controlled carrier concentrations down to about 10^{15} cm^{-3} [45]. Extremely high electron Hall mobilities of more than 600,000 cm^2/volt-sec at 4.2°K have been obtained by Harman et al. [51]. Many investigators [44,45] have measured n-type crystals with various carrier concentrations in HgTe and have established the low electron effective mass m_e^* and the non-parabolic character of the (Γ_8) conduction band at K=0. The gap $E_g = E\Gamma_6 - E\Gamma_8$ for HgTe is very sensitive to temperature, that is the energy gap separation E_g is smaller at room temperature than at 4.2°K. Consequently, the resistivity decreases as a function of temperature by nearly one order of magnitude between the temperatures 4.2° to 300°K [51].

In the inverted band structure (about K=0), the energy-momentum (E-K) relationship of the conduction band (c in Figure 2.8) and the light-hole valence band (v_2 in Figure 2.8) can be expressed [11,44,51], following

Kane's theory [52] by :

$$E_c = -\left|\frac{E_g}{2}\right| + \frac{1}{2}\left[E_g^2 + \frac{8}{3}G^2K^2\right]^{\frac{1}{2}} \qquad (2.6)$$

$$E_{v_2} = -\left|\frac{E_g}{2}\right| - \frac{1}{2}\left[E_g^2 + \frac{8}{3}G^2K^2\right]^{\frac{1}{2}} \qquad (2.7)$$

where E_g is the energy gap between (Γ_6) and (Γ_8) states (but not necessarily the thermal gap), that is

$$E_g = E\Gamma_6 - E\Gamma_8$$

G is Kane's momentum matrix element and K is the momentum space vector. Equation (2.6), together with the electron effective mass

$$m_e^* = \hbar^2 K \left(\frac{dE_c}{dK}\right)^{-1} \qquad (2.8)$$

were used by Wright et al. [40] to derive the relationship

$$\left(\frac{m_e^*}{1-m_e^*}\right)^2 = 32.5 \times 10^{-32}\,\frac{E_g^2}{G^4} + \frac{8.27 \times 10^{-30} n^{2/3}}{G^2} \qquad (2.9)$$

which applies when the Fermi level E_F (the highest valence band in a semimetal) is 4kT or greater above the conduction band edge E_c [44]; n is the electron concentration. It can be seen that if a plot of $[m_e^*/(1-m_e^*)]^2$ versus $n^{2/3}$ yields a straight line, then the slope of the line is proportional to $1/G^2$ and the intercept is

proportional to E_g^2/G^4 . Such a plot was given originally by Wright et al. [40] for HgSe and reviewed later by Harman [44], yielding straight lines for HgSe and HgTe. Harman estimated the corrected energy gap E_g for HgSe and HgTe at room temperature to be approximately -0.15 ev and -0.14 ev, respectively [45] .

Lombos et al. [11] gave an expression for the electron concentration n in the conduction band (Γ_8), following Kane's theory [52] and according to the inverted band scheme, as follows :

$$n = \frac{\sqrt{2}}{\pi^2}\left(m_e^* \frac{4\pi^2 kT}{h^2}\right)^{3/2} [F_{1/2}(\eta) + \beta(5/2 - 5\xi)F_{3/2}(\eta) + \beta^2(1 - \frac{21}{2}\xi)F_{5/2}(\eta) - 4\xi\beta^3 F_{7/2}(\eta)] \qquad (2.10)$$

where

$$\beta = \frac{kT}{|E_g|}, \quad \xi = \frac{m_e^*}{m}, \quad \eta = \frac{E_F}{kT} = \frac{3h|E_g|}{16\pi^2 G^2}$$

k is Boltzmann's constant, T is the temperature, E_F is the Fermi level relative to the bottom of the conduction band, and $|E_g| = |E\Gamma_6 - E\Gamma_8|$. m_e^* is the band curvature effective mass of the electron at the edge of the conduction band, m is the free electron mass, h is Planck's constant and G is Kane's momentum matrix element. $F_j(\eta)$ is the Fermi-Dirac Integral of order j :

$$F_j(\eta) = \int_0^\infty \frac{\varepsilon^j \, d\varepsilon}{1 + \exp(\varepsilon - \eta)} \qquad (2.11)$$

The hole concentration p in the heavy-hole valence band [v_1 in Figure 2.8] is expressed [11,34,44] by :

$$p = \frac{\sqrt{2}}{\pi^2} \left(m_h^* \frac{4\pi^2 kT}{h^2}\right)^{3/2} F_{1/2}\left(-\eta - \frac{E_t}{kT}\right) \qquad (2.12)$$

where m_h^* is the density of state effective mass in the heavy-hole valence band and E_t, the thermal gap, is defined as in equation (2.5).

2.6 ENERGY BAND STRUCTURE AND TRANSPORT PROPERTIES OF MERCURY CHALCOGENIDES AT HIGH PRESSURE

High pressure measurements for HgTe assured that the inverted band structure, similar to that used for Sn [29], is the most appropriate structure for this material. It is known [53] from all diamond and zinc-blende type compounds examined so far that the level (Γ_6) rises as a function of pressure faster than (Γ_8) . This means that $\frac{d}{dP}(E_{\Gamma_6} - E_{\Gamma_8})$ is positive or $(\partial E_g / \partial P)_T > 0$, for positive energy gap materials, i.e. $E_g > 0$. However, for the inverted band structure where $E_g < 0$, it has to be noted that $\frac{d}{dP}(E_{\Gamma_6} - E_{\Gamma_8}) < 0$, i.e. $(\partial E_g / \partial P)_T < 0$. Thus the pressure coefficients of the (Γ_8) and (Γ_6) states depend on the symmetry of these wave functions rather than on their relative energetic positions [54] .

The pressure dependence of the thermoelectric power of extrinsic n-type HgTe with electron concentration $n=1.1\times10^{18}$ cm^{-3} was measured by Piotrzkowski et al. [55]. These investigators deduced from the change of sign of the thermoelectric power that the Fermi level has increased with pressure. This was supported by Groves et al. [54] who determined that a decrease of the conduction band mass indicates a decrease in $(\Gamma_8 - \Gamma_6)$ separation as a function of pressure. They also have analyzed some unpublished data for HgTe and HgSe under pressure, using thermoelectric power and optical absorption measurements. In the case of HgTe, they confirmed the pressure dependence of thermoelectric power given by Piotrzkowski et al. [55], however, they reported that for the HgSe compound having the same concentration, the opposite sign of pressure dependence was noticed. They attributed the latter to the problem of obtaining samples of high concentration n-type to show extrinsic behaviour, yet with a small enough number of electrons to give a measurable change of thermoelectric power under pressure.

Measurements of the temperature dependence of the Hall constant in intrinsic HgTe samples under pressure were examined by Porowski and Zakrzewski [56] and Piotrzkowski et al. [55]. A linear relation exists between the Hall constant R_H and $T^{-3/2}$, where T is the temperature. This dependence which was found at pressures of one atmosphere and 5 kbar

is a characteristic of a zero thermal energy gap E_t . Thus, the zero thermal gap E_t which was obtained from the inverted band structure and found in materials such as HgTe and HgSe [15,33,45] does not change with pressure or temperature. This confirms Groves' and Paul's [29] original observation in the case of Sn. The expression "zero gap semiconductor", or alternatively, zero overlap semimetal, stresses the fact that these materials belong to a special class of semiconductors [33] .

According to Piotrzkowski and Porowski [57] , the electron effective mass m_e^* in semimetal materials is independent of pressure. Experiments with HgTe and HgSe [8] and in this work with HgSe showed that the conductivities of these materials under pressure are constants up to their transition pressures, substantiating Piotrzkowski's and Porowski's observation. Unfortunately, up to date, no transport measurements are known to be published on the high pressure phase (the cinnabar structure) of mercury chalcogenides [15] . However, due to the pressure induced polymorphic phase transition, detected by the large resistance increase, the low pressure phase (zinc-blende) characterized by the inverted band structure [15,33,45] changes to Kane's normal band structure [57] and the effective masses increase [15] . The high pressure phase electron effective masses m_e^* for HgTe and HgSe were determined to be 0.04 m and 0.046758 m, respectively [15],

where m is the free electron mass. The energy gaps E_g of the high pressure phase of the mercury chalcogenides are then positive as in a normal semiconductor, i.e. the conduction band (Γ_6) is higher than the valence band (Γ_8) at K=0.

2.7 KINETIC MECHANISMS OF TRANSFORMATION

The term "transformation" in connection with phases has been used generally by many authors to mean an extensive rearrangement of the atomic structure. Such a rearrangement results from some driving forces under the influence of strain energy, surface energy or other external forces. In a typical phase transformation, the new phase grows at the expense of the old phase by migration of atoms across the interphase boundary [59] . The reaction will proceed at a given temperature and a given pressure and the formation of the new phase advances with time [60,p. 50].

Most chemical kinetics are originally based on a statistical theory developed by Glasstone et al. [61]. The basic assumption of their theory is that the whole reaction can be divided into steps. Each unit step appears from the interaction of a group of atoms or molecules to form a new configuration. However, before this can be accomplished, the group must pass through an intermediate state which has higher energy than either the initial (of the reactants)

or the final (of the products) states. Furthermore, there is a critical dimension which each group must attain if the final state is to be reached; hence, an increase in the system's free energy is required to form these groups. Such an activation energy is needed by the system to enable the reaction to proceed before it stabilizes in its final state.

2.7.1 Homogeneous and Heterogeneous Systems

A system is considered to be homogeneous when it maintains only one phase during the entire course of its reaction [62,p. 2] . Thus, transformation takes place simultaneously in all parts of the assembly.

Heterogeneous systems include not only those in which reactants are of different phases, but also those in which a difference in composition may exist between the various phases of the system [62, p. 3]. These systems therefore always encounter a surface of separation (interface) between the reactants and the products.

Transformation classification is well discussed by Christian [63] , but since HgSe and HgTe transform from the zinc-blende into the hexagonal cinnabar structure under pressure, therefore this investigation is concerned only with the heterogeneous type of kinetics.

2.7.2 Nucleation and Growth

Avrami [64] indicated in his development of the theory of kinetics of phase change that the new phase is nucleated by potential nuclei already existing in the parent phase, whose number can be altered by previous treatment. The potential nuclei are groups of atoms or molecules, located throughout a sample, with sizes less than a critical dimension required for the growth nuclei. Growth nuclei or simply nuclei are only those centers which have reached the critical size, possessing a number of atoms in the new phase (the number is being different for different reactions, consisting of a few atoms or molecules), and are ready to grow. The potential nuclei can be those points in a crystal lattice consisting of defects, impurities or both. When a potential nucleus reaches its critical size, i.e. becomes a growth nucleus, it then grows instantaneously in the new phase within the old one, until all the material is transformed. The number of potential nuclei or growth nuclei vary for various reactions. For example, when a transformation process is characterized by a single growth nucleus, created perhaps at a corner of a sample and with a single moving interface, this process is called mono-nucleation. However, most of the heterogeneous transformations contain large numbers of growth nuclei [60 - 64].

Nucleation and growth are two distinct processes. Nucleation at any site within the lattice requires the

accumulation of a given number of atoms or molecules, i.e. to become a critical size nucleus, at that site before it is ready to grow, and therefore it is microscopic. On the other hand, growth which is a macroscopic process, characterizes a continuous phase transformation with a moving interface and can mathematically be in one, two or three dimensions. The growth interface in some transformations moves inward, starting from the material surfaces, and in others it moves outward towards the surfaces. Furthermore, when the potential nuclei reach their critical size with a composition of the new phase, the free energy of the system rises first from the initial state to a higher state, i.e. transition state. This increase of energy (transformation energy barrier) which is due to an increase in the number of atoms or molecules at the sites of the potential nuclei, is followed by a decrease of energy to a level (final state) lower than both, the transition and the initial state [17,60 p. 8-9]. Therefore, the increase of energy from the initial state to the transition state corresponds to nucleation, while the decrease of energy from the transition state to the final state corresponds to growth. More detailed discussion on the energy profile will be given in Chapter V.

In most heterogeneous systems, the nucleation process starts with a given number of potential nuclei, a fraction of which acquires sufficient energy enabling them

to reach the critical size of growth nuclei and then grow. As soon as more energy is supplied to the system, the remaining potential nuclei will grow gradually after reaching their critical size, following up the previous growth [62, p. 394] . Thus, in this process the number of growth nuclei is generally a function of energy and time. It is not necessary that all of the existing potential nuclei become growth nuclei; depending upon the model and the supporting experimental evidences, for example growth nuclei may easily "swallow" nearby potential nuclei [63, p.19]. It is also possible for growth nuclei to ingest (overlap) other growth nuclei or be interrupted by the surfaces of the sample before the completion of transformation, thus affecting the growth rate [62, p. 401] .

2.7.3 Growth Rates

The rate of growth or the rate of transformation is a very important parameter in kinetics. The exact mathematical expression and derivation for the rate depends upon the particular model and situation [62, p. 397]. However, for the work of the present investigation, based on the developed model and the experimental results, the growth rate was determined to be proportional to the change of the degree of advancement of the reaction with respect to a change in time. It is important to note that in heterogeneous transformations the physically observable changes are usually attributed to growth rather than nucleation and thus can be quite useful in elucidating the kinetics of many reactions.

CHAPTER III

EXPERIMENTAL APPARATUS AND PROCEDURE

3.1 MATERIAL PREPARATION

This Chapter is basically composed of three sections, sample preparations under the given conditions, equipment used and the experimental procedures.

3.1.1 Crystal Growing

Mercury selenide crystals were prepared by the modified Bridgman technique, using direct synthesis from their semiconductor grade elements, i.e. tridistilled mercury and semiconductor purity selenium from Noranda Company of Canada Ltd.. Carefully weighed stoichiometric amounts of Hg and Se with a calculated excess amount of Hg were put into a quartz boat to maintain dissociation pressure at the melting point of the compound. The boat was then sealed inside a quartz ampule at a pressure of 10^{-5} mm Hg. This ampule was suspended in a horizontal zone refiner, using a Silicon Carbide tube. The hot zone of the zone refiner, similar to the one described by Harman et al. [38] for HgTe, was set at 803°C[1], while the flat background furnace was adjusted for approximately 35 cm at 580°C. This was done to ensure a mercury vapor pressure of 20 atmospheres inside the ampule to avoid compound dissociation. A sample

---

[1] The melting point of HgSe is 798°C [16].

calculation is provided in Appendix A-I. The temperature in this furnace was controlled within ± 1°C. A travelling rate of 0.35 cm/hr was selected to synthesize the compound and zone refine it. After 3 zone refining passages, polycrystals containing segments of single crystals (typical grain size 10x4x4 mm) were obtained.

3.1.2 Sample Type and Geometry

Three sample types of HgSe were obtained:

1) Samples from the ingot including single and polycrystals.
2) Powdered samples of HgSe including samples with impurities of HgS or HgTe.
3) Annealed crystal samples under different temperatures.

The first type was obtained after the process of zone refining; the ingots were attached to a metal base of a wire saw, designed at Concordia University for crystal cutting purposes, by means of a molten wax to ensure sample stability during the wire movements. Slices with a typical thickness of 3 mm of single crystals as well as polycrystals were carefully cut, using fine Aluminum Oxide powder (0.3 μm). These slices were then further cut into small samples of approximately 3x3x8 mm in dimensions. They were then lapped, using the same powder, to approximately 2.4x2.5x5 mm washed in distilled water and immersed in Tricholoroethylene to dissolve and clean any remaining wax. This type of samples was used in all the experiments for comparison.

Due to the softness of HgSe (comparable to Pyrophyllite), the second type was prepared by weighing a given amount of HgSe, grinding it into fine powder (with an average diameter of 40 μm) and mixing it with the necessary impurities (powder of HgS or HgTe, see p. 63). Then it was poured into the chamber of the Simplimet Press made by Buehler Ltd. of Illinois, USA. A precompression was applied of about 4,000 lb/in^2 for a couple of minutes, followed by decompression and a final compression of about 10,000 lb/in^2 which was maintained for at least thirty minutes and decompressed again. The obtained cylindrical specimen having a diameter of 2.56 cm and a thickness of approximately 3 mm was then cut, using the same saw, to small sizes as mentioned earlier. Some powder samples of HgSe were prepared and employed in the high pressure experiments without introducing any impurities to investigate the behaviour of the powder compared to that of the single and polycrystals of HgSe compounds.

The third type was prepared by first cutting single crystal samples from the ingot, maintaining the same size as before. These were then placed in small quartz tubes of 13 cm in length and 1.1 cm in diameter. After evacuation the tubes were carefully sealed. Four such tubes, each with three or more samples, were annealed under different conditions as follows:

1) 328°C for 20 hrs + 500°C for 20 hrs
2) 350°C for 48 hrs
3) 400°C for 48 hrs
4) 500°C for 48 hrs.

At the ends of each sample, a thin good conducting silver coated wire approximately 7.0 cm long, was tightly coiled around the sample to ensure good mechanical contact as shown in Figure 3.1-A. This was followed by a layer of "44" resin solder made by Kester Solder Company of Canada Ltd., to ensure good electrical contacts between the coiled part of the wires and the two far ends of the samples, creating ring-like solder as shown in Figure 3.1-B. Indium solder was then used of approximately twice the amount of the Kester solder, covering up the two far ends of the sample cross-section and reinforcing the contacts between the sample, Kester solder and the coiled parts of wires as in Figure 3.1-C, forming plate-like contacts at each end. The coiled part of the sample at each end was about 1 mm in thickness. Therefore, the effective length of the sample has been taken to be intermediate between the length between the end faces and the length between the inside edges of the coils. The contact resistance of these ohmic electrical connections compared to the resistance of HgSe, particularly right after the outset of the upstroke transition, becomes negligible. This technique of establishing good wire contacts to a sample proved to be far superior than just soldering wires into samples with either of the mentioned solder or few other kinds of solder that were tried independently. By this new technique, the wire-sample contacts cannot be separated by pulling the wires from the sample without

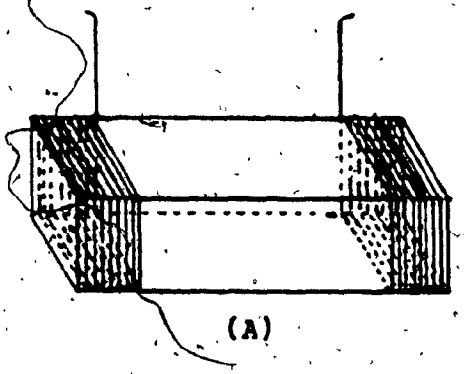

(A)

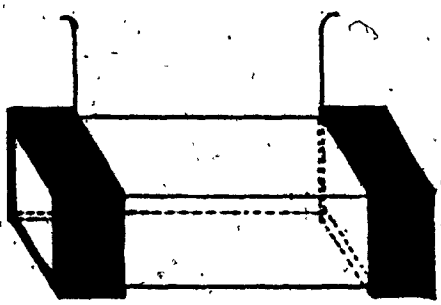

(B)

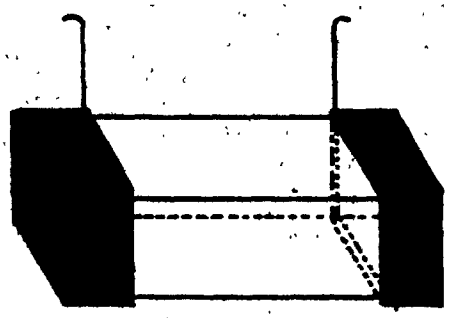

(C)

Fig. 3.1-(A) - Coiled wires to secure mechanical contacts with the sample
(B) - "44" resin solder applied
(C) - Indium solder applied

breaking the sample itself into pieces. The first few experiments with mercury chalcogenides were often interrupted by poor contacts under high pressure, before this technique was developed.

Furthermore, with the new contact arrangements, when a voltage is applied to the wires, current will flow uniformly between the two plates through the sample. This allows better resistance measurements than just soldering a wire to a point at each end of the sample. The other two ends of the wires are soldered to the high pressure obturator wires after ensuring their isolation from each other and from the obturator itself.

3.2 HIGH PRESSURE APPARATUS

The high pressure apparatus used in these experiments is shown in Figure 3.2; it is manufactured by Basset-Bretagne-Loire in France.

3.2.1 High Pressure Press

The upper part of the apparatus is a four column press with a thrust capability of 120 tons. Two pistons, primary and mobile were incorporated in the system. The primary piston has a diameter of 25.0 cm (cross-sectional area of 490.6 cm^2), while the mobile piston has a diameter of 1.996 cm. The maximum pressure corresponds to a maximum attainable pressure of 32 kbar in the high pressure chamber.

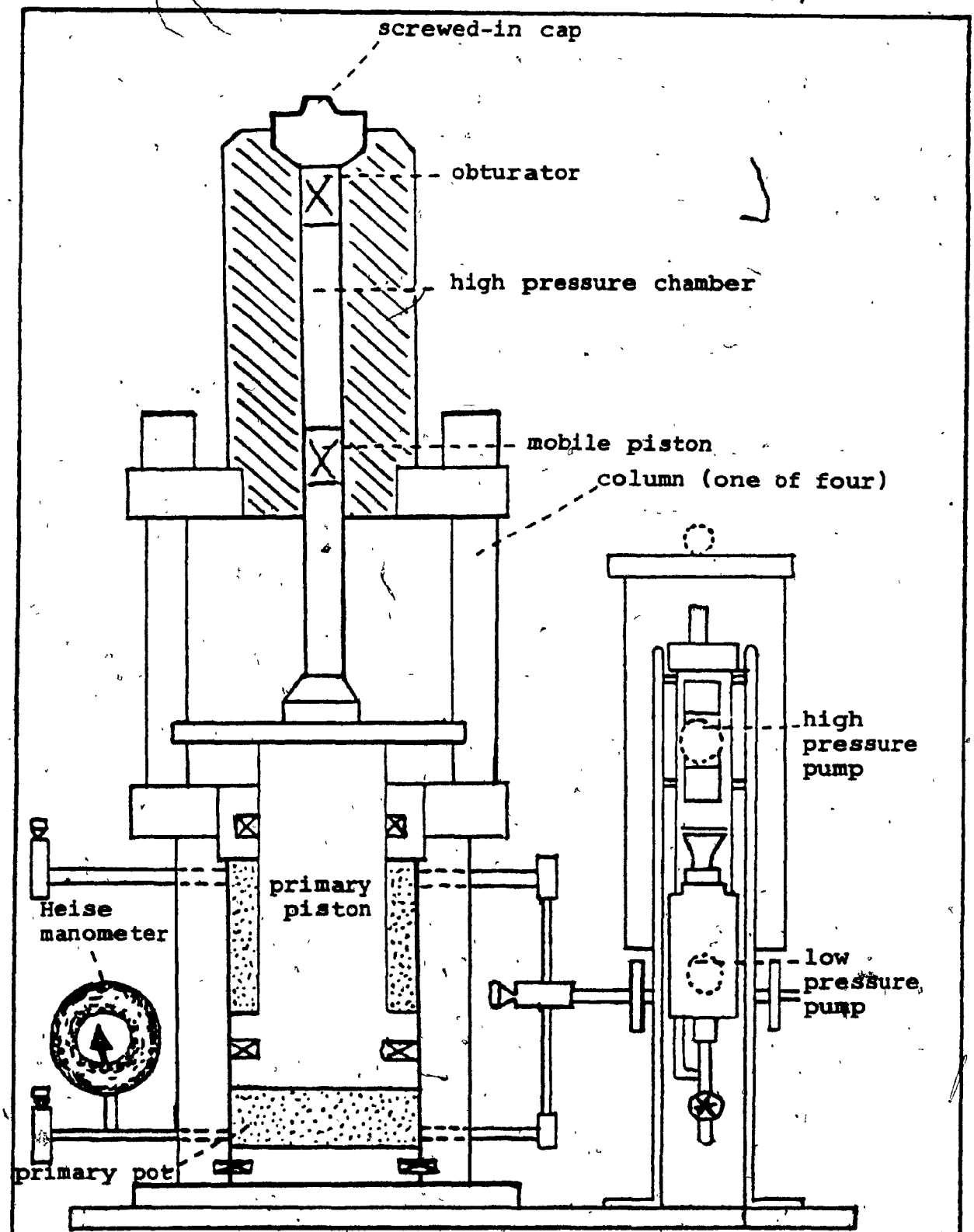

Fig. 3.2 - High pressure instrument

3.2.2 Pressure Pumps

A two-pump design was chosen in this system to provide the ability to vary in large proportions the pressures as well as the pressure rates. Both pumps are hydraulic and can be used independently. The low pressure pump, with a large flow for fast compressions, is used in these experiments mainly to settle the Teflon joints, which undergoes a phase transition of around 4 kbar; also in order to avoid any leaks, due to the sudden volume change of the joints, it was necessary to pass over this 4 kbar point very fast (500 bar/min to 700 bar/min). The high pressure pump with a fine regulation of flow allowed compressions at small controlled rates (a few bar/min to nearly 100 bar/min).

3.2.3 High Pressure Chamber

This chamber is placed on the top of the press. The body of the chamber itself is made of steel multilayer type, with an inside cylinder made of Vascomax 385 steel, finely polished; periodical polishings with an alumina powder (maximum grain size of 0.03 um) reduce friction and permit a good conservation of the interior surface. The interior diameter of the chamber is compatible to that of the piston at atmospheric pressure. The dilatation of the chamber is in the order of 0.006 mm/kbar. The maximum useful pressure chamber volume is in the order of 60 cm^3.

An equivolume mixture of n-pentane and iso-pentane served as pressure transmitting medium and was used in all the experiments. This liquid environment was confirmed as truly hydrostatic by Barnett and Bosco [65] . Through its viscous flow this liquid environment takes a few seconds to be hydrostatic when subjected to pressure below 50 kbar, while taking a few minutes if the pressure exceeds 60 Kbar.

3.2.4 Mobile Piston

When the mobile piston moves through the chamber, a friction force is exerted on the mobile piston by the pressure chamber walls. In order to reduce this friction, and more important to prevent piston-chamber leak, it was necessary to employ as in Figure 3.3-A a Teflon O-ring and two copper rings. Just before starting any experiment, the rings were covered with a molybdenum bisulfur grease to allow an easy displacement of the rings in the chamber. The softness of the copper rings assists in minimizing a possible degradation of the interior fine polish of the chamber.

3.2.5 Obturator

The obturator is shown in Figure 3.3-B along with the necessary rings that ensure the pressure vessel to remain leak-proof during any experiment. The piling order including the rubber O-ring, as in the above figure, is found

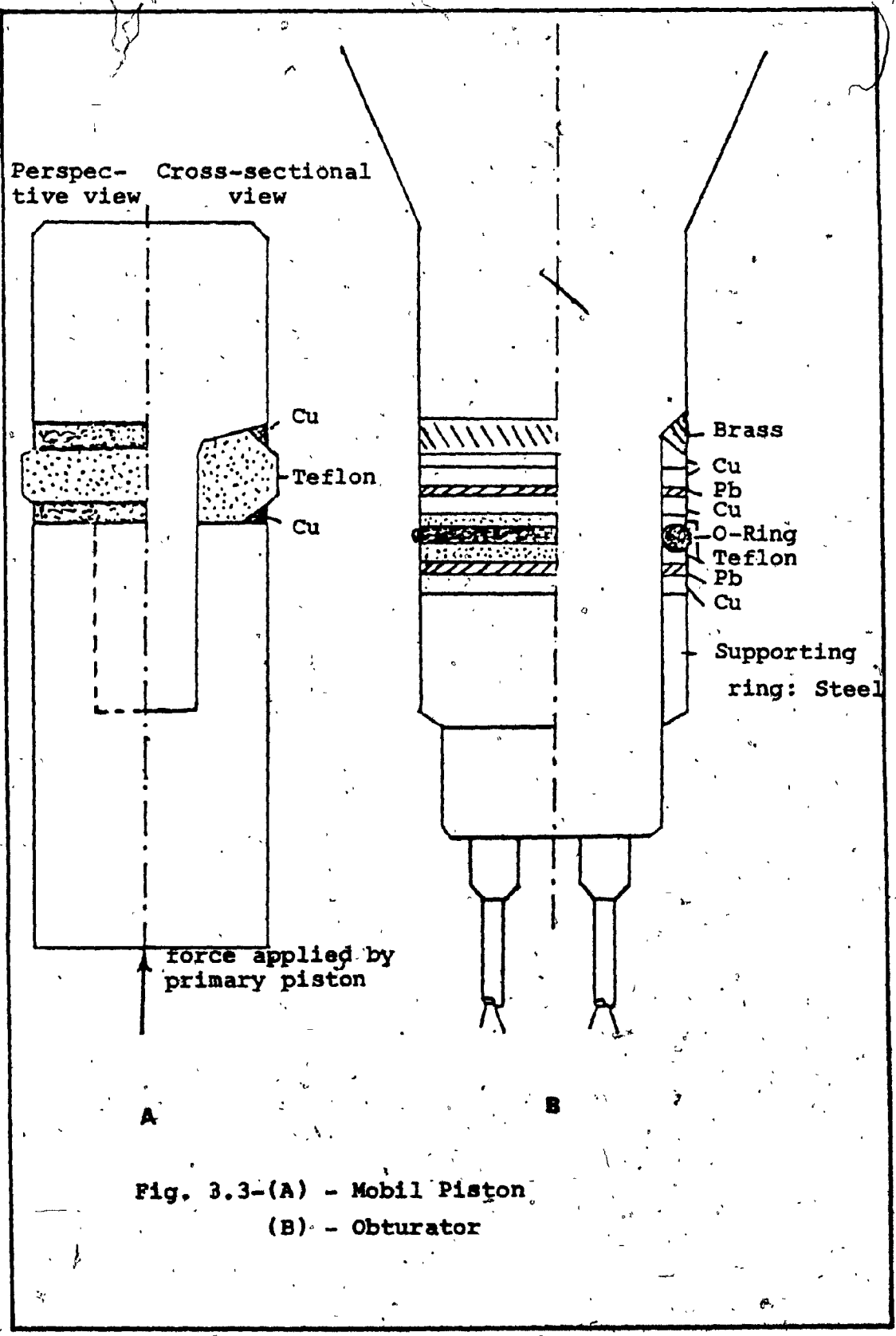

Fig. 3.3-(A) - Mobil Piston
(B) - Obturator

experimentally to allow better fitting and deformation of the soft elements at the beginning of each experiment.

3.2.6 Electrical Feed-throughs

The obturator has five electrical feed-throughs made by Société Anonyme d'Etudes et Réalisations Nucléaires, Suresnes, France, as shown in Figure 3.4. Each feed-through with a diameter of 1.0 mm, made of a stainless steel tube, embeds two isolated electrical conductors. The isolation used is magnesia powder, sufficient[2] to isolate the conductors from the feed-through and from each other. Each conductor wire which is very brittle has a resistance of 0.02 ohm/cm and a diameter of 0.18 mm. One feed-through is used for the manganin coil and the remaining four to measure resistance variations of the samples.

A screwed-in cap is used to hold the obturator in place and to protect the electrical entries against possible mechanical damage.

3.2.7 Holder

The holder as shown in Figure 3.5 was designed to provide good electrical contacts stability and protect the

---

[2] An insulation resistance of the order of 5 megohms is obtained for a dry magnesia powder.

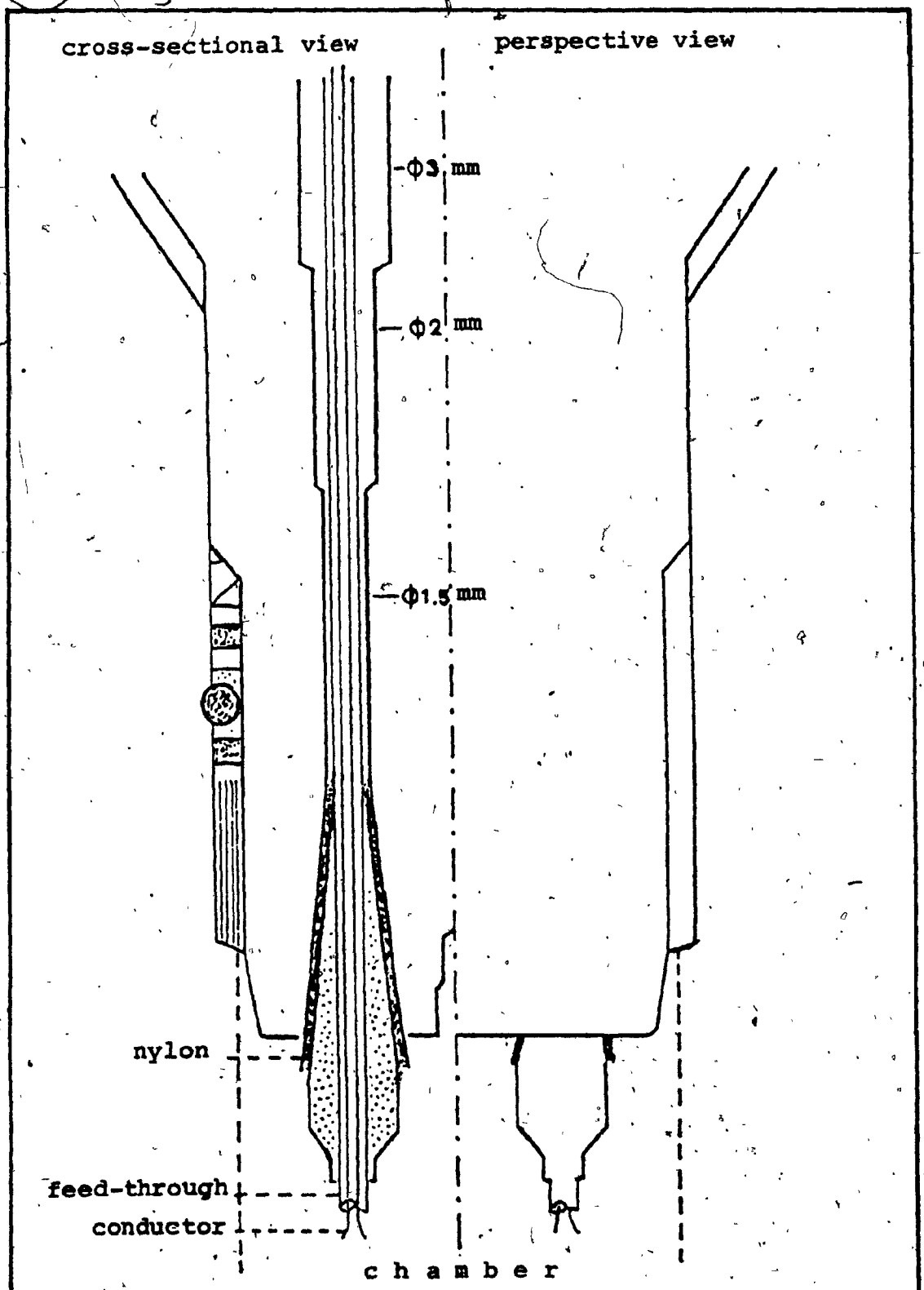

Fig. 3.4 - Obturator with electrical feed-throughs (two out of five are shown)

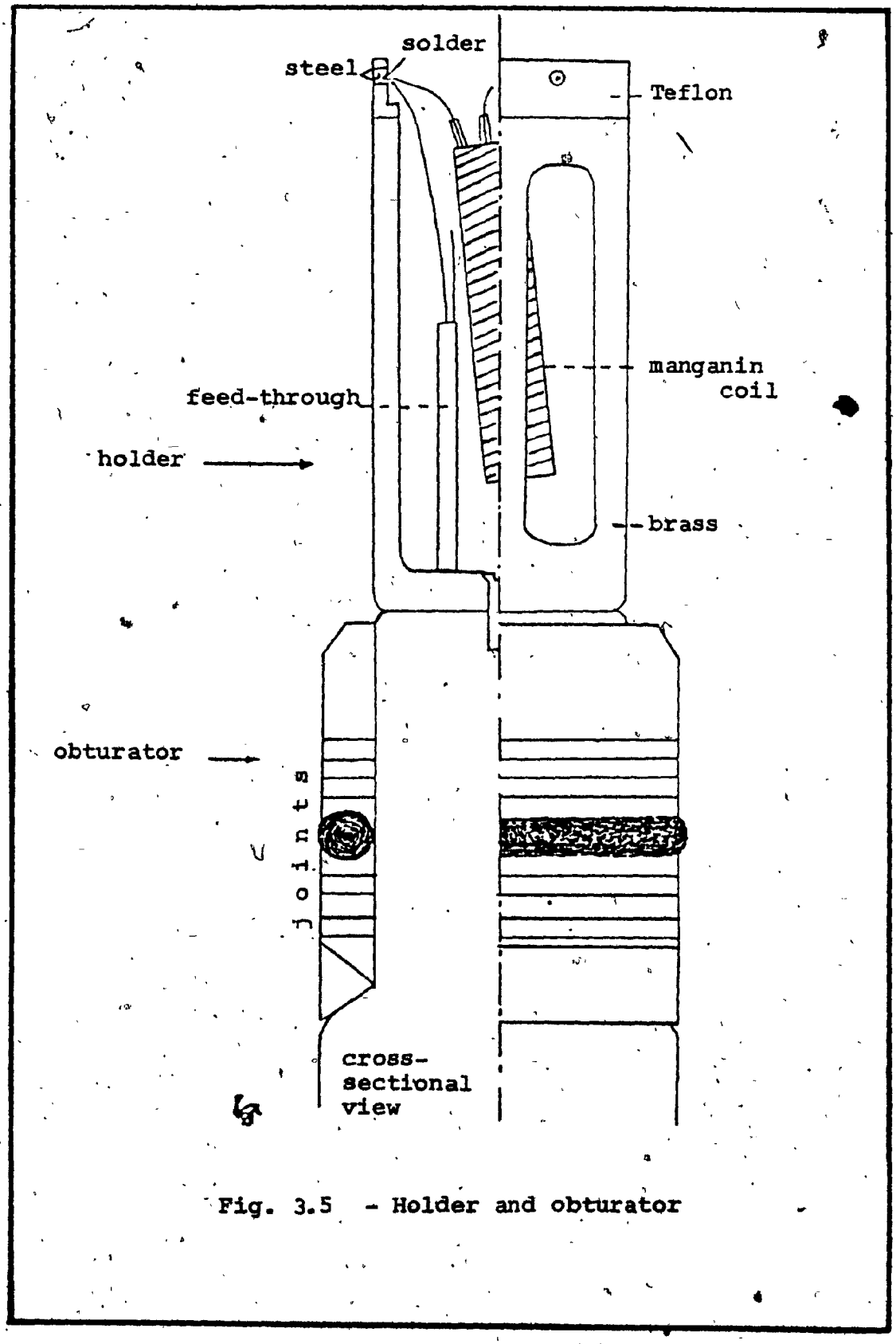

Fig. 3.5 - Holder and obturator

manganin coil against mechanical damage during an experiment. The upper plate of the holder is made of Teflon with independent holes for the wires to ensure good isolation.

3.2.8 The Primary Pressure Pot

A manometer is connected directly to the primary pot with a measuring precision of approximately 1.0 %. This measurement is necessary to evaluate the friction of the joints during any experiment.

3.3 FRICTION

Working with high pressure equipment, one has to evaluate the friction presence for a particular pressure; since it changes as a function of pressure, it has to be evaluated repeatedly during any experiment.

The pressure inside the chamber depends on the ratio between the cross-sectional areas of the primary and mobile pistons and on the friction between the rings of the mobile piston and the walls of the chamber. If one designates p' for the pressure reading on the manometer in the primary pot, and P for the pressure inside the chamber, then

$$P = \frac{S}{s} p' + f(P) \qquad (3.1)$$

where S and s are the cross-sectional areas of the primary and mobile pistons respectively and f (P) is an expression

of the friction forces.[3] Thus knowing $S = 490.6\ cm^2$, $s = 3.13\ cm^2$ and reading p' from the manometer and P from the manganin coil, one can determine f (P) from equation (3.1). In most of these experiments the friction is calculated to be in the range between 7.0 % to 15.0 % for pressures up to 15 kbar.

3.4 PRESSURE MEASUREMENTS

The manganin pressure gauges are widely used in liquid hydrostatic pressures because of their large pressure coefficient of the resistance (P.C.R.) and their small temperature coefficient of the resistance (T.C.R.)[66].

The manganin wire insulated with silk is wound non-inductively on a paper support with a total resistance at one atmospheric pressure in the order of 120 ohms. The coils were seasoned by a special treatment consisting of heating to 150°C and quenching with liquid nitrogen repeatedly, followed by a pressure cycle to 25 kbar [66].

The two leads of the manganin coil were soldered to the conductor wires of the feed-throughs. The total length of the conductor wires which were exposed to pressure inside the chamber were less than 2 cm. The resistance of these wires as given before was 0.02 ohm/cm, while that

---

[3] $f(P) < 0$ on the upstroke and $f(P) > 0$ on the downstroke

of the coil was above 120 ohms. Since manganin has a rather high pressure coefficient of resistance, the pressure coefficient of the conductor wires was ignored. The possible error due to the latter was estimated to be less than 0.033 %.

A wheatstone bridge[4] was used with the manganin coil as one of the arms and low temperature coefficient resistors as the other arms. A Keithley Microvolt Ammeter type 150 B was employed to monitor the balanced condition of the bridge circuit. In such a configuration any unbalancing of the bridge would be due to the variation of the resistance of the manganin coil alone.

The relation between pressure and the change of resistance of the coil used was

$$P = 420 \frac{\Delta R}{R_o} \qquad (3.2)$$

where P is in kbar, R_o is the coil resistance at atmospheric pressure in ohms, and ΔR is the respective change in the resistance of the coil (ohms). The coil calibration determining the pressure coefficient of 420 was performed at Laboratoire des Hautes Pressions, CNRS, 92-Bellevue, France, by means of the transition pressure of Potassium Bromide (KBr) and a free piston gauge. However, the manganin manufacturer's (Isabellenhuette, Heusler KG, Dillenburg, W. Germany) specification gave a pressure coefficient of 426.4

[4] The maximum error for this bridge was 2.75 %.

without seasoning. But the calibrated value was used, which is close to the value published in the literature [66].

Independent constant current sources of 0.1 mA, 1.0 mA, 10 mA and 21 mA were used to pass currents through samples under pressure. Hence, the measured voltage drop across a given sample provided a measure of its resistance at any time during an experiment. These voltages along with the coil voltage$^{\emptyset}$ were continuously detected, displayed and recorded on a four channel strip chart recorder. The sensitivity of the pressure measurement in the order of 1.0 bar was easily detected, as shown in Appendix A-II. All measurements were performed at room temperature (22^{o}C).

3.5 EXPERIMENTAL PROCEDURES

The first goal was to find a correlation between volume and resistance changes during the solid-solid phase transformation in HgSe. Therefore, in a set of experiments samples were used to measure resistance changes with typical dimensions of 2.4x2.4x5 mm, cut from the prepared crystals of HgSe. Ohmic contacts as described earlier were applied and soldered to the electrical wires of the feed-throughs near the holder. The other terminals of these wires were connected to constant current sources and to the strip chart recorder. The ratio of the volumes of the resistance sample to that of the high pressure chamber (50.0 cm^3) is approximately 5.7x10^{-4}. Hence, the

effect of the sample volume variation on the pressures maintained in the relatively large chamber volume can be neglected. A large sample with a typical volume of 10.0 cm^3 was used simultaneously to follow the volume change for one experiment to correlate resistance with volume variations.

In the correlation experiment the sample volume variation was detected by monitoring the position of the base plate of the pump, which displaced the mobile piston, with a micrometer giving a precision of 0.01 mm [67]. The resistance variations of the samples were followed with a sensitivity of better than 0.003 ohm [Appendix A-III].

The experimental results and analyses of the simultaneous measurements of volume and resistance variations during the phase transformations were used to develop the conversion function between volume and resistance variations and will be given later.

A second set of experiments was done to investigate the effect of nucleation on the upstroke and downstroke outset of transition pressure. Since the high-pressure phase of HgSe is hexagonal, corresponding to the red HgS hexagonal structure [12], the latter was mixed with the powdered HgSe as the nucleation centers for the upstroke transition. The various amounts of nucleation concentrations of HgS were in molecular weight percentages of 0.01, 0.05, 0.1, 0.5, 1.0, 2.0 and 3.0. The upstroke transition pressure of HgSe was reported

to be at 9.3 kbar and the downstroke one at 5 kbar while the upstroke transition pressure of HgTe is at 15.3 kbar and the downstroke one at 13 kbar [8]. Furthermore, HgTe is known to have the same low and high pressure structures as that of HgSe [14], respectively. Based on this data, HgTe was selected and used as the downstroke nucleating agent for HgSe, since the low pressure phase of HgTe retained its structure at least up to above 15 kbar, a pressure at which HgSe had transformed into the high pressure phase. Before reaching the transition pressure of HgTe, pressure was decreased slowly towards the downstroke transition. Therefore, just prior to the downstroke transition which occurred, the structure of the material at the high pressure phase containing a number of active centers and maintaining the low pressure phase, were ready to grow. The specific amounts[5] of nucleation concentratidns of HgTe in HgSe were similar to that used for the upstroke case. The results of these experiments are presented in the next Chapter.

The third set of measurements was examined to determine the fast rate of transformation in HgSe, using the previously described annealed samples. The rates were compared with the nucleated and unnucleated samples, as will be discussed later.

---

[5] The amount of impurities is expressed in units of molecules per cm^3, as the nucleation concentration.

CHAPTER IV

EXPERIMENTAL RESULTS

4.1 INTRODUCTION

This Chapter presents only the important experimental results within the scope of the total investigation; the analysis of these results is discussed in Chapter VI. Some of the results given in this Chapter depend partially upon the theoretical model presented in Chapter V as will be indicated.

4.2 VOLUME AND RESISTANCE HYSTERESES

There are two types of volume change for HgSe under pressure: volume change due to compressibility and volume change due to phase transformation. Bridgman [13] measured the compressions of mercury chalcogenides and the compressibilities were determined from his data for HgSe at low pressure phase 1.5392×10^{-3} kbar^{-1} and at high pressure phase 2.272×10^{-3} kbar^{-1}. The relative change of volume due to the polymorphic phase transition in this material was reported by Jayaraman et al. [16] to be 9.0 % of the total sample volume, and by Lacam et al. [8] as 8.2 %. In this investigation, however, the analysis of the measurements[6] gave a value of 8.29 %.

---

[6] One set of the raw data analyzed here was obtained from Laboratoire des Hautes Pressions, CNRS, 92-Bellevue, France, through the courtesy of Drs. A. Lacam and J. Peyronneau.

The experimental results of the simultaneous measurements of volume (solid line) and resistance (dotted line) of HgSe, displayed in their typical hystereses, are shown in Figure 4.1 [8]. In this figure the ordinate contains two scales: plate displacement and normalized resistances to sample resistance at atmospheric pressure R'_o, while the abscissa displays only the pressure scale. The pressure as a function of base plate displacement clearly depicts the effect of the volume change of the large sample due to phase transition superimposed on the experimentally adjusted pressure variation. Consequently, the rate of volume change is superior to the rate of change of pressure and hence the increase of pressure is being modulated by the large sample volume reduction. This pressure interruption, as indicated by A for the upstroke transition (A' for the downstroke transition) in Figure 4.1, was already observed in the case of RbCl and called "retropressure" [68,69]. The period of retropressure in HgSe was about 12.5 minutes for a rate of change of pressure $\frac{\Delta P}{\Delta t} = 82$ bar/min. The resistance sample volume, taking into account its compressibility, was determined to be 2.84×10^{-2} cm^3 at the outset of the upstroke transition. Its resistance increased first slowly during the period of retropressure, then in a much faster rate, changing by several orders of magnitude, as pressure was increased. In Figure 4.2 the measured resistance variation is depicted as a function of the measured volume variation (small circles), during the period of retropressure.

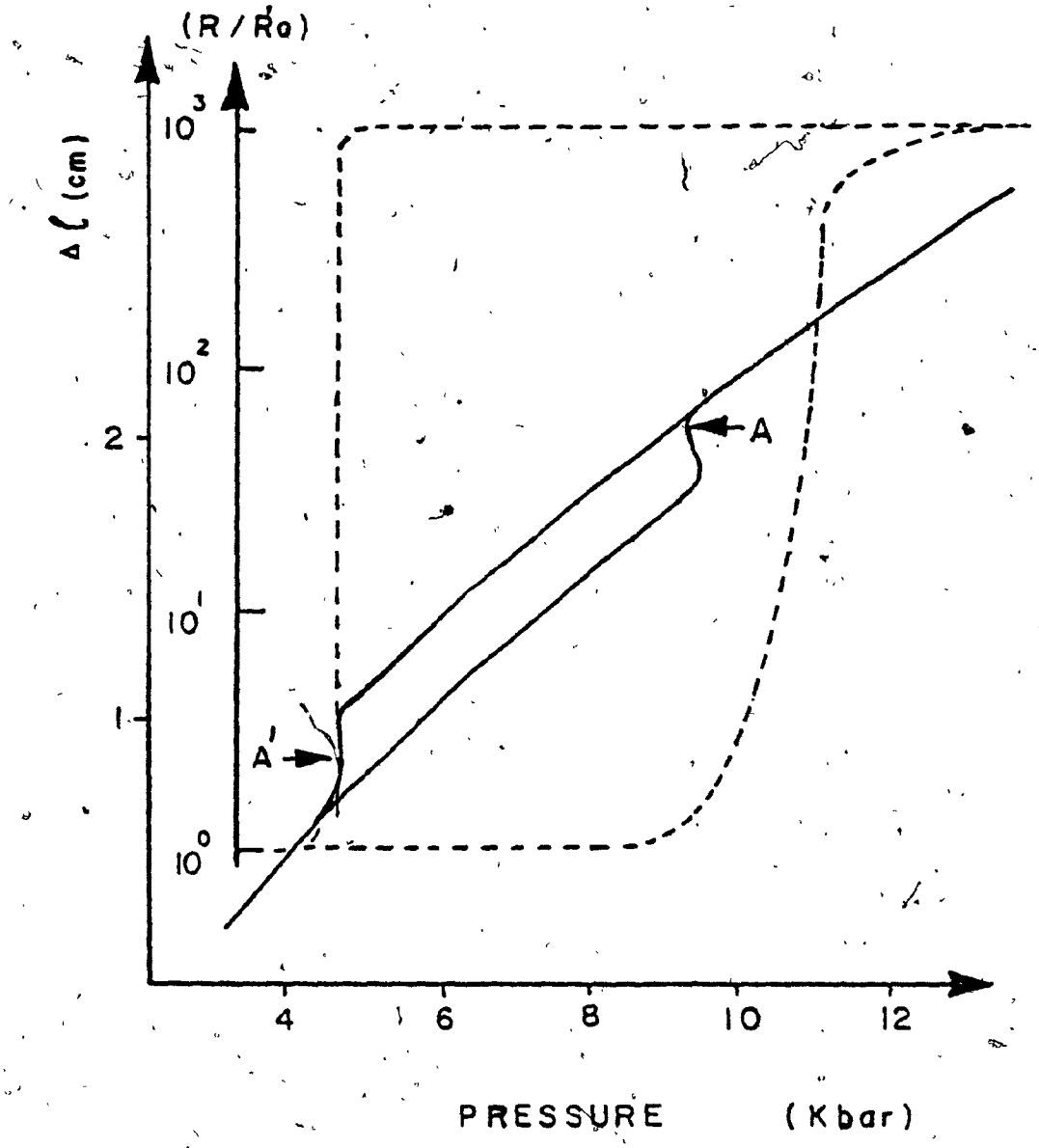

Fig. 4.1 - The experimentally obtained simultaneous variations of the base plate displacement (cm), expressing the volume change due to the polymorphic phase transition in HgSe (solid line) and the relative sample resistance R/R_o (dotted line) as a function of pressure (kbar) in the high pressure chamber.

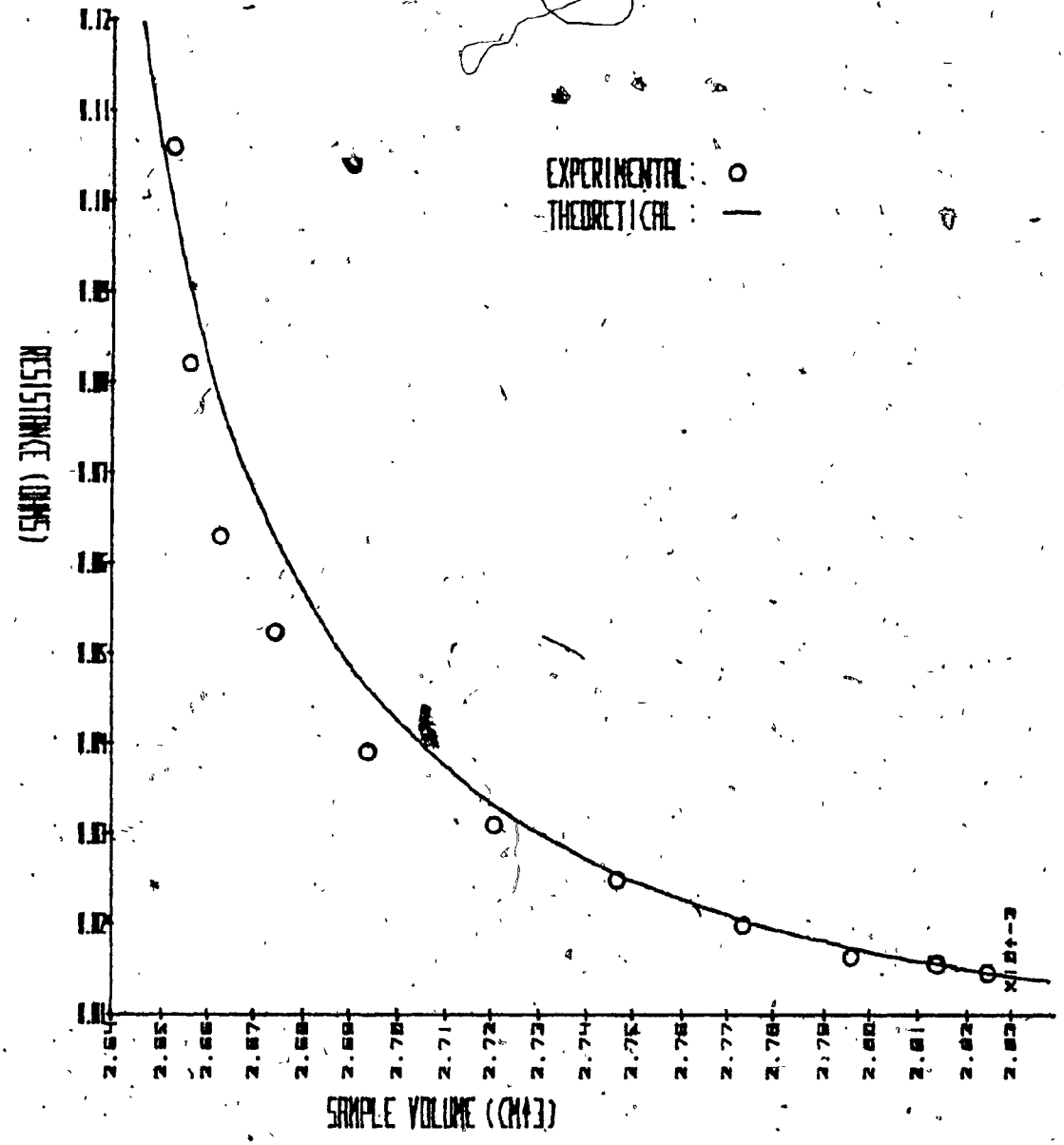

Fig. 4.2 - Sample resistance (Ω) as a function of sample volume , determined experimentally from region A of Fig. 4.1 , (small circles) and computed using equation (5.8),(solid line) in the case of upstroke transition.

The total volume V(t) under pressure as a function of time and the advancement of the reaction α can be given [68,69] as :

$$V(t)=V_L(t) + V_1(t) + V_2(t)$$

$$=V_L[1-B_L P(t)]+V_1[1-B_1 P(t)](1-\alpha)+V_1\frac{D_1}{D_2}[1-B_2 P(t)]\alpha \qquad (4.1)$$

where $V_L(t) = V_L[1-B_L P(t)]$

$V_1(t) = V_1[1-B_1 P(t)](1-\alpha)$

$V_2(t) = V_1 \frac{D_1}{D_2}[1-B_2 P(t)]\alpha$

Then the degree of advancement of the reaction α can be expressed as:

$$\alpha = \frac{\Delta V(t) - (V_L B_L + V_1 B_1) P(t)}{V_1 [(1 - \frac{D_1}{D_2}) + (B_2 \frac{D_1}{D_2} - B_1) P(t)]} \qquad (4.1\text{-a})$$

where $\Delta V(t) = V_L + V_1 - V(t)$ (4.1-b)

Here $P(t)$ is the pressure at time t ; V_L is the volume of the pressure transmitting liquid and V_1 is the volume of the sample, both volumes being at atmospheric pressure. $V_L(t)$, $V_1(t)$ and $V_2(t)$ which are the respective volumes of the liquid, and phase I and phase II of the sample are considered as a function of time during the transition. B_L, B_1 and B_2 are the corresponding compressibilities of the liquid, low and high pressure phases of the sample. D_1 and D_2 are the densities of the low and high pressure phases. They were reported by Kafalas et al. [12] to have the values of 8.239 gr/cm^3 and 8.946 gr/cm^3, respectively. $\Delta V(t)$ is the volume change determined from the measured displacement of the pressure generating base plate as a function of time. The detailed measurements and calculations

of both samples during retropressure are found in Table 4.1 and Appendix B.

4.3 TRANSITION PRESSURES AND NUCLEATION

HgSe in the forms of single and polycrystals as well as powder, did not show any difference in the outset of upstroke and downstroke transition pressures, using the direct resistance measurement technique. However, pressure dispersion was noticed with respect to upstroke transition pressure that had an average value of 9.6 kbar. A similar result was obtained for the downstroke transition pressure with an average value of 5 kbar. In the case of upstroke, transition pressure dispersion of approximately 600.0 bar, and downstroke, of approximately 300.0 bar for single, polycrystals and powder HgSe, were found. In fact, a range of transition pressures of 1.0 kbar was previously noticed and reported for HgSe by Lacam et al.[8], for samples exposed to almost identical conditions.

The results of upstroke and downstroke transition pressures as a function of different nucleation concentrations (by molecular weight percents), are illustrated in Figure 4.3. Each experimental curve contains a set of points detected in the same pressure cycle. The rate of applied pressure $\frac{\Delta P}{\Delta t}$ is varied for each cycle ranging between 10 to 100 bar/min. It can be seen from this figure that the outset of upstroke transition pressure decreased as the number of active centers increased in a non-linear manner and

Table 4.1

Summary of the measured and calculated data for both, the large and small samples during retropressure.

Time (t) min	Volume of large sample $V'(t)$ cm^3	Volume of Resistance sample $V(t) \times 10^{-2}$ cm^3	α	Normalized measured Resistance (Ω)	Calculated sample Resistance (Ω)
0	9.85	2.8	0	0.01	0.0135
1	9.82	2.8	0.046	0.01	0.0145
2	9.76	2.8	0.110	0.02	0.0153
3	9.68	2.8	0.203	0.02	0.0171
4	9.58	2.8	0.321	0.02	0.0199
5	9.49	2.7	0.440	0.02	0.0249
6	9.38	2.7	0.566	0.03	0.0309
7	9.28	2.7	0.673	0.04	0.0430
8	9.23	2.7	0.741	0.05	0.0500
9	9.20	2.6	0.779	0.06	0.0625
10	9.18	2.6	0.799	0.08	0.0760
11	9.17	2.6	0.812	0.11	0.0972
12	9.15	2.6	0.839	0.14	0.1413

The volume of the large sample $V'(t)$ was directly measured as indicated in Appendix B, while that of the small sample $V(t)$ was calculated proportionally to that of $V'(t)$. α is calculated from the measured values of equation (4.1-a). The measured resistance values were obtained directly on the small sample from the experimental chart calculated, using the model of Chapter V.

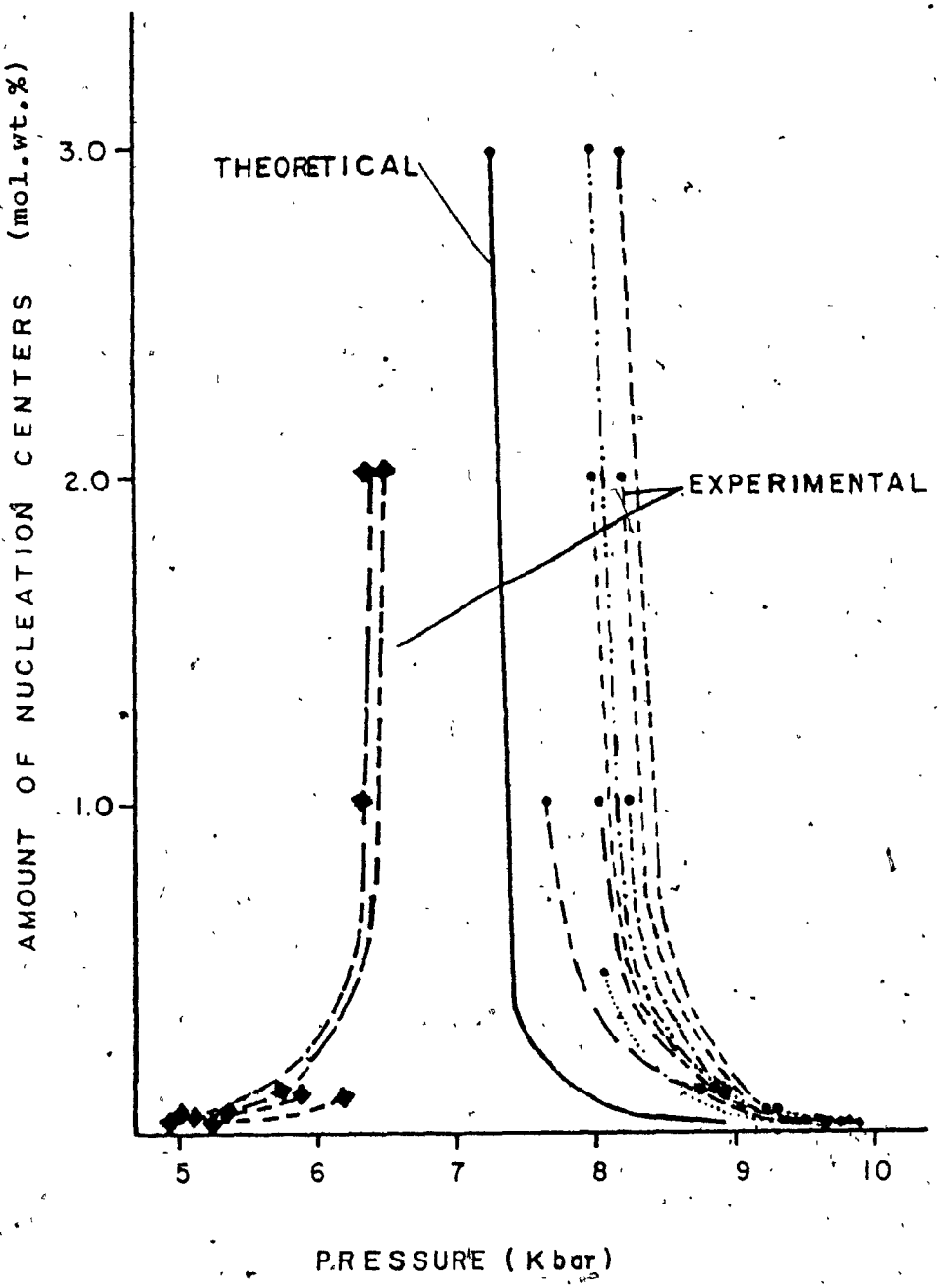

Fig. 4.3 - Upstroke (r.h.s.) and downstroke (l.h.s.) outset of transition pressures (kbar) are plotted as a function of heterogeneous nucleation concentrations (mol.wt.%), (dotted lines). The computed outset of upstroke transition pressures using equation (5.9), (solid line) are also shown. The theoretical curve for the downstroke transition was not computed due to the difficulty of the observation of the retropressure cycle (A of Fig.4.1) needed for the experimental adjustment of the conversion function.

reached saturation. No adiabatic heating effect was observed during these transitions. The start of downstroke transition pressures as a function of nucleation concentrations (shown in Figure 4.3) displayed a very similar behaviour in the opposite direction of transformations.

4.4 DETERMINATION OF THE NUMBER OF NUCLEI IN HgSe CRYSTALS

In a given piece of crystal there are a number of possible imperfections, such as impurities and defects. These points of imperfections can be considered as potential nuclei; when given sufficient energy under pressure, some will reach the critical size and become growth nuclei. This section discusses how to determine experimentally a number that is assumed to be proportional to the number of growth nuclei at the outset of upstroke transition pressure for HgSe.

It is noticed from Figure 4.3 that the outset of upstroke transition pressures were shifting, i.e. the upstroke transition pressure decreased as a function of nucleation concentration. These shifts or changes of transition pressures as a function of nucleation concentration from the normal transition pressures of the non-nucleated HgSe, were decreasing non-linearly up to a nucleation concentration of approximately 1.0 %. Above 1.0 % and up to 3.0 %, no significant transition pressure changes were noticed, due to the saturation effect and hence this region is ignored here. In the non-linear region, the change or difference between transition pressures (ΔP_t)

reached saturation. No adiabatic heating effect was observed during these transitions. The start of downstroke transition pressures as a function of nucleation concentrations (shown in Figure 4.3) displayed a very similar behaviour in the opposite direction of transformations.

4.4 DETERMINATION OF THE NUMBER OF NUCLEI IN HgSe CRYSTALS

In a given piece of crystal there are a number of possible imperfections, such as impurities and defects. These points of imperfections can be considered as potential nuclei; when given sufficient energy under pressure, some will reach the critical size and become growth nuclei. This section discusses how to determine experimentally a number that is assumed to be proportional to the number of growth nuclei at the outset of upstroke transition pressure for HgSe.

It is noticed from Figure 4.3 that the outset of upstroke transition pressures were shifting, i.e. the upstroke transition pressure decreased as a function of nucleation concentration. These shifts or changes of transition pressures as a function of nucleation concentration from the normal transition pressures of the non-nucleated HgSe, were decreasing non-linearly up to a nucleation concentration of approximately 1.0 %. Above 1.0 % and up to 3.0 %, no significant transition pressure changes were noticed, due to the saturation effect and hence this region is ignored here. In the non-linear region, the change or difference between transition pressures (ΔP_t)

of non-nucleated and nucleated samples can be expressed by

$$\Delta P_t = P_t\Big|_{N=N_o} - P_t\Big|_{N=N_{HgS}} \qquad (4.2)$$

Here $P_t\Big|_{N=N_o}$ is the start of upstroke transition pressure of HgSe with the unknown nucleation concentration N_o, and $P_t\Big|_{N=N_{HgS}}$ is the start of upstroke transition pressure of HgSe with the known number of a given nucleation concentration of HgS.

Figure 4.4 shows the points obtained experimentally as the differences in the outset of upstroke transition pressures (ΔP_t), plotted as a function of the logarithm of the number of the corresponding nucleation concentration (log N). A straight line was obtained, based on the average values of ΔP_t for a given concentration, and was extrapolated to zero ΔP_t . The intercept of the extrapolated line with the axis of logarithm N, gave a value of 18.72 with an antilogarithm value for $N_o = 5.31 \times 10^{18}$ cm^{-3}. Hence, the value N_o, obtained at $\Delta P_t = 0$, was assumed to be the number of equivalent nucleation concentration caused by crystal imperfections in HgSe. The nucleation concentration N_o, when compared with the HgSe material concentration, gave a percentage ratio of 0.03 %, as was calculated in Appendix C.

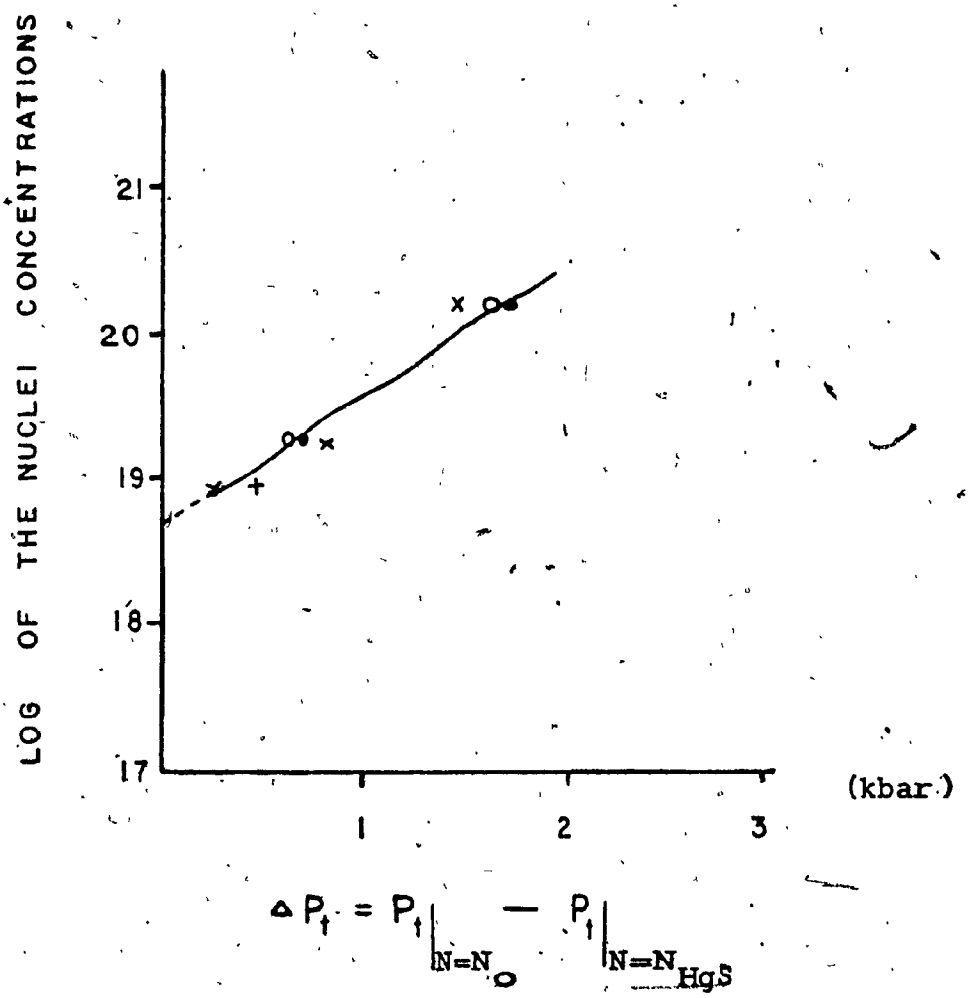

Fig. 4.4 – Plot of the experimentally determined difference at the start of upstroke transition pressure (ΔP_t) versus the log of the nuclei concentrations. Each set of marks represents different samples at the same pressure cycle.

the reaction can then be given by the following expression:

$$\alpha = \frac{V_1\,[1-B_1P(t)] - V(t)}{V_1\,[1 - \frac{D_1}{D_2} + (\frac{D_1}{D_2}B_2 - B_1)P(t)]} \qquad (5.7)$$

where the notations correspond to those defined with respect to equation (4.1). Continuing the development of the conversion function, one has to note that equation (5.5) does not take into account that during the pressure induced phase transition there is a volume change due to the change of crystal structure, which has to be considered. Expressing this volume change of transition with densities of the low and high pressure phases, and taking into account the corresponding compressibilities, equation (5.5) can be written in the following form :

$$R(\alpha) = \frac{\rho_1 V_1[\,1-B_1P(t)] + (\frac{\rho_1^2}{\rho_2} - \rho_1)N''z(\alpha)w(\alpha)[\,1-2B_2P(t)/3](\frac{D_2}{D_1})^{2/3} A}{ZW[1-2B_1P(t)/3]\left[B + \frac{\rho_1}{\rho_2}N''\,z(\alpha)w(\alpha)[\,1-2B_2P(t)/3](\frac{D_2}{D_1})^{2/3}\right]} \qquad (5.8)$$

where $A = L'[1-B_1P(t)/3] - N'\,\ell(\alpha)[1-B_2P(t)/3]\,(\frac{D_2}{D_1})^{1/3}$

and $B = ZW[1-2B_1P(t)/3] - N''\,z(\alpha)w(\alpha)[1-2B_2P(t)/3]\,(\frac{D_2}{D_1})^{2/3}$

Equation (5.8) gives the sample resistance as a function of the advancement of transition, α . The details are developed in Appendix D .

Using equation (5.8), the sample resistance as a function of pressure during the cycle of retropressure is computed. The resulting curve is shown in Figure 4.2. It can be seen that, taking into consideration experimental errors, especially the relatively large series resistance introduced by the electrical feed-throughs, the calculated curve follows satisfactorily the experimental data.

5.3 NUCLEATION DEPENDENCE OF THE OUTSET OF TRANSITION PRESSURE

The outset of transition pressure P_t as a function of nucleation concentration can be derived from equation (5.8), neglecting the small difference between the compressibilities of the low and high pressure phases and letting $P_t = P(t)$ [see Appendix D], as:

$$P_t = \frac{1}{B_1}\left[1-\left\{\frac{\rho_1 V_1+(\frac{\rho_1^2}{\rho_2}-\rho_1)N''z(\alpha)w(\alpha)(\frac{D_2}{D_1})^{2/3}[L-N'\ell(\alpha)(\frac{D_2}{D_1})^{1/3}]}{R(\alpha)ZW[ZW+(\frac{\rho_1}{\rho_2}-1)N''z(\alpha)w(\alpha)(\frac{D_2}{D_1})^{2/3}]}\right\}^3\right] \quad (5.9)$$

The result of the calculation using the last equation is shown in Figure 4.3. It follows satisfactorily the experimentally measured values, taking into account different sample sizes used and different rates of applied pressures. The influence of the latter is not included in this model.

5.4 THERMODYNAMICAL EQUILIBRIUM, ACTIVATION VOLUME AND REACTION KINETICS

Consider a reaction described by the Von't Hoff rule as follows:

$$aA + bB + ... \underset{r_2'}{\overset{r_1'}{\rightleftharpoons}} \ell L + mM + ... \qquad (5.10)$$

where A, B.... etc. are the reactants, L, M.... etc. are the products, and a, b...., ℓ, m.... are the number of moles. If the rate of transformation from one form to the other (r_1') is equal to the rate of the reverse transformation (r_2'), then the system is said to be in equilibrium.

When two phases of a crystal are in equilibrium, the thermodynamic potentials of the two phases are equal, that is:

$$U_1 - TS_1 + PV_1 = U_2 - TS_2 + PV_2 \qquad (5.11)$$

where the symbols are the usual symbols used in thermodynamics and the subscripts 1 and 2 represent the low and high pressure phases, respectively. Based on equation (5.11), Jacobs [71] derived an expression to calculate the equilibrium pressures of the polymorphic phase transitions in metallic halides. He suggested that the temperature terms in isothermal pressure analysis can be neglected. The expression is in the form of :

$$P = \frac{E_2(r) - E_1(r)}{V_1 - V_2} \qquad (5.12)$$

where $E_1(r)$ and $E_2(r)$ are the lattice energies and V_1 and V_2 are the volumes of the respective phases. According to the absolute rate theory [17], if temperature is employed as the thermodynamical variable, the energy change during a reaction will follow the path schematically depicted in Figure 5.2-A. Thus, during the reaction, the reactants with initial energy (E_1) must gain an energy of activation (E_a) greater than that of either the reactants (E_1) or the products (E_2). The change in internal energy of the system or the heat of reaction (ΔE), is given by

$$\Delta E = E_1 - E_2 \qquad (5.13)$$

When pressure is employed as the thermodynamical variable, an analogous concept to that of "activation energy" is encountered and is called the "activation volume". Figure 5.2-B clearly illustrates a sample volume path during the polymorphic phase transition, where crystal volumes for the stable low pressure state (V_I), transition state ($V^{\#}$) and the stable high pressure state (V_{II}) are indicated. Thus, during the pressure induced polymorphic phase transition, the system with an initial volume (V_I) has to pass through the transition state characterized by its volume of $V^{\#}$ (representing only a small fraction of the material) to be able to reach the final volume (V_{II}), [see Appendix F].

The activation volume ($\Delta V^{\#}$) or the volume change between the initial state (V_I) and the transition state ($V^{\#}$)

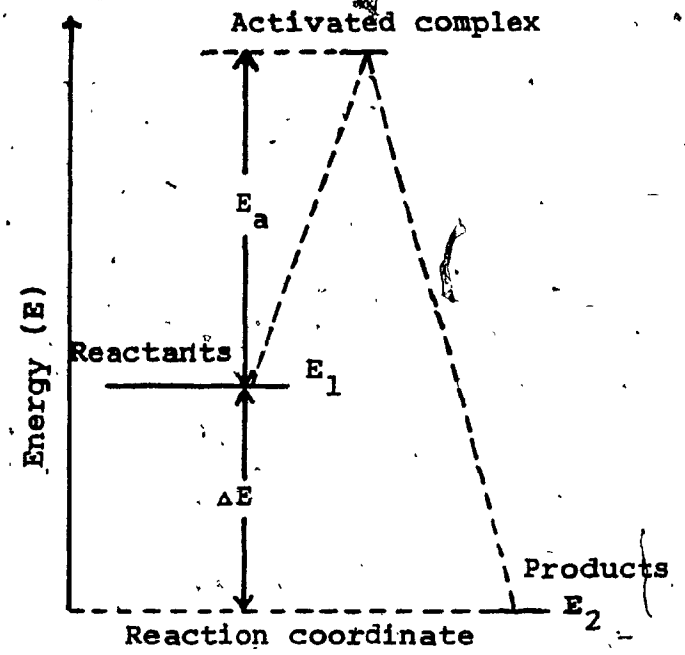

Fig. 5.2-(A) - Energy path and states within the course of a reaction showing the activation energy E_a for temperature induced reaction.

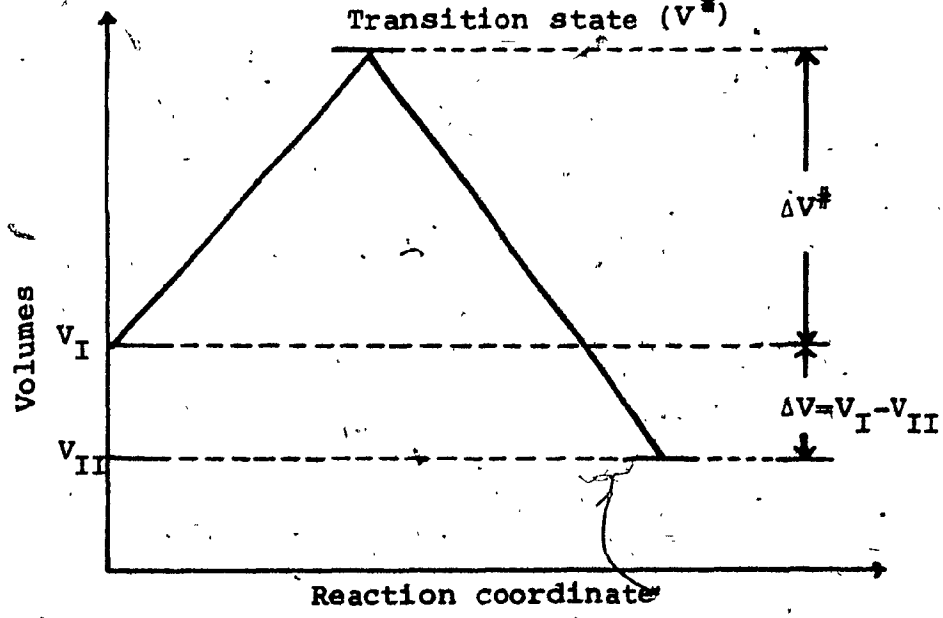

Fig. 5.2-(B) - Polymorphic volume path within the course of a reaction showing the activation volume $\Delta V^{\ddagger}$ for pressure induced reaction.

as defined by Evans and Polanyi [17] is given by :

$$\Delta V^{\ddagger} = V^{\ddagger} - V_I \qquad (5.14)$$

No confusion should arise between this volume change, i.e. the activation volume ($\Delta V^{\ddagger}$), with the change of volume between the initial state (V_I) and the final state (V_{II}). The latter has been established experimentally in the case of HgSe to be 8.29 % of the original volume at atmospheric pressure, and can be expressed symbolically as:

$$\Delta V = V_I - V_{II} \qquad (5.15)$$

Thermodynamics can predict only the feasibility of a reaction, but are not concerned with the reaction process itself. On the other hand, the mechanism of a reaction based on the kinetic data involves steps so as to provide how events occur as a function of time.

Therefore, the principal experimental approach to study the reaction process is to measure the rate of change of species when a reaction proceeds, and the dependence of this reaction rate on the concentrations of the reacting species and on pressure and/or temperature.

5.5 ACTIVATION VOLUMES AND RATES OF TRANSITIONS

The rate of transformation characterizes the change in material concentration per unit time. The rate equation

describing the behaviour of the reaction depends on the order of the reaction. The latter is strictly an experimental quantity and merely provides information about the way which the rate depends on concentration. The reaction of the pressure induced polymorphic phase transitions in mercury chalcogenides has been shown to be of first order [7]. Thus, the rate equation can be written as:

$$\text{Rate} = \frac{d\ \Delta V(t)}{dt} = r' \Delta V(t) \qquad (5.16\text{-a})$$

where r' is the rate constant, and $\Delta V(t)$ is the change of volume as a function of t [see Appendix E].
From equation (5.16-a), the rate constant can be given as:

$$r' = \frac{d\ \Delta V(t)}{\Delta V(t) dt} \quad (\text{sec}^{-1}) \qquad (5.16\text{-b})$$

Since this is a first order reaction, the unit of the rate constant is sec^{-1}. Data for $\Delta V(t)$ can be obtained using the direct resistance measurement technique. The change in resistance is measured on the sample and transformed into the corresponding change of volume using the model developed in this Chapter.

Activation volume $\Delta V^{\#}$ is the difference in volume between the transition state and the reactants. In the case of solid-solid phase transitions, where only the low and high pressure phases with the transition state V_I, V_{II} and $V^{\#}$ are present, no solvent effect has to be considered. However, in the case of kinetic studies in solutions, the role of the solvent and its rearrangement during the transition results

in a much more complex system as discussed by Evans and Polanyi [17], and is not the subject of this investigation.

It has been a common practice to analyze experimental results of transitions on the basis of the Van't Hoff equation, in the form which was first introduced, using the transition state theory developed by Evans and Polanyi [17]. Thus, the expression relating the rate constant of the pressure induced phase transition (r') to $\Delta V^{\#}$, is

$$\frac{d \ln r'}{dP} = - \frac{\Delta V^{\#}}{R' T} \qquad (5.17\text{-a})$$

where R' is the gas constant and T is the absolute temperature. Thus, the activation volume at room temperature from equation (5.17-a) is given as:

$$\Delta V^{\#} = -R' T \frac{d \ln r'}{dP} = -24.205 \times 10^3 \frac{cm^3 \ atm}{gr\text{-}mole} \frac{d \ln r'}{dP} \qquad (5.17\text{-b})$$

It is evident from equation (5.17-b) that the activation volume depends on the rate constants and the pressure variations. The rate constants and the pressure variations are in turn dependent upon the nucleation concentration, as is shown by the experimental results (see Chapter IV), and their kinetic interpretation (see the following Chapter).

5.6 REACTION MECHANISM BASED ON THE THREE-DIMENSIONAL HETEROGENEOUS MODEL

Following up the assumptions stated at the beginning of this Chapter, some of the potential nuclei existing in a sample must acquire sufficient atoms or molecules to reach

their critical size before they start to grow. Hence, in the case of the upstroke transition, phase II is assumed to grow geometrically in three-dimensional cubes with a number of nuclei within phase I. Furthermore, as the reaction proceeds, the total volume of phase II increases, while that of phase I decreases. It is therefore necessary to deduce equations to express both volumes as a function of time during the reaction. The total volumes of the growth nuclei in phase II at any time will constitute the volume of the high pressure phase, $V_2(t)$, and hence:

$$V_2(t) = N' \ell(\alpha) N'' z(\alpha) w(\alpha) \qquad (5.18)$$

where $\ell(\alpha)$, $w(\alpha)$ and $z(\alpha)$ are the length, width and thickness of a cubic nucleus (see p. 80).

The volume of the low pressure phase is then expressed [Appendix E] as :

$$V_1(t) = V_I - V_2(t) \frac{D_2}{D_1} \qquad (5.19)$$

where V_I is the volume of the low pressure phase at the outset of the upstroke transition and the rest of the symbols carry the same meanings as before. The total volume of the sample as a function of time will consist of the sum of $V_1(t)$ and $V_2(t)$, as given previously in equation (5.6), that is:

$$V(t) = V_1(t) + V_2(t)$$

$$= V_1[1-B_1P(t)](1-\alpha) + V_1 \frac{D_1}{D_2}[1-B_2P(t)]\alpha$$

The last equation satisfies the boundary conditions for the volume of a sample before, during and after transition, therefore :

a) at the outset of upstroke transition pressure

$t = t_o = 0$, $\alpha = 0$, $V_2(t_o) = 0$, hence

$$V(t_o) = V_1(t_o) = V_I$$

b) after the transition is completed

$t = t_f$, $\alpha = 1$, $V_1(t_f) = 0$, hence

$$V(t_f) = V_2(t_f) = V_{II}$$

The initial volume of a sample at the outset of upstroke transition pressure (V_I) is equal to the sum of the volume of the sample during transition, $V(t)$, plus the accompanied volume change $\Delta V(t)$, [Appendix E]. This can be re-expressed as :

$$\Delta V(t) = V_I - V(t) \qquad (5.20)$$

Substituting equation (5.6) into (5.20), one obtains

$$\Delta V(t) = V_I - [V_1(t) + V_2(t)] \qquad (5.21)$$

which is the volume variation accompanying the pressure induced polymorphic phase transition. Experimentally, $\Delta V(t)$ is determined from the directly measured change of sample resistance using equation (5.8) and normalizing

to a unit volume of 1.0 cm^3 (see the following Chapter). The rate of change of this volume characterizes the rate of transition as in equation (5.16-a), i.e.

$$\text{Rate} = \frac{d\,\Delta V(t)}{dt} = r'\,\Delta V(t)$$

Since the degree of advancement of the reaction (α) is by definition a parameter that measures the amount of material transformed with respect to the available material, it can be easily expressed according to this model [see Appendix E] as :

$$\alpha = \frac{V_2(t)\; D_2/D_1}{V_I} \qquad (5.22)$$

Although this model is simple enough to explain the kinetics and the mechanism of phase transition in HgSe under pressure, showing a good agreement with the experimental data, it is only valid for 86.0 % of the reaction, as indicated in Table 5.1. The last part of the transition, that is just before completion, might involve ingestion [62], i.e. overlapping of many of the growth nuclei among themselves. This phenomenon is not investigated in this work.

The numerical differences between the two values of α, using equations (5.7) and (5.22) are given in Table 5.1, which obviously are not very significant.

Table 5.1

The degree of advancement of the reaction α obtained separately from equation (5.7) and from equation (5.22).

Time(t) min	α using eq.(5.7)	α using eq.(5.22)
0	0	0.057
1	0.048	0.057
2	0.112	0.104
3	0.205	0.182
4	0.323	0.276
5	0.441	0.391
6	0.566	0.502
7	0.673	0.617
8	0.741	0.654
9	0.780	0.712
10	0.802	0.762
11	0.816	0.810
12	0.845	0.860

The verification of the evaluated α's (equation 5.7) based on the experimental data of Figure 4.1, and the calculated α's (equation 5.22) used to fit the complete model. The rate of applied pressure in this experiment as stated before was 82 bar/min.

CHAPTER VI

ANALYSIS OF THE EXPERIMENTAL RESULTS

6.1 INTRODUCTION

The purpose of this Chapter is to analyze the experimental data based on the developed model. The results of the direct resistance measurement technique will be compared with the results of the conventional indirect volumetric measurement technique. Furthermore, the analysis includes the experimental values of the activation volumes as a function of nucleation concentration and other related data.

6.2 COMPARISON OF THE DIRECT ELECTRICAL WITH THE INDIRECT VOLUMETRIC TECHNIQUES

The conventional volumetric measurement technique for the solid-solid polymorphic phase transition, as was pointed out earlier, requires large sample volumes, i.e. in the range of 20 % of the usable chamber volume. Such a requirement is essential in order to enable one to analyze the transition satisfactorily. If the applied rate of pressure ($\Delta P/\Delta t$) is kept constant, the volume reduction of the sample due to the transformation causes pressure reduction in the chamber. This pressure reduction is propagated by means of the liquid pressure transmitting medium and is detected by the manganin coil resistance.

Although the pressure detection was sentitive to ±1.0 bar, as indicated in Appendix A-II , the measurements are considered:

1) Indirect, since the solid volume variation is being detected through the liquid by pressure variation.
2) Cannot be relied on for rate measurements due to liquid relaxation time interference.
3) Do not provide information for activation volume, since it depends on rate measurements at constant pressures.
4) The pressure rate inside the chamber during transition cannot be kept constant despite the fact that the applied pressure rate can be constant. This is because of the large sample volume variation during the period of retropressure.
5) The slope of the indirectly measured volume change during the retropressure includes volume variations of the solid due to its transition and of the liquid due to its compressibility. Furthermore, for most of the reaction (up to $\alpha \approx 0.8$), the volume variation due to the solid transition is much larger than the volume variation of the liquid due to compressibility and hence the former dominates the latter. However, near the end of the reaction ($\alpha > 0.8$) the volume variation of the solid is difficult to obtain. This is because the volume variation of the solid becomes smaller and smaller, comparable to the volume variation of

the liquid, and hence it is difficult to measure the former precisely.

The volumetric technique, however, provided plenty of information concerning transformations of many materials under various pressure ranges and their related compressibilities. It is also important to remember that the great work of Bridgman was based on this technique.

The electrical or resistance measurement technique, on the other hand, proved to be very fruitful; in addition to the fact that it can provide information on the band structure of the material, it requires only small sample volumes (less than 10^{-3} of the usable chamber volume). Its transition measurement is direct, with a resistance change by four or five orders of magnitude. The concept of this technique is not unknown, but the elucidation, the reaction mechanism interpretation and relation to the transformation were well explained by the heterogeneous model presented in this work.

Furthermore, from the practical point of view, if for example one desires to measure the influence of various nucleation concentrations on transition pressures (as has been done as part of this investigation with the results given in Chapter IV), employing the volumetric measurement technique, the amount of material needed would be enormous. The total volume change during

transition in the volumetric technique is less than one order of magnitude as compared to that of several orders of magnitude for the direct technique.

6.3 RESISTANCE VARIATION AND ACTIVATION VOLUMES

The resistance variation of a sample under pressure can only be noticed at and above the outset of the upstroke transition pressure. This is determined experimentally from the simultaneous volumetric and resistance measurements, summarized in Figure 4.1. It was stated earlier that the detection resolution was about $\pm$ 2 mΩ (see Appendix A-III) in this investigation. No noticeable resistance change was observed until transition actually took place. The resistance change depicting the polymorphic phase transformation started first by increasing slowly for a few minutes (during retropressure), and then at a faster rate to several orders of magnitude. Figure 6.1 shows a plot of typical experimental data for the resistance of HgSe which began to change during the first few minutes of the transformation with an applied pressure rate $\Delta P/\Delta t$ of 80 bar/min. It is this portion of the resistance change that determines the activation volume of the material and its transformation rates.

The following steps are taken to determine the rate constants of transition, i.e. a normalized partial volume change $d\,\Delta V(t)/\Delta V(t)$ within a given interval of time dt (usually one

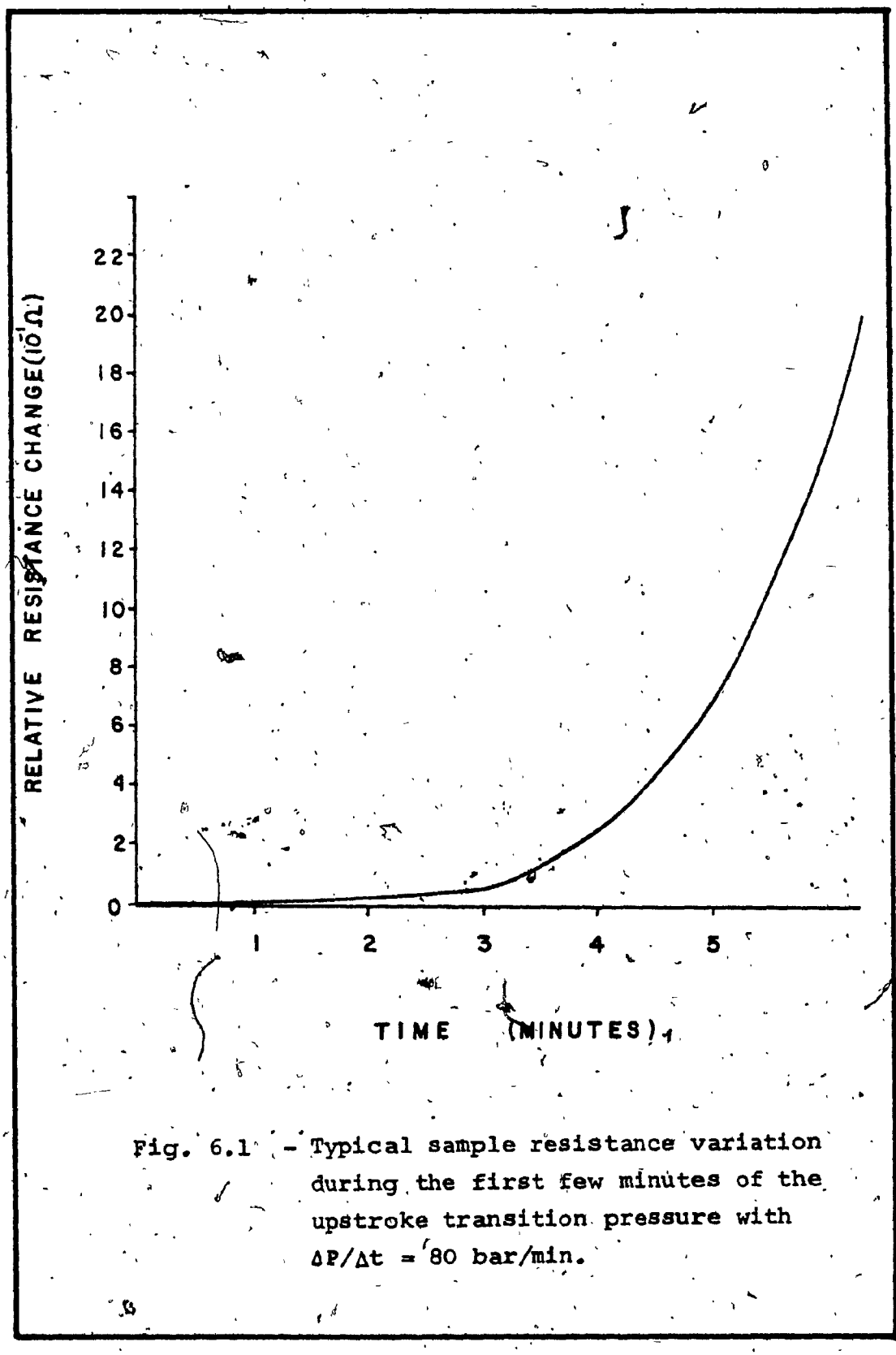

Fig. 6.1 - Typical sample resistance variation during the first few minutes of the upstroke transition pressure with $\Delta P/\Delta t = 80$ bar/min.

minute), as a function of α, at a particular pressure :

1) The resistance value of a sample with a given nucleation concentration N is measured at the beginning of the time interval dt.
2) The conversion function, i.e. equation (5.8) as a function of α, is used to calculate a resistance value identical to that of the measured value.
3) The values used for the length $\ell(\alpha)$, the width $w(\alpha)$ and the depth $z(\alpha)$ of a growth nuclei, to evaluate step (2) at the given nucleation concentration N of step (1), serve to determine $V_2(t)$ in equation (5.18).
4) The volume of the low pressure phase $V_1(t)$ of equation (5.19) is calculated by using the obtained value of $V_2(t)$ of equation (5.18).
5) The total volume V(t) of the low pressure phase $V_1(t)$ and the high pressure phase $V_2(t)$ is obtained by employing equation (5.6).
6) $\Delta V(t)$ of equation (5.20) is evaluated by using the value acquired for V(t) from step (5), and then normalized to a sample of a unit volume of 1.0 cm^3; that is, to calculate a corresponding $\Delta V(t)$ for a sample of 1.0 cm^3.
7) The steps (1) through (6) are repeated for another value of $\Delta V(t)$, except that this time the resistance measurement of step (1) is performed at the end of the time interval dt.

8) Thus, a value of $\frac{d\Delta V(t)}{\Delta V(t)dt}$ is acquired for the transition rate constant of equation (5.16-b) at a given pressure.

By iterating the above procedure at different pressures (during the first few minutes of transition), several values for $\frac{d\Delta V(t)}{\Delta V(t)dt}$ are obtained. Plotting the natural logarithm of these values versus pressure, a straight line is constructed, using the least square method. These results are shown in Figure 6.2 for a non-nucleated ($N=5.3\times10^{18}$ cm^{-3}) HgSe sample. The activation volume, as defined in equation (5.17-b), is then easily determined by measuring the slope of the line and multiplying it by $-RT$. The obtained value is the difference in partial molar volume between the transition state and the initial state (reactants).

6.4 NUCLEATION CONCENTRATIONS, TRANSITION RATES AND ACTIVATION VOLUMES

Using the technique described in section 6.3, the transition rate measurements of samples containing different amounts of nucleation concentrations of HgS (0.05 %, 0.1 %, 1.0 % and 3.0 %), in the case of the upstroke transitions were performed. The results which displayed different transition rates for the different nucleation concentrations are summarized in Figure 6.3. In this figure, it is clear that the rate linearly increases as the logarithm of the nucleation concentration decreases. A straight line was fitted using the least square method on a Hewlett Packard

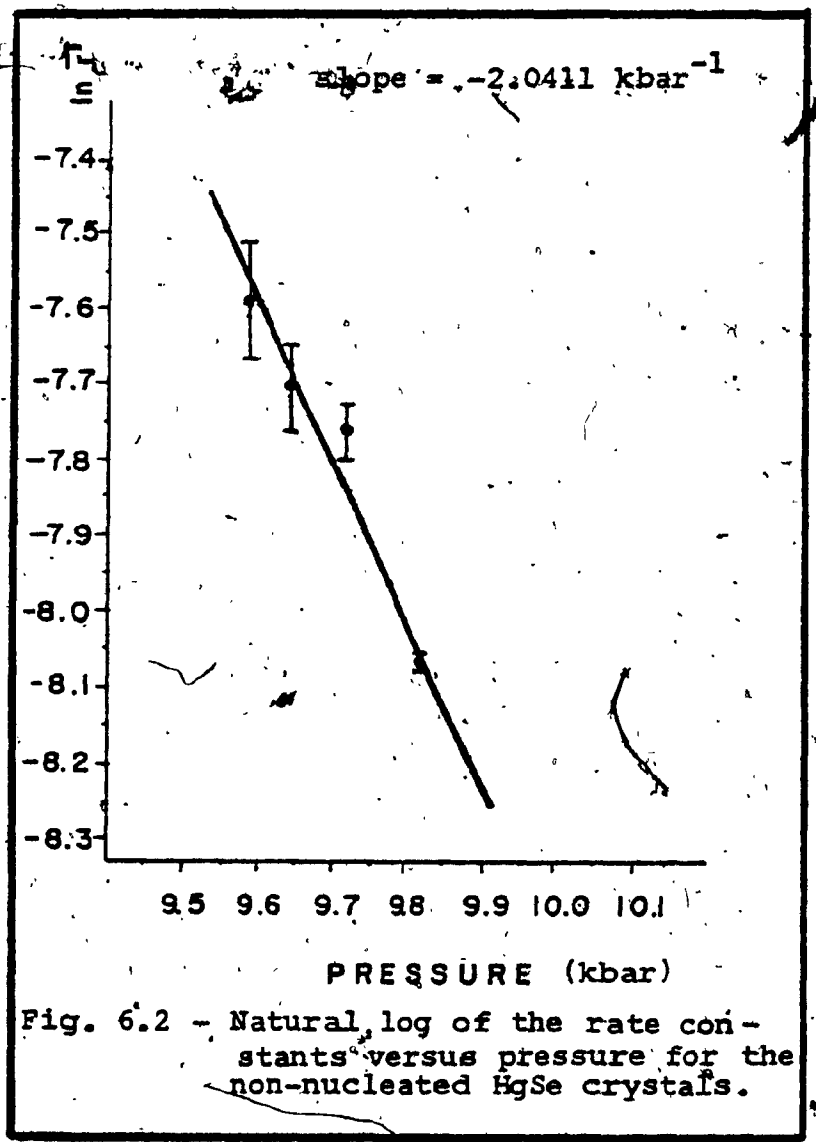

Fig. 6.2 - Natural log of the rate constants versus pressure for the non-nucleated HgSe crystals.

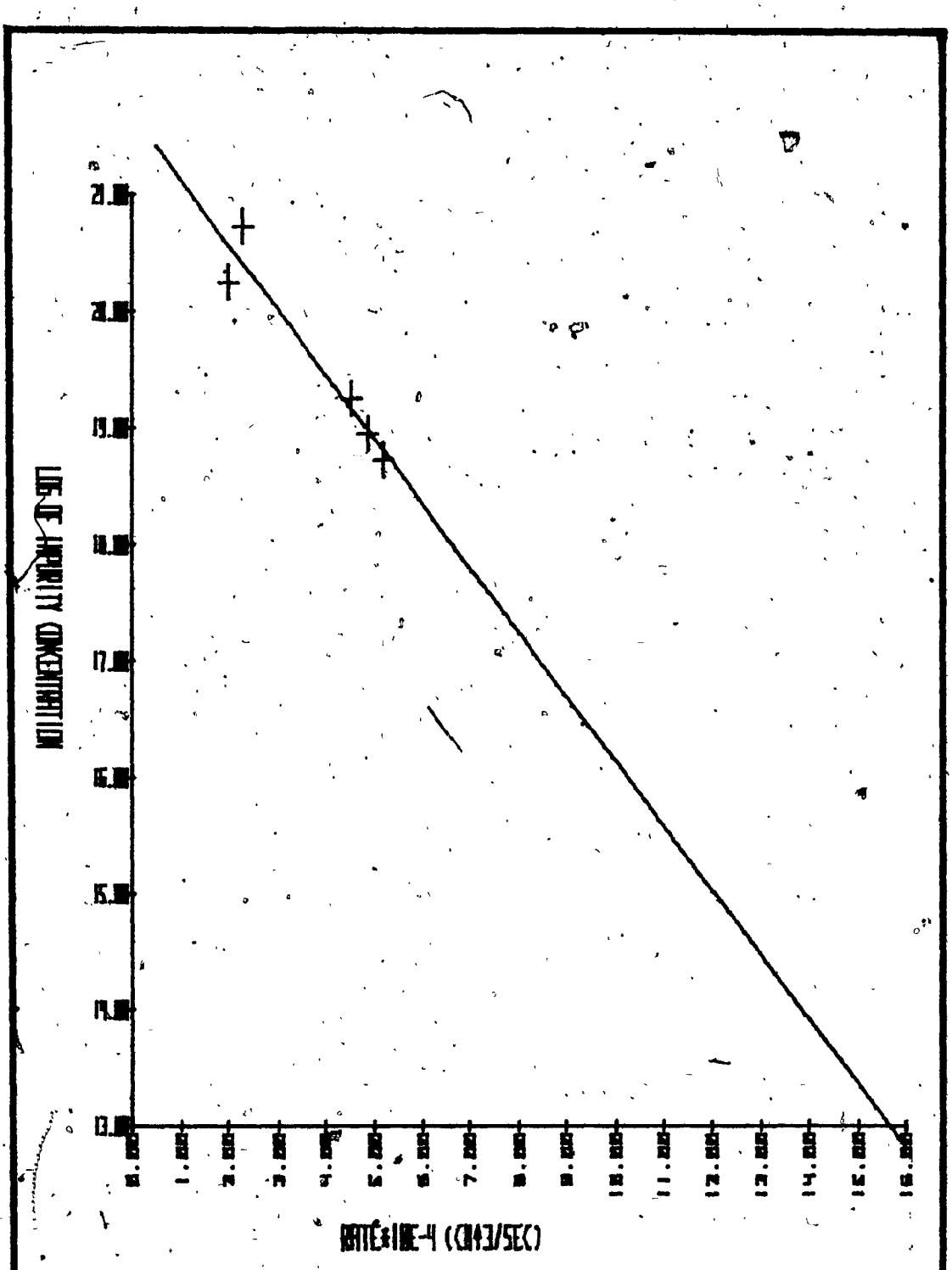

Fig.6.3 - The log of impurity (nucleation) concentration versus the measured transition rates, where the former is extrapolated to a concentration of $10^{13} cm^{-3}$.

Minicomputer Model 9830 A. This line, however, when extrapolated as in the figure to a low semiconductor grade impurity concentration (1 p.p.b.), i.e. an impurity concentration of $10^{13} cm^{-3}$, gave a corresponding transition rate of 1.56×10^{-3} cm^3/sec. This extrapolated transition rate was done for the purpose of comparison with the measured transition rates of the annealed samples, which will be discussed later.

The activation volumes for the nucleated samples were also determined as a function of nucleation concentration following the steps given in section 6.3. The experimental points which determined the activation volumes were collected and plotted as follows:

1) Figure 6.4 shows the logarithm of the rate constant as a function of pressure for a sample with 0.05 % nucleation concentration.
2) Figure 6.5 is similar to Figure 6.2, except that it is for a sample with 0.1 % nucleation concentration.
3) Figure 6.6 is similar to Figure 6.2, except that it is for a sample with 1.0 % nucleation concentration.
4) Figure 6.7 is similar to Figure 6.2, except that it is for a sample with 3.0 % nucleation concentration.

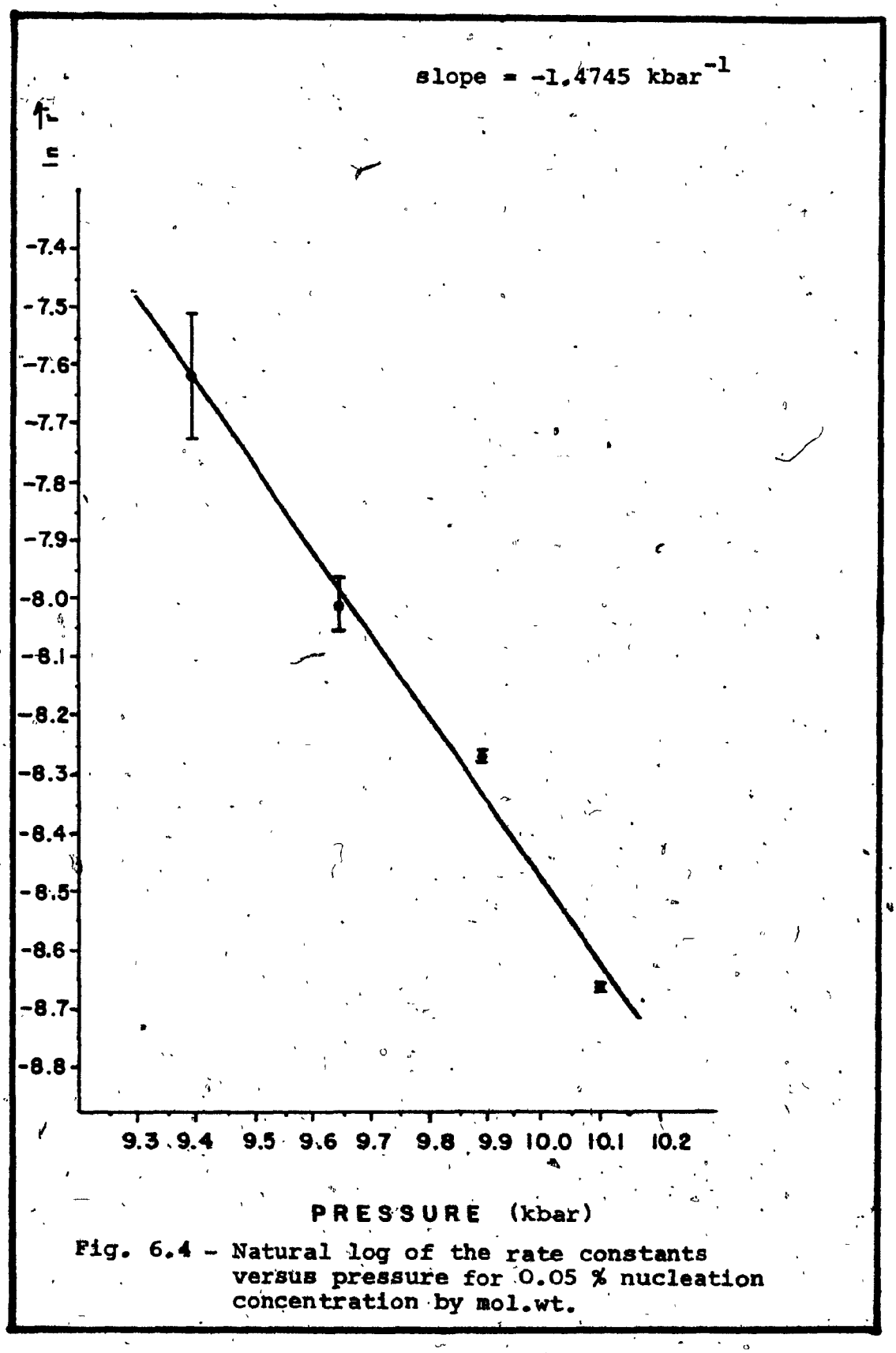

Fig. 6.4 - Natural log of the rate constants versus pressure for 0.05 % nucleation concentration by mol.wt.

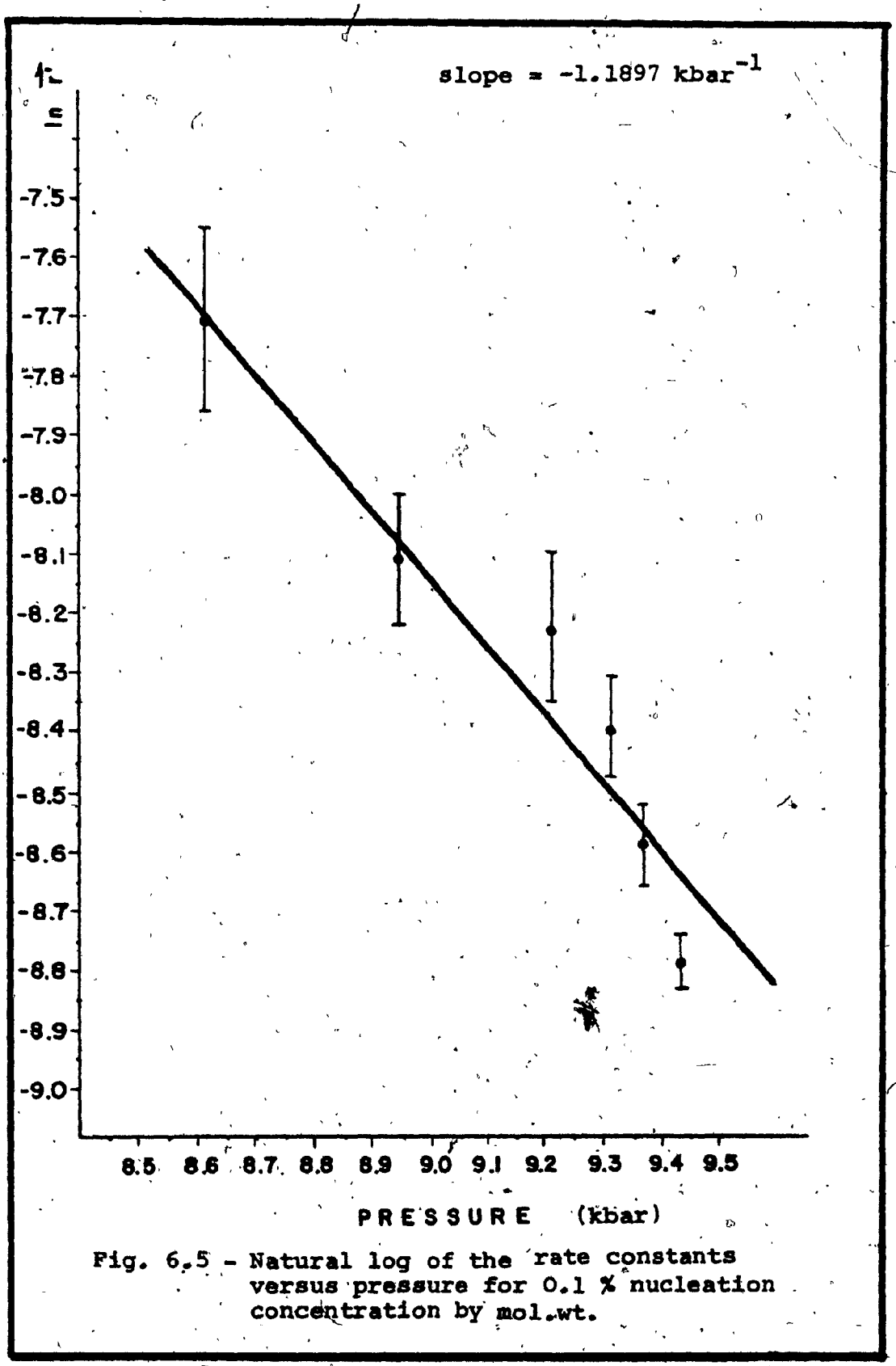

Fig. 6.5 - Natural log of the rate constants versus pressure for 0.1 % nucleation concentration by mol.wt.

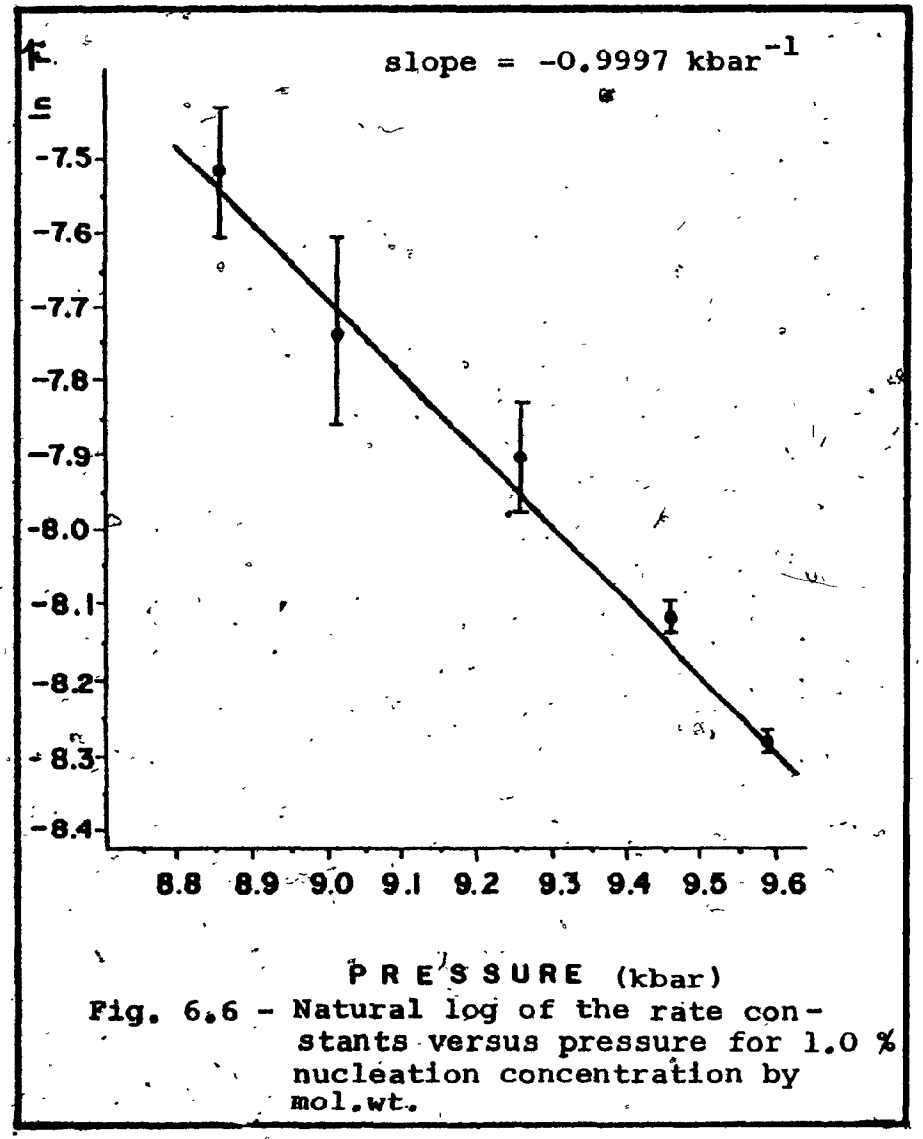

Fig. 6.6 - Natural log of the rate constants versus pressure for 1.0 % nucleation concentration by mol.wt.

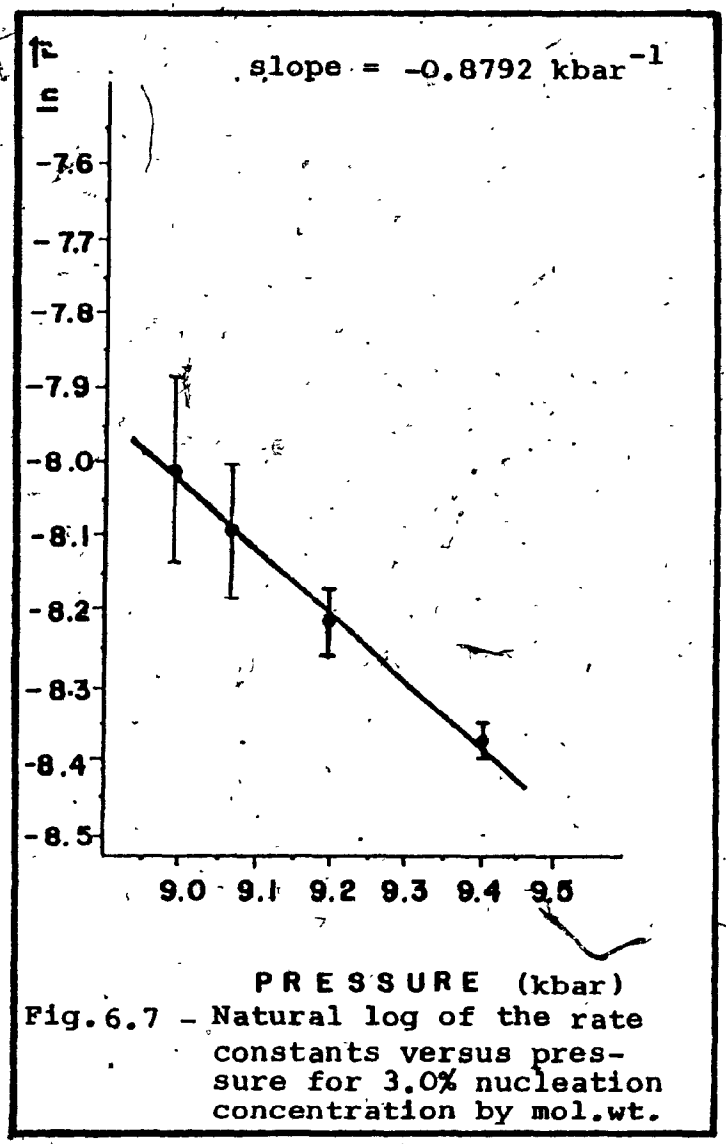

Fig. 6.7 - Natural log of the rate constants versus pressure for 3.0% nucleation concentration by mol.wt.

The obtained data, i.e. activation volumes, outset of upstroke transition pressures, their rate of transitions during the first one minute, and the corresponding nucleation concentrations are summarized in Table 6.1.

Reading small resistance values and more important their very small variations, within a time interval (dt) at the beginning of the transition, from the experimental charts, involved uncertainty in the reading precision. Therefore, it was necessary to determine the range of uncertainty for all the resistance values and their corresponding volume values used to determine Figures 6.2, 6.4, 6.5, 6.6 and 6.7. This uncertainty was taken to be the chart resistance reading resolution of ±2 mΩ. Thus, each resistance value read from the chart was considered as the mean value with possible deviation values (uncertainties) of ± 2 mΩ . The corresponding mean and deviated volume values were calculated, each as specified in section 6.3. The uncertainty ranges determined for the volume values and hence for the transition rates, are indicated for all the experimental points in the above-mentioned figures.

It can be seen from the data given in Table 6.1 and the above-mentioned figures that the amount of nucleation concentration affects the activation volume of transition directly. Thus, the higher the number of nucleation concentration in the material, up to the saturation

Table 6.1

Kinetic data experimentally obtained for different amounts of nucleation concentrations

Nucleation Concentration			Activation Volume $\Delta V^{\ddagger}$ $\left(\frac{cm^3}{gr\ mole}\right)$	Upstroke transition pressure P_t (kbar)	Rate of transition at its outset ($\times 10^{-4}\ \frac{cm^3}{sec}$)
(% mol.wt.)	$\frac{molecules}{cm^3}$	$\frac{nuclei}{cm^3}$ [7]			
0.03	5.3×10^{18}	4140	50 ± 7	9.67	5.21
0.05	8.8×10^{18}	6875	36 ± 3	9.21	4.86
0.1	1.8×10^{19}	14063	29 ± 2	8.91	4.54
1.0	1.8×10^{20}	140629	24 ± 3	8.32	2.02
3.0	5.3×10^{20}	414075	21 ± 5	8.25	2.28

[7] size of nucleus $(40\ \mu m)^3$

concentration of 3.0 %, the lower the activation volume needed for the transition to proceed.

6.5 TRANSITION PRESSURES AND ACTIVATION VOLUMES

Figure 6.8 displays the outset of upstroke transition pressures versus activation volumes of HgSe with different amounts of nucleation concentrations, as given in Table 6.1. These experimental points were plotted, and using the least square method, were fitted to a straight line and extrapolated to zero activation volume. The purpose of this extrapolation was to attempt the determination of the thermodynamic equilibrium pressure. However, due to the measurements' errors of the activation volumes, the intercepts with the pressure axis gave values between 7.22 - 7.26 kbar. These values are comparable with the theoretically determined value of 7.28 kbar, using equation (5.9) with the saturation nucleation concentration of 3.0 %. All these values fall well within the hysteresis curves published in the literatures [12,13,16,72], but are lower than the ones calculated from the lattice energies by Lombos et al. [15].

The outset of transition pressure P_t can be defined as

$$P_t = P_{th} + P_k \qquad (6.1)$$

where P_{th} and P_k are the nucleation independent thermodynamic equilibrium pressure and nucleation dependent kinetic pressure, respectively. Thus, if the pressure

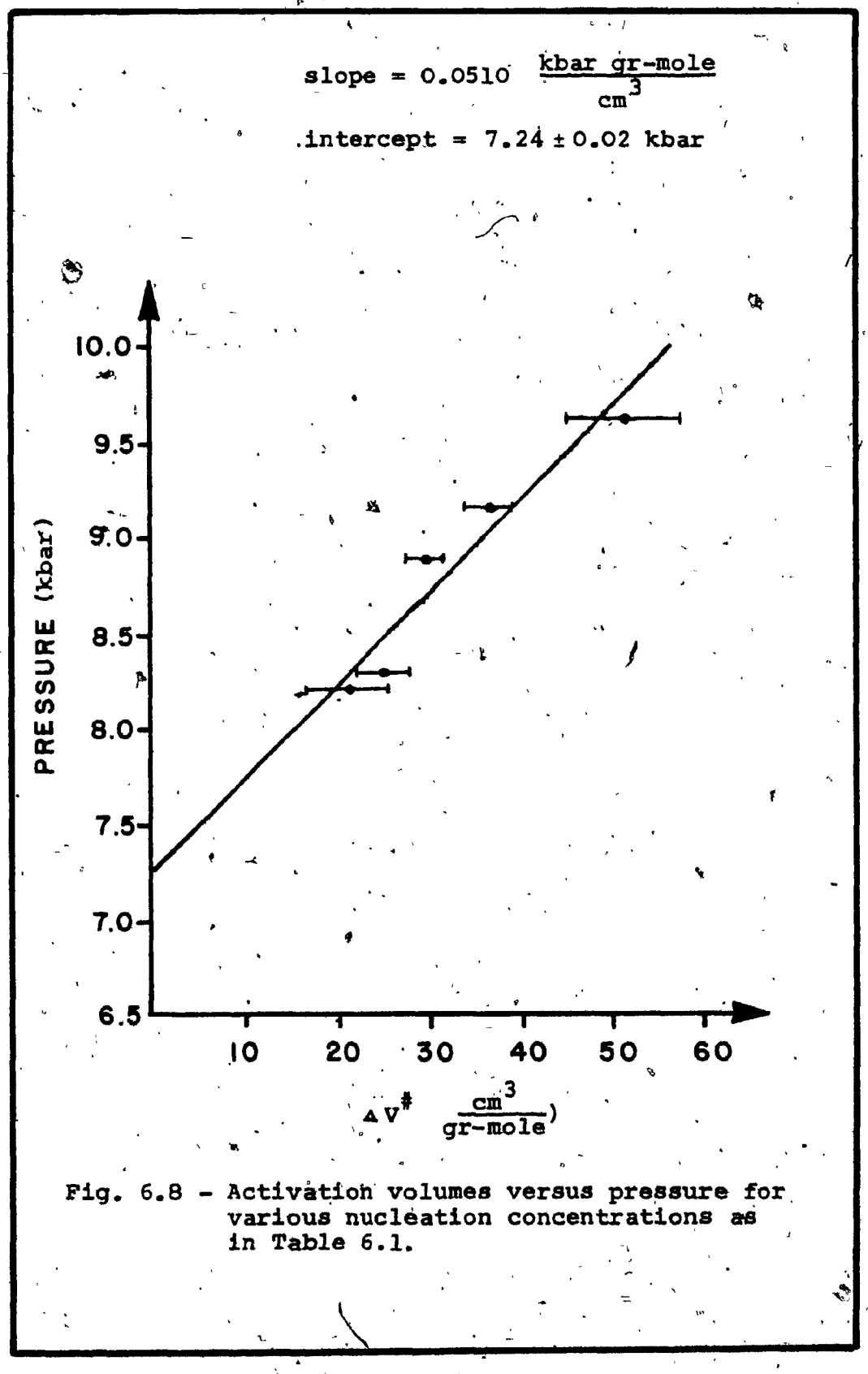

Fig. 6.8 - Activation volumes versus pressure for various nucleation concentrations as in Table 6.1.

induced polymorphic phase transition is associated with a zero activation volume, then the kinetic pressure needed is also zero. In this case the transition pressure is equal to the thermodynamic equilibrium pressure. Furthermore, as the activation volume is increased (as a function of decreasing nucleation concentration), the kinetic pressure is also increased, thus increasing the required transition pressure. This argument is consistent with the measured data of Table 6.1.

6.6 TRANSITION RATE MEASUREMENTS WITH ANNEALED MERCURY SELENIDE CRYSTALS

Brebrick and Strauss [10] reported that the amount of carrier concentration increased when annealing HgSe crystals with saturated Hg or Se. Similar results were obtained by Rodot [73] by annealing HgTe crystals with saturated Hg or Te. However, HgSe annealed in vacuum at 240°C, reduced the carrier concentration from 4×10^{18} to 1.4×10^{17}, as published by Blue and Kruse [46]. Lehoczky et al. [35] measured the decrease of impurities of HgSe annealed in vacuum under different conditions (time and temperature). In the present investigation, the vacuum annealed samples of HgSe revealed faster transition rates than the non-annealed samples, indicating that annealing in a vacuum decreased the number of nuclei in these samples, substantiating the previous observations [35,46].

In the case of the upstroke transitions for the various nucleation concentrations, the measured rates, normalized to a sample volume of 1.0 cm^3, were presented in section 6.4. The curve that fitted the experimental points was extrapolated to a nucleation concentration of $1x10^{13}cm^{-3}$, giving a corresponding rate of $1.56x10^{-3}cm^3$/sec. The rate measurements obtained from the annealed samples (also normalized to 1.0 cm^3) showed no significant deviations in spite of their different annealing conditions, as presented in Chapter III.

The upstroke transition rates of six independently performed experiments maintained an average value of $2.5x10^{-2}cm^3$/sec. This value is one order of magnitude higher than the extrapolated rate of $1.56x10^{-3}cm^3$/sec, as obtained in Figure 6.3. This is probably due to the assumption that more crystal defects were eliminated by annealing than, as predicted, by means of extrapolation, i.e. $1x10^{13}cm^{-3}$, since the nucleation concentration, as was pointed out earlier, consisted of both, foreign particles and crystal defects. The predicted concentration value was selected arbitrarily, based on the generally accepted semiconductor grade purity of 1 p.p.b. The outset of upstroke transition pressures of these samples gave an average value of 8.16 kbar with a dispersion of over 1.0 kbar. Unfortunately, all these samples broke during the upstroke transitions and hence, did not provide any further data on the full transformation cycle.

CHAPTER VII

SUMMARY AND CONCLUSIONS

This thesis has elaborated on the heterogeneous nucleation aspects of the pressure induced polymorphic phase transitions in mercury chalcogenides, using the direct resistance measurement technique. Based on the empirical results, a model is derived and verified by the experimental data. The influence of nucleation on transition pressures is clearly demonstrated. Furthermore, by means of transition pressures and activation volumes of the absolute rate theory, the thermodynamical equilibrium pressure is determined.

Figure 4.3 demonstrates the following theoretical and experimental results:

1) The upstroke transition pressures will decrease as a function of nucleation concentrations.
2) The upstroke transition pressures dispersions can be noticed for all the nucleated and non-nucleated samples.
3) The downstroke transition pressures show similar phenomena as in 1 and 2 .
4) These results effectively reduce the width of the reported hysteresis [8,15,16] of the pressure induced polymorphic phase transition in the case of HgSe.

Although the experimental investigations of this work include both, the upstroke and the downstroke transition pressures, the theoretical values have been evaluated for the upstroke transition pressures only. For the downstroke transition pressures, the theoretical values can be obtained, using the same model, by inverting the conversion function and evaluating it as a function of nucleation concentration.

A range of pressure was identified around the thermodynamical pressure, where, although the system was in a thermodynamically metastable state with both phases coexistant, the kinetic pressure for a particular nucleation concentration was not reached. Thus, the potential nuclei did not attain the critical size of growth nuclei and the rate of reaction was undetectably small (i.e. this was the process of nucleation as compared to that of growth). In fact, this was very similar to the phenomenon observed and originally reported by Bridgman [72] during his rate studies of the polymorphic phase transitions. He called this phenomenon "the region of indifference". By means of transition velocity, using the indirect volumetric measurement technique, he detected in many cases a pressure range within which the rates of transition become nearly zero. No correlation has yet been proposed between the region of indifference and the size of the critical nuclei at or above the saturation concentration (3.0 % mol.wt.).

Therefore, based on the kinetic data given in Table 6.1 and on the determined thermodynamical equilibrium pressure (7.22-7.26 kbar), it is proposed that the "region of indifference" is directly related to the kinetic pressures which in turn are dependent upon the number and size of the critical nuclei,present in the material.

Furthermore, it is proposed that the region of indifference, instead of the hysteresis curve, can be utilized to characterize the pressure induced polymorphic phase transition.

It was assumed that when the potential nuclei reached the critical dimension, that is at the outset of a transition pressure, growth nuclei were formed and the reaction started to proceed with measurable rates. These were related to the fractional volume transformed and consequently, the rates of transition were easily detectable by both, the indirect volumetric and the direct resistance measurement technique.

The kinetic data in Table 6.1 and section 6.6 provide the necessary information to demonstrate the dependence of transition rates on the nucleation concentration. Thus, the reported sluggish phase transformation of HgSe under pressure [8,16] either

i) increased (i.e. slower rates of transformation), by increasing the number of nucleation concentration;

ii) decreased (i.e. faster rates of transformation), by decreasing the number of nucleation concentration.

Moreover, the annealed samples provide a very fast transition with an average rate (during the first minute) of 2.5×10^{-2} cm^3/sec for an estimated nucleation concentration of less than 1×10^{13} cm^{-3}. This is a considerably larger transition rate than the one for the non-annealed samples which is 5.2×10^{-4} cm^3/sec. Such a fast transition rate suggests that a large number of crystal defects were removed by the annealing process.

Although the rate of the applied pressure ($\Delta P/\Delta t$) was kept constant for a given nucleation concentration, the measured transition rates varied with time. This was expected from the basic theory of kinetics of chemical reactions [74]. Thus, the transition rates, starting with a given value, will diminish as a function of time to zero when the transition is completed. At a constant pressure and within the first minute of the outset of the upstroke transition, each tabulated value of the transition rates in Table 6.1 as well as in section 6.6 was taken as the average of several measured values for the respective concentrations and the annealing.

The heterogeneous nucleation model presented in Chapter V has been employed in this investigation to elucidate the mechanism of transformation in a totally new and simple approach. It describes closely the transformation during $0 \leq \alpha \leq 0.86$. It is not valid for the last portion of the transition (i.e. $0.86 < \alpha \leq 1.0$),

possibly due to the involvement of ingestion [62], i.e. the overlap of growth nuclei among themselves.

The conversion function for the upstroke transition pressures, deduced from the model, serves as a bridge between the theory and the experiments. This is performed by taking a sample resistance reading at a given time during a transition, and finding the corresponding resistance value of the conversion function. Hence, values such as $V_1(t)$, $V_2(t)$, $\Delta V(t)$ and α were easily obtained. Furthermore, the conversion function contributed additional data when reworked as in equation (5.9). Here the transition pressure dependence of nucleation concentration was also easily obtained.

The transition rate measurements, based on the absolute rate theory [17,61], provide the values of the activation volumes as a function of nucleation concentration. The outset of the upstroke transition pressures for different nucleation concentrations and their corresponding activation volumes (Table 6.1) have been used to determine the thermodynamical equilibrium pressure of the HgSe compound, as in Figure 6.3. These results would have been very difficult, if not impossible to obtain without the developed kinetic model and the direct resistance measurement technique. This is because in Bridgman's region of indifference [72], including the thermodynamical equilibrium pressure, the rate of transition is undetectably small.

The decrease of the activation volumes as a function of nucleation concentration exemplified the decrease of the

transition barrier between phase I and phase II. Defining the transition pressure P_t in Chapter VI as the sum of thermodynamic and kinetic pressures, i.e. $P_t = P_{th} + P_k$, it can be seen that any decrease in the transition pressure as a function of nucleation concentration must have been due to a decrease in the kinetic pressure. The energy necessary to climb and overpass the activated state given by $\Delta G^{\#}$, i.e. the variation of free energy between the initial and the transition state (hindering potential), was supplied in the form of PV [Appendix F]. Therefore, a decrease in the activation volume (the pressure derivative of the hindering potential at a constant temperature) for a given nucleation concentration, corresponds to a decrease in the required energy to overpass the barrier and consequently, to a decrease in the transition pressure. Furthermore, if there were no potential barrier during the course of transition (resulting in a zero activation volume), then the transition would have taken place at the thermodynamical equilibrium pressure with zero rate of reaction. It then becomes clear that the kinetic pressure was needed to supply the necessary energy in the form of PV to enable the system to overcome the activation volume barrier, upon which the transition was dependent to proceed.

The resistance measurement technique provides a direct means of following the polymorphic phase transition under pressure. In the case of HgSe, this technique has proven to be more precise than the indirect conventional

volumetric measurement technique. The resistivity variation of the former is also related to the material band structure variation, as discussed in Chapter II.

Therefore, for pressures up to their transition pressures, the resistance invariance of the mercury chalcogenides indicates strongly that these materials are zero gap semiconductors or zero overlap semimetals. This is because, in the case of the normal band structure for the diamond or zinc-blende compounds, the energy gap ($E_g = E_{\Gamma_6} - E_{\Gamma_8}$) is also the thermal gap E_t. Since $E_g > 0$, and the level (Γ_6) rises upward with pressure faster than (Γ_8), [53,55], i.e. $\frac{d}{dP}(E_{\Gamma_6} - E_{\Gamma_8})$ is positive, then E_g which is equal to E_t, increases with pressure and a resistivity variation is expected. On the other hand, in the inverted band structure, the energy gap ($E_g = E_{\Gamma_6} - E_{\Gamma_8}$) is not the same as the thermal gap [$E_t = E_c - E_{v_1}$ as given by equation (2.5)]. The thermal gap E_t is zero and is independent of pressure and temperature [55,57], while the energy gap $E_g < 0$, and the level (Γ_6) still rises upward with pressure faster than (Γ_8), [54], i.e. $\frac{d}{dP}(E_{\Gamma_6} - E_{\Gamma_8})$ is negative, thus E_g decreases with pressure. However, since E_t is zero and does not change with pressure, a resistivity invariance is expected. Therefore, hydrostatic pressure experiments can provide data enabling a choice between these two models.

In the case of HgSe, since there was no noticeable resistance variation under pressures up to the transition

pressure throughout this investigation, the inverted band structure or the zero gap concept is the suitable choice for this compound. In this, E_t is zero and independent of pressure, whereas $\frac{d}{dP}(E_{\Gamma_6}-E_{\Gamma_8})$ is negative; hence E_g would decrease with pressure up to the transition pressure. As soon as the transition pressure is reached, the crystal structure changes (i.e. from the zinc-blende to the hexagonal cinnabar); consequently, the band structure changes from the inverted band type into the normal band type, where E_g is positive. This is supported by the fact that at transition pressure the resistivity of HgSe changes by several orders of magnitude, reflecting the band structure change from the inverted type to the normal type. Based on these grounds, HgSe can be considered a zero gap semiconductor.

The transition resistivity variations, when transformed into volume changes, can be of great value in geology to facilitate understanding such phenomena as earthquakes which might be related to the polymorphic phase transition. It has been suggested by Fermor [75] as early as 1914, and reviewed lately by Birch [6] that the volume change caused by a pressure induced polymorphic phase transition might be related to earthquakes. Moreover, Press [76] has published some data on the resistivity variation of the earth's crust prior to earthquakes. These measurements were made by feeding currents into the

ground and observing voltage variations a few kilometers away. Press indicated that generally it has been observed that earthquakes are preceded by a decrease in crustal resistivity. Therefore, since the crustal rocks of the deep earth experience great pressures as well as very high temperatures, nucleating these rocks might be of importance if they undergo polymorphic phase transitions to produce the disastrous earthquakes. This initiates the transition in a controlled manner (i.e. earlier and with slower transition rates). Such investigation may improve earthquake predictability and thus, reduce mankind's fear in one of the biggest catastrophes of nature.

In conclusion, the author hopes that the results obtained in this thesis would be useful in further understanding the kinetics of the pressure induced polymorphic phase transitions [77-80], and that zero gap materials such as HgSe and HgTe would provide valuable engineering device applications. Presently, one of the most promising applications would be photovoltaic infrared detectors, possibly working at room temperature. This would be a very valuable addition to laser communication systems.

REFERENCES

[1] P.W. Bridgman, The Physics of High Pressure, London, G. Bell and Sons Ltd., 1945.

[2] V.N. Zharkov and V.A. Kalinin, Equations of State for Solids at High Pressures and Temperatures, New York: Consultants Bureau of Plenum Pub. Corp., 1971.

[3] P.W. Bridgman, Collected Experimental Papers, Harvard University Press, Mass., Vol. I-VII, 1964.

[4] J.W. Stewart, The World of High Pressure; New Jersey: D. Van Nostrand Inc., Ch. I, 1967.

[5] H. Brooks, "Review and Prospect", in: W. Paul and D. Warschauer (eds.), Solids Under Pressure, New York: McGraw-Hill, pp.421-427, 1963.

[6] F. Birch, "Some Geophysical Applications of High-Pressure Research", in: W. Paul and D. Warschauer (eds.), Solids Under Pressure, New York: McGraw-Hill, pp.137-162, 1963.

[7] A. Lacam, B.A. Lombos and B. Vodar, "Pressure Effect on the Rate of Phase Transition in Mercury Telluride", Phys. Earth Planet Interiors, Vol. 3, pp.511-512, 1970.

[8] A. Lacam, J. Peyronneau, L.J. Engel and B.A. Lombos, "Pressure Induced Phase Transitions in Mercury Chalcogenides", Chem. Phys. Letters, Vol. 18, pp.129-131, Jan. 1973.

[9] A. Onodera, "Kinetics of Polymorphic Transitions of Cadmium Chalcogenides Under High Pressure", Rev. Phys. Chem. Japan, Vol. 41, pp.1-17, 1971.

[10] R.F. Brebrick and A.J. Strauss, "Homogeneity Range and Concentration Pressure Isotherms for HgSe", in: D.G. Thomas (ed.), International Conference on II-VI Semiconducting Compounds, New York: W.A. Benjamin Inc., pp.425-438, 1967.

[11] B.A. Lombos, E.Y.M. Lee, A.L. Kipling and R.W. Krawczyniuk, "Mercury Chalcogenides, Zero Gap Semiconductors", J. Phys. Chem. Solids, Vol. 36, No. 11, pp.1193-1198, Nov. 1975.

[12] J.A. Kafalas, H.C. Gatos, M.C. Lavine and M.D. Banus, "High Pressure Phase Transition in Mercury Selenide", J. Phys. Chem. Solids, Vol. 23, pp.1541-1544, June-Dec. 1962.

[13] P.W. Bridgman, "The Compression of 46 Substances to 50,000 kg/cm^2", Proc. Am. Acad. Arts and Sci., Vol. 74, pp.21-51, 1940.

[14] A.N. Mariano and E.P. Warekois, "High Pressure Phases of Some Compounds of Group II-VI", Science, Vol. 142, pp.672-673, Oct.-Dec. 1963.

[15] B.A. Lombos, B. Ghicopoulos, S. Bhattacharyya and B.C. Pant, "Pressure Induced Transitions of Mercury Chalcogenides", Can. J. Phys., Vol. 54, pp.48-55, Jan. 1976.

[16] A. Jayaraman, W. Klement Jr. and G.C. Kennedy, "Melting and Polymorphic Transitions for Some Group II-VI Compounds at High Pressures", Phys. Rev., Vol. 130, No. 6, pp.2273-2283, June 1963.

[17] M.G. Evans and M. Polanyi, "Some Applications of the Transition State Method to the Calculation of Reaction Velocities, Especially in Solution", Transactions of the Faraday Society, Vol. 31, pp.875-894, 1935.

[18] J.P. McKelvey, Solid State and Semiconductor Physics, New York: Harper and Row Pub., 1966.

[19] S.M. Sze, Physics of Semiconductor Devices, New York: Wiley-Interscience, pp.18-19, 1969.

[20] L.M. Falcov, "The Influence of Pressure on the Band Structure of Solids", in: C.T. Tomizuka and R.M. Emrick (eds.), Proceedings of the First International Conference on the Physics of Solids at High Pressures, New York: Acad. Press, pp.30-45, 1965.

[21] M.L. Cohen and Y.W. Tsang, "Theory of the Electronic Structure of Some IV-VI Semiconductors", in: D.L. Carter and R.T. Bate (eds.), Proceedings of the Conference on the Physics of Semimetals and Narrow-Gap Semiconductors, 1970, New York: Pergamon Press, pp.303-317, 1971.

[22] P.W. Bridgman, "The Effect of Pressure on the Electrical Resistance of Certain Semiconductors", Proc. Amer. Acad. Arts and Sci., Vol. 76, pp.127-148, 1951.

[23] W. Paul and H. Brooks, "Pressure Dependence of the Resistivity of Germanium", Phys. Rev., Vol. 94, pp. 1128-1134, June 1954.

[24] W. Paul, "Pressure Dependence of Resistivity of Germanium", Phys. Rev., Vol. 90, pp. 336-337, Jan. 1953.

[25] W. Paul, "Band Structure of the Intermetallic Semiconductors from Pressure Experiments", J. Appl. Phys. Supp., Vol. 32, No. 10, pp.2082-2094, Oct.1961.

[26] S. Minomura and H.G. Drickamer, "Pressure Induced Phase Transitions in Silicon, Germanium and Some III-V Compounds", J. Phys. Chem. Solids, Vol. 23, pp. 451-456, Jan.-June 1962.

[27] W. Paul and G.L. Pearson, "Pressure Dependence of the Resistivity of Solicon", Phys. Rev., Vol. 98, No. 6, pp.1755-1757, June 1955.

[28] A.L. Edwards, T.E. Slykhouse and H.G. Drickamer, "The Effect of Pressure on Zinc-Blende and Wurtzite Structure", J. Phys. Chem. Solids, Vol. 11, pp.140-148, 1959.

[29] S.H. Groves and W. Paul, "Band Structure of Gray Tin", Phys. Rev. letters, Vol. 11, No. 5, pp.194-196, Sept. 1963.

[30] H. Ehrenreich, "Band Structure and Electron Transport of GaAs", Phys. Rev., Vol. 120, pp.1951-1963, Dec. 1960.

[31] W.G. Spitzer, M. Gershenzon, C.J. Frosch and D.F. Gibbs, "Optical Absorption in n-type Gallium Phosphide", J. Phys. Chem. Solids, Vol. 11, pp.339-341, 1959.

[32] A. Onodera, N. Kawai, K. Ishizaki and I.L. Spain, "Semiconductor-to-Metal Transition in GaP Under High Pressure", Solid State Comm., Vol. 14, No. 7, pp.803-806, April 1974.

[33] S.H. Groves, "Recent Experiments on Zero Gap Semi-Conductors", in: D.L. Carter and R.T. Bate (eds.), Proceedings of the Conference on the Physics of Semimetals and Narrow-Gap Semiconductors, 1970, New York: Pergamon Press, pp.447-460, 1971.

[34] T.C. Harman and A.J. Strauss, "Band Structure of HgSe and HgSe-HgTe Alloys", J. Appl. Phys. Vol. 32, No. 10, pp.2265-2270, Oct. 1961.

[35] S.L. Lehoczky, J.G. Broerman, D.A. Nelson and C.R. Whitsett, "Temperature-Dependent Electrical Properties of Mercury Selenide , Phys. Rev., Vol. 9, No. 4, pp.1598-1620, Feb. 1974.

[36] R.O. Carlson, "Electrical Properties of Mercury Telluride", Phys. Rev., Vol. 111, No. 2, pp.476-478, July 1958.

[37] J. Black, S.M. Ku and H.T. Minden, "Some Semiconducting Properties of HgTe", J. Electrochem.Soc., Vol. 105, No. 12, pp.723-728, Dec. 1958.

[38] T.C. Harman, M.J. Logan and H.L. Goering, "Preparation and Electrical Properties of Mercury Telluride", J. Phys. Chem. Solids, Vol. 7, pp.228-235, 1958.

[39] T.C. Harman, W.H. Kleiner, A.J. Strauss, G.B. Wright, J.G. Mavroides, J.M. Honig and D.H. Dickey, "Band Structure of HgTe and HgTe-CdTe Alloys", Solid State Comm., Vol. 2, pp.305-308, 1964.

[40] G.B. Wright, A.J. Strauss and T.C. Harman, "Nonparabolic Conduction Band in HgSe and $HgSe_{0.5}Te_{0.5}$", Phys. Rev., Vol. 125, pp.1534-1536, March 1962.

[41] C.R. Whitsett, "Oscillatory Magnetoresistance in Mercuric Selenide", Phys. Rev., Vol. 138, pp.A829-A839, May 1965.

[42] R.R. Galazka, W.M. Becker and D.G. Seiler, "Warping and Symmetry of Conduction Band in HgSe from Shubnikov-de Haas-Measurements", in: D.L. Carter and R.T. Bate (eds.), Proceedings of the Conference on the Physics of Semimetals and Narrow-Gap Semiconductors , 1970, New York: Pergamon Press, pp.481-491, 1971.

[43] J.G. Broerman, "Ionized-Impurity-Limited Mobility and the Band Structure of Mercuric Selenide", Phys. Rev., Vol. 183, No. 3, pp.754-757, July 1969.

[44] T.C. Harman, "Properties of Mercury Chalcogenides", in: M. Aven and J.S. Prener (eds.), Physics and Chemistry of II-VI Compounds, Amsterdam: North Holland Pub. Co., Ch. XV, 1967.

[45] T.C. Harman, "Band and Transport Parameters of Hg-Chalcogenides", in: D.G. Thomas (ed.), International Conference on II-VI Semiconducting Compounds, New York: W.A. Benjamin, pp.982-1006, 1967.

[46] M.D. Blue and P.W. Kruse, "Preparation and Electrical properties of Mercury Selenide", J. Phys. Chem. Solids, Vol. 23, pp.577-586, Jan.-June 1962.

[47] C.R. Pidgeon, S.H. Groves, "Low Temperature Reflection Studies of Interband Magneto-Optical Transitions in HgTe", in: D.G. Thomas (ed.), International Conference on II-VI Semiconducting Compounds, New York: W.A. Benjamin Inc., pp.1080-1089, 1967.

[48] M. Rodot and H. Rodot, "Quelques Propriétés du Tellurure de Mercure", C.R. Acad. Sci., Vol. 248, pp.937-940, Feb. 1959.

[49] T.C. Harman, "Determination of the Effective Scattering Mechanism Parameter of Electron Transport Theory", Phys. Rev., Vol. 118, No. 6, pp. 1541-1542, June 1960.

[50] M. Rodot, H. Rodot and R. Triboulet, "Some properties of HgSe-HgTe Solid Solutions", J. Appl. Phys., Vol. 32, pp.2254-2256, Oct. 1961.

[51] T.C. Harman, J.M. Honig and P. Trent, "Hall Coefficient and Transverse Magneto-Resistance in HgTe at 4.2°K and 77°K", J. Phys. Chem. Solids, Vol. 28, pp.1995-2001, Sept. 1967.

[52] E.O. Kane, "Band Structure of Indium Antimonide", J. Phys. Chem. Solids, Vol. 1, pp.249-261, Sept.1957.

[53] W. Paul and H. Brooks, "Effect of Pressure on the Properties of Germanium and Silicon", in: A.F. Gibson and R.E. Burgess (eds.), Progress in Semiconductors, Series of Monographs, New York: Wiley and Sons, Vol. 7, pp.135-235, 1963.

[54] S.H. Groves, R.N. Brown and C.R. Pidgeon, "Interband Magnetoreflection and Band Structure of HgTe", Phys. Rev., Vol. 161, No. 3, pp.779-793, Sept. 1967.

[55] R. Piotrzkowski, S. Porowski, Z. Dziuba, J. Ginter, W. Giriat and L. Sosnowski, "Band Structure of HgTe", Phys. Stat. Sol., Vol. 8, pp.K135-K139, 1965.

[56] S. Porowski and T. Zakrzewski, "Measurements of the Temperature Dependence of the Hall Constant in HgTe Under Pressure", Phys. Stat. Sol., Vol. 11, pp.K39-K41, 1965.

[57] R. Piotrzkowski and S. Porowski, "Temperature Dependence of the Band Structure of HgTe from Pressure Measurements", in: D.G. Thomas (ed.), International Conference on II-VI Semiconducting Compounds, New York: W.A. Benjamin Inc., pp. 1090-1100, 1967.

[58] W.D. Lawson, S. Nielson, E.H. Putley and A.S. Young, "Preparation and Properties of HgTe and Mixed Crystals of HgTe-CdTe", J.Phys. Chem. Solids, Vol. 9, pp.325-329, 1959.

[59] B. Chalmers, Physical Metallurgy, New York: Willey and Sons Inc., Ch. 8, 1959.

[60] M.E. Fine, Introduction to Phase Transformations in Condensed Systems, New York: McMillan Series in Materials Science, 1964.

[61] S. Glasstone, K.J. Laidler and H. Eyring, The Theory of Rate Processes, New York: McGraw-Hill, 1941.

[62] G. Pannetier and P. Souchay, Chemical Kinetics, translated by H.D. Gesser and H.H. Emond, Barking, Essex: Elsevier Pub.Co.Ltd., 1967.

[63] J.W. Christian, The Theory of Transformations in Metals and Alloys, Oxford: Pergamon Press, 1965.

[64] M. Avrami, "Kinetics of Phase Change I", J. Chem. Phys., Vol. 7, pp.1103-1112, Dec. 1939.

[65] J.D. Barnett and C.D. Bosco, "Technique for Obtaining True Hydrostatic Pressures to 60 kbars", The Rev. of Scientific Instrument, Vol. 38, pp. 957-963, July 1967.

[66] R.J. Zeto and H.B. Vanfleet, "Pressure Calibration to 60 kbar Based on the Resistance Change of a Manganin Coil Under Hydrostatic Pressure", J. Appl. Phys., Vol. 40, No. 5, pp.2227-2231, April 1969.

[67] A. Lacam and J. Peyronneau, "Transition Polymorphique de RbCl Sous Haute Pression. Influence des Paramètres Expérimentaux Sur l'Effet d'Hystérésis", J. de Physique, Vol. 34, No.11-12, pp.1047-1053, Nov.-Dec. 1973.

[68] L. Lacam, J. Peyronneau and J.L. Kopystynski, "Transitions Polymorphiques des Solides Induites par la Pression", J. de Physique, Vol. 34, No. 11-12, pp.1055-1059, Nov.-Dec. 1973.

[69] J.L. Kopystynski, J. Peyronneau and A. Lacam, "Etude Cinétique de l'Effet d'Hystérésis dans les Transitions Polymorphiques.Influence de la Surpression", J.de Physique, Vol. 35, pp.609-614, July-Aug. 1974.

[70] W. Jander, "Reactions in Solid State at High Temperatures I", Z. Anorg. Allgem. Chem., Vol. 163, pp.1-30, April 1927.

[71] R.B. Jacobs, "Polymorphic Transitions in Metallic Hallides", Phys. Rev., Vol. 54, pp.468-474, Sept.1938.

[72] P.W. Bridgman, "The Velocity of Polymorphic Changes between Solids", Proc. Amer. Acad. Arts Sci., Vol. 52, pp.57-88, 1916.

[73] H. Rodot, "Etude de l'Equilibre de Phases dans le Tellurure de Mercure", J. Phys. Chem. Solids, Vol. 25, pp.85-93, Jan.-June 1964.

[74] G.M. Barrow, Physical Chemistry, New York: McGraw-Hill, Ch. 15, 1966.

[75] L.L. Fermor, "The Relation of Isostasy, Earthquakes and Vulcanicity to the Earth's Infra-plutonic Shell", Geol. Mag., Vol. 1, pp.65-70, 1914.

[76] F. Press, "Earthquake Prediction", Scientific American, Vol. 232, No. 5, pp.14-23, May 1975.

[77] B.A. Lombos, H.M. Mahdaly and B.C. Pant, "Nucleations of Pressure Induced Phase Transitions in Mercury Selenide", Can. J. Phys., Vol. 55, No.3, pp.222-226, Feb. 1977.

[78] B.A. Lombos, H.M. Mahdaly, "Electrical Characterization of Pressure Induced Phase Transitions in Mercury Chalcogenides", IEEE-Trans-Geoscience Electronics, Vol. GE-15, No. 4, p.p.203-207, Oct. 1977.

[79] H.M. Mahdaly, "Kinetics Aspects of Mercury Chalcogenides Under High Pressures", The Young Authors' Symposium of the Electrochemical Society, held at the Royal Military College, St. Jean, Que., Oct. 1975.

[80] B.A. Lombos, H.M. Mahdaly, and B.C. Pant, "Electrical Characterization of Pressure Induced Phase Transitions", 6th AIRAPT Conference, Boulder, Colorado, July 1977.

APPENDIX A-I

A TYPICAL CALCULATION OF THE EXCESS MERCURY NEEDED TO CONTROL THE PRESSURE IN AN AMPULE

A cylindrical ampule with a typical diameter ϕ = 32.0 mm (inside) and a length L = 60.0 cm is used. The desired pressure inside the ampule is 20 atm. The melting point of HgSe is 798°K and the background temperature is 580°K.

The ampule volume $V = \pi \left(\frac{\phi}{2}\right)^2 L = 3.14 \times 2.56\ cm^2 \times 60\ cm$

$= 4.82 \times 10^2\ cm^3$

Molecular wt. of Hg = 200.59 $\frac{gr}{mole}$

Molecular wt. of Se = 78.96 $\frac{gr}{mole}$

If one takes a measured wt. of Hg of 188.38 gr, then the corresponding 1:1 ratio by molecular wt. of Se to form HgSe = 62.89 gr. To maintain a pressure of 20 atm. inside the ampule, n' extra moles of Hg is required.

$$n'(mole) = \frac{P \cdot V}{R' \cdot T} = \frac{20\ atm \times 4.82 \times 10^2 cm^3}{8.205 \times 10^1 \frac{atm\ cm^3}{mole\ ^\circ K} \times 880^\circ K} = 0.134\ mole$$

where R' is the gas constant

∴ the needed excess weight of Hg to control the pressure inside the ampule

$= 0.134\ mole \times 200.59 \frac{gr}{mole} = 26.88\ gr.$

APPENDIX A-II

PRESSURE MEASUREMENT PRECISION

A full scale deflection in the Keithley Instrument Model 150 B Microvolt Ammeter of 600 μv corresponds to a manganin coil resistance change ΔR of 0.1 Ω. The coil resistance, R_o, at atmospheric pressure is 128.6 Ω. The pressure P is related to ΔR and R_o by [see equation (3.2)]

$$P = 420 \frac{\Delta R}{R_o} \text{ kbar}$$

For $\Delta R = 0.1\,\Omega$, $R_o = 128.6\,\Omega$, one gets

$$P = 420 \times \frac{0.1}{128.6} = 3.3 \times 10^{-1} \text{ kbar} = 330 \text{ bar}.$$

Consequently 330 bar give a maximum deflection of 600 μv, i.e. 2 μv deflection corresponds to 1 bar.

The strip chart recorder was set up such that the 600 μv output from the Microvolt Ammeter drives the pen 100 divisions (10 in). Therefore, 2 μv output, which corresponds to 1 bar, drives the pen 1/3 of a division (0.03 in), which is detectable. Thus, the pressure can be read within a precision of ±1 bar.

At the upstroke transition, the outset of the transition pressure is determinable within about 20 bar. Since the average transition pressure is 9.6 kbar, the percentage error is given as

$$\frac{20}{9.6 \times 10^3} \times 100 = 0.21\ \%.$$

APPENDIX A-III

RESISTANCE MEASUREMENT PRECISION

For a constant current of 21 mA through the sample the strip chart recorder was set up so that 50 mv full scale corresponds to 100 divisions (10 in) on the strip chart.

The corresponding resistance is

$R = \frac{50 \text{ mv}}{21 \text{ mA}} = 2.381\,\Omega$. With a strip chart resolution of one tenth of a division, the resistance change can be read within $\frac{2.381}{100} \times \frac{1}{10} = 2.381 \text{ m}\,\Omega$.

APPENDIX B

CALCULATIONS OF VOLUMES DURING RETROPRESSURE

The volume of the resistance sample at atmospheric pressure (V_1) was $2.88 \times 10^{-2} cm^3$. The volume of the same sample at the outset of the upstroke transition pressure (V_I) was $2.84 \times 10^{-2} cm^3$, calculated from the relation

$$V_I = V_1(1-B_1P_t)$$

where B_1 is the compressibility of phase I and P_t is the upstroke transition pressure. The volume of the large sample at atmospheric pressure (V_1') was 10 cm^3. The volume of the large sample at the outset of the upstroke transition pressure was

$$V_I' = V_1'(1-B_1P_t) = 9.86 \text{ cm}^3$$

The rate of the applied pressure ($\frac{\Delta P}{\Delta t}$) read from the strip chart = 0.082 $\frac{\text{kbar}}{\text{min}}$. The transition time (t) read from the chart = 12 min, while the plate displacement during transition $\Delta \ell$ = 0.26 cm. The total volume reduction of the large sample due to transition ΔVR = 0.829 cm^3 (estimated via $\Delta \ell$). The total pressure reduction (ΔP) due to sample volume reduction, was evaluated as follows:

$$\Delta P = \frac{\Delta P}{\Delta t} t = 0.98 \text{ kbar}$$

The instantaneous volume reduction of the large sample as a function of time during the transition is given by :

$$\Delta VR(t) = \frac{\Delta VR}{\Delta P} \Delta P(t) \qquad (B.1)$$

where $\Delta P(t)$ is the instantaneous pressure change, obtained from the strip chart at time (t). Therefore, the large sample volume as a function of time during the transition can be expressed as

$$V'(t) = V'_I - \Delta VR(t) \qquad (B.2)$$

The small sample volume variation as a function of time was obtained by assuming that its variation is proportional to the large sample volume variation, i.e.

$$V(t) = \frac{V'(t)V_I}{V'_I} \qquad (B.3)$$

Table B.1 lists the measured pressure (inside the chamber) and $\Delta VR(t)$ during the retropressure cycle. The calculated values for equations (B.2) and (B.3) are given in Table 4.1 together with other related data.

Table B.1

Supplementary measured data to Table 4.1

Time (t) min	Pressure in Chamber P(t), kbar	Volume Reduction of the large samples $\Delta V_R(t)$, cm^3
0	9.39	0
1	9.43	0.04
2	9.44	0.09
3	9.43	0.17
4	9.40	0.27
5	9.36	0.37
6	9.32	0.48
7	9.29	0.57
8	9.31	0.62
9	9.35	0.66
10	9.41	0.67
11	9.48	0.69
12	9.53	0.71

APPENDIX C

PERCENTAGE CALCULATION OF THE GROWTH NUCLEI IN MERCURY SELENIDE

The molecular volume (V_m) of a unit cell of HgSe at phase I is given by Ref. [15] = 56.46×10^{-24} cm^3/molecule. The concentration (n) of HgSe at phase I is thus given by

$$n = \frac{1}{V_m} = \frac{\text{molecules}}{56.46 \times 10^{-24} cm^3} = 1.77 \times 10^{22} \frac{\text{molecules}}{cm^3}$$

From Fig. 4.4, the intercept of the line with the axis of log N at $\Delta P_t = 0$ gave a value of 18.72. Therefore, the estimated concentration of growth nuclei in a non-nucleated sample of HgSe, N_o, is given by

$$N_o = \log^{-1} 18.72 = 5.31 \times 10^{18} \ cm^{-3}$$

Thus, the ratio of the growth nuclei concentration (N_o) to the concentration of HgSe (n) is

$$\frac{N_o}{n} = 5.31 \times 10^{18} / 1.77 \times 10^{22} = 3 \times 10^{-4}$$

Consequently, the growth nuclei occupy about 0.03 % of the concentration of HgSe crystals as-grown, using the modified Bridgman technique.

APPENDIX D

THE CONVERSION FUNCTION OF THE HETEROGENEOUS MODEL

Fig. 5.1-A in the text shows a typical parallelepiped sample of HgSe of length (L), width (W) and depth (Z), together with the distributed nuclei within the sample. The resistance of the sample is proportional to its length (L) and inversely proportional to its cross-sectional area (ZW), i.e.

$$R = \rho \frac{L}{ZW} \qquad (D.1)$$

Let N be the concentration of the nuclei in the material, N' and N'' be the number of nuclei along L and on the surface ZW, respectively. Also, let $\ell(\alpha)$, $w(\alpha)$ and $z(\alpha)$ be the length, width and depth of a cubic adjusted nucleus (see p.80), along L, W and Z, respectively. Suppose that the sample is divided, following L, into cross-sectional surfaces (ZW), as illustrated in Fig. 5.1-B and D. The type of surfaces of Fig. 5.1-D (first type) is for the untransformed (phase I) parts of the sample, whereas the type of Fig. 5.1-B and C is for those surfaces containing the growth nuclei (second type); both are considered as a function of α.

The sample length contributed by the surfaces of the first type is obviously $L - N' \ell(\alpha)$. Therefore, the sum

of all the resistances of the first type at any time during the reaction can be written as:

$$R_o = \rho_1 \frac{L - N' \ell(\alpha)}{ZW} \qquad (D.2)$$

where ρ_1 is the resistivity of phase I.

The second type of surfaces (Fig. 5.1-B) contains two parallel resistances due to the coexistance of both phases. The total length of these surfaces is $N' \ell(\alpha)$. The cross-sectional area occupied by phase I is $[ZW-N'' z(\alpha)w(\alpha)]$ and that occupied by phase II is $N'' z(\alpha)w(\alpha)$. Therefore, these resistances can be expressed as:

$$R_I = \rho_1 \frac{N' \ell(\alpha)}{ZW - N'' z(\alpha)w(\alpha)} \qquad (D.3)$$

and

$$R_{II} = \rho_2 \frac{N' \ell(\alpha)}{N'' z(\alpha)w(\alpha)} \qquad (D.4)$$

where R_I and R_{II} are the resistances of phase I and II, respectively, ρ_2 is the resistivity of phase II. The total resistance of the surfaces of the second type is given by the parallel combination of R_I and R_{II}, that is

$$R_p = \frac{1}{\frac{1}{R_I} + \frac{1}{R_{II}}} = \frac{\rho_1 \rho_2 N' \ell(\alpha)}{\rho_2 [ZW-N'' z(\alpha)w(\alpha)] + \rho_1 N'' z(\alpha)w(\alpha)} \qquad (D.5)$$

Since the two types of surfaces are in series, the total sample resistance as a function of α from eqs. (D.2) and (D.5) become:

$$R(\alpha) = R_o + R_p = \rho_1 \frac{L - N' \ell(\alpha)}{ZW} + \frac{\rho_1 \rho_2 N' \ell(\alpha)}{\rho_2 [ZW - N'' z(\alpha) w(\alpha)] + \rho_1 N'' z(\alpha) w(\alpha)}$$

$$= \frac{\rho_1 V_1 + (\frac{\rho_1^2}{\rho_2} - \rho_1) N'' z(\alpha) w(\alpha) [L - N' \ell(\alpha)]}{ZW [ZW - N'' z(\alpha) w(\alpha) + \frac{\rho_1}{\rho_2} N'' z(\alpha) w(\alpha)]} \qquad (D.6)$$

which is identical to eq. (5.5) of Chapter V.

The change of the volumes of both phases due to their compressibilities and transition, can be taken into account by considering their compressibility and density factors. These can be written as:

$$V_1(P) = V_1[1 - B_1 P(t)]$$

and (D.7)

$$V_2(P) = V_2[1 - B_2 P(t)]$$

where $V_1(P)$ and $V_2(P)$ are the volumes as functions of pressure, of phase I and phase II, respectively. B_1 and B_2 are their respective compressibilities and $P(t)$ is the pressure at time t. From eq. (E.6) of Appendix E, one obtains:

$$V_I = V_{II} \frac{D_2}{D_1} \qquad (D.8)$$

which expresses the total volume relations due to transition by their density factors. Consequently, during transition, the volume of the sample in phase II, $V_2(\alpha)$, is related to the parent partial volume $V_1(\alpha)$ which induced it by

$$V_1(\alpha) = V_2(\alpha)\frac{D_2}{D_1} \qquad (D.9)$$

Note that $V_1(\alpha)$ is not equivalent to $V_1(t)$ which is the untransformed portion of the volume of the sample at a given time t (see Appendix E).

The linear compressibility is approximately 1/3 of the volume compressibility of a homogeneous material under hydrostatic pressure. Therefore, following eq. (D.7) one may write:

$$\begin{aligned} L(P) &= L[1-B_1P(t)/3] \\ W(P) &= W[1-B_1P(t)/3] \\ Z(P) &= Z[1-B_1P(t)/3] \\ \ell(\alpha,P) &= \ell(\alpha)[1-B_2P(t)/3] \\ w(\alpha,P) &= w(\alpha)[1-B_2P(t)/3] \\ z(\alpha,P) &= z(\alpha)[1-B_2P(t)/3] \end{aligned} \qquad (D.10)$$

Substituting these values and the transition density factors [see eq.(D.9)] into eq. (D.6), it becomes:

$$R(\alpha)=\frac{\rho_1 V_1[1-B_1P(t)]+(\frac{\rho_1^2}{\rho_2}-\rho_1)N''z(\alpha)w(\alpha)[1-2B_2P(t)/3](\frac{D_2}{D_1})^{2/3}A}{ZW[1-2B_1P(t)/3]\left\{B+\frac{\rho_1}{\rho_2}N''z(\alpha)w(\alpha)[1-2B_2P(t)/3](\frac{D_2}{D_1})^{2/3}\right\}} \qquad (D.10)$$

where $A = L[1-B_1P(t)/3]-N'\ell(\alpha)[1-B_2P(t)/3](\frac{D_2}{D_1})^{1/3}$

and $B = ZW[1-2B_1P(t)/3]-N''z(\alpha)w(\alpha)[1-2B_2P(t)/3](\frac{D_2}{D_1})^{2/3}$

Equation (D.10) is given in the text as eq. (5.8).

The outset of the upstroke transition pressure P_t as a function of nucleation concentration can be deduced from eq. (D.10) by neglecting the small difference between the compressibilities of the low and high pressure phase [i.e. $\{1-B_1P(t)\}$ and $\{1-B_2P(t)\}$]; also, P(t) converges to P_t at the outset of the upstroke transition pressure, hence it is given as:

$$P_t = \frac{1-\left[\dfrac{\rho_1V_1+(\frac{D_2}{D_1})^{2/3}(\frac{\rho_1}{\rho_2}-\rho_1)N''z(\alpha)w(\alpha)\{L-N'\ell(\alpha)(\frac{D_2}{D_1})^{1/3}\}^3}{R(\alpha)ZW[ZW+(\frac{D_2}{D_1})^{2/3}(\frac{\rho_1}{\rho_2}-1)N''z(\alpha)w(\alpha)]}\right]}{B_1} \qquad (D.11)$$

which is identical to eq. (5.9) of the text.

APPENDIX E

THE VOLUMES OF THE PHASES DURING THE UPSTROKE TRANSITION

Let V_1 be the volume of a sample in phase I at atmospheric pressure. Also let $V_1(P)$ be its volume as a function of pressure which is given by

$$V_1(P) = V_1(1-B_1P) \qquad (E.1)$$

where B_1 is the compressibility of phase I, and P is the applied hydrostatic pressure. At the outset of the upstroke transition pressure (P_t), $V_1(P)$ becomes V_I, i.e.

$$V_I = V_1(1-B_1P_t) \qquad (E.2)$$

Similarly, let V_2 be the volume of the sample when it is transformed into phase II; and let $V_2(P)$ be its volume in phase II, as a function of pressure, given by

$$V_2(P) = V_2(1-B_2P) \qquad (E.3)$$

where B_2 is the compressibility at phase II and $P \geq P_t'$; P_t' being the pressure at which transition is completed. When transition is completed at pressure P_t', $V_2(P)$ becomes V_{II}, i.e.

$$V_{II} = V_2(1-B_2P_t') \qquad (E.4)$$

Note that the subscripts I and II represent phase I and phase II, respectively.

The mass conservation law requires that the total mass of a sample must remain constant. Thus,

$$m_I = m_1(t) + m_2(t) = m_{II} \qquad (E.5)$$

where m_I is the sample mass at the beginning of the transition, $m_1(t)$ and $m_2(t)$ are the masses of the first and the second phase at time (t) during the transition (when both phases co-exist), and m_{II} is the mass of the sample at the end of the transition. The previous equation can be re-expressed by:

$$V_I D_1 = V_1(t) D_1 + V_2(t) D_2 = V_{II} D_2 \qquad (E.6)$$

where D_1 and D_2 are the densities of the first and the second phase, respectively.

During the transition, the total sample volume V(t) is given by :

$$\begin{aligned} V(t) &= V_1(t) + V_2(t) \\ &= V_1[1-B_1P(t)](1-\alpha) + V_1 \frac{D_1}{D_2}[1-B_2P(t)]\alpha \end{aligned} \qquad (E.7)$$

where $V_2(t)$ is the fractional sample volume transformed into phase II, and $V_1(t)$ is the remaining, untransformed fractional sample volume of phase I. When transition starts at time $t=t_o=0$, the degree of advancement of the reaction $\alpha=0$ and the sample volume is V_I. Similarly, when transformation is completed, $t=t_f$ (final time), $\alpha=1$, and the

sample volume becomes V_{II}. Therefore, since for $t_o \leq t \leq t_f$, $0 \leq \alpha \leq 1$, then α is a time dependent parameter, proportional to the amount of material transformed, hence $V_2(t)$ is given as :

$$V_2(t) = V_2 \ [1-B_2P(t)\ ]\ \alpha \qquad (E.8)$$

Using the approximation $[1-B_1P_t] \approx [1-B_2P'_t\ ]$ and the mass conservation law, it can be shown that:

$$V_2 = V_1 \frac{D_1}{D_2} \qquad (E.9)$$

Substituting eq. (E.9) into eq. (E.8), it becomes

$$V_2(t) = V_1 \frac{D_1}{D_2}[\ 1-B_2P(t)]\ \alpha \qquad (E.10)$$

However, when $V_2(t)$ increases as a function of α, $V_1(t)$ decreases and is given by

$$V_1(t) = V_1\ [\ 1-B_1P(t)](1-\alpha) \qquad (E.11)$$

Furthermore, substituting eqs. (E.10) and (E.11) into eq. (E.7), one obtains

$$V(t) = V_1\ [1-B_1P(t)](1-\alpha\ ) + V_1\left\{\frac{D_1}{D_2}\right.[1-B_2P(t)]\alpha \qquad (E.12)$$

Hence,

$$\alpha = \frac{\Delta V(t)}{V_1\ [1-\frac{D_1}{D_2} + (\frac{D_1}{D_2}\ B_2-B_1)P(t)\ ]} \qquad (E.13)$$

where

$$\Delta V(t) = V_1 [1-B_1 P(t)] - V(t)$$

$$= V_1 [1-B_1 P_t] - V(t) = V_I - V(t) \qquad (E.14)$$

Substituting eq. (E.7) into the last equation, it becomes

$$\Delta V(t) = V_I - [V_1(t) + V_2(t)] \qquad (E.15)$$

where according to the model[text eq.(5.18)],

$$V_2(t) = N' \ell(\alpha) N'' w(\alpha) z(\alpha) \qquad (E.16)$$

and from eq. (E.6),

$$V_1(t) = V_I - V_2(t) \frac{D_2}{D_1} \qquad (E.17)$$

Applying the following boundary conditions to eq. (E.15), one observes that:

1) When transition starts, $t=t_o=0$, $V_2(0)=0$ and $V_1(0)=V_I$

$$\therefore \Delta V(t) = 0$$

2) When transition is completed, $t=t_f$, $V_2(t_f)=V_{II}$ and $V_1(t_f)=0$

$$\therefore \Delta V(t) = V_I - V_{II}$$

hence, the total volume change due to transition is

$$\Delta V(t_f) = \Delta V ,$$

Now, approximating $[1-B_2P(t)]$ to $[1-B_2P'_t]$, eqs. (E.8) and (E.4) can be written for α as

$$\alpha = \frac{V_2(t)}{V_{II}} = \frac{V_2(t)\frac{D_2}{D_1}}{V_I} \qquad \text{(E.18)}$$

which is much simpler than eq. (E.13). It also satisfies the boundary conditions:

1) When transition starts, $t=t_o=0$, $V_2(0)=0$

$$\therefore \alpha = 0$$

2) When transition is completed, $t=t_f$, $V_2(t_f) = V_{II}$

$$\therefore \alpha = \frac{V_{II}\frac{D_2}{D_1}}{V_I} = \frac{V_I}{V_I} = 1$$

APPENDIX F

EFFECT OF PRESSURE ON REACTION VELOCITY

The equilibrium constant K for the reaction

$$aA + bB + \ldots \underset{r_2'}{\overset{r_1'}{\rightleftharpoons}} lL + mM + \ldots \qquad (F.1)$$

(where the symbols are as in p.85) is defined as

$$K = \frac{A^a x B^b x \ldots}{L^l x M^m x \ldots} \qquad (F.2)$$

is related to the free energy change or chemical potential ΔG by

$$K = \frac{r_1'}{r_2'} = \exp\left(-\frac{\Delta G}{RT}\right) \qquad (F.3)$$

where r_1' and r_2' are the rate constants of the forward and reverse reactions, respectively, R' is the gas constant and T is temperature, then

$$\ln r_1' - \ln r_2' = -\frac{\Delta G}{RT} \qquad (F.4)$$

The last equation may be split as follows

$$\ln r_1' = -\frac{\Delta G_1^{\ddagger}}{R'T} + \text{const.} \qquad (F.5)$$

and

$$\ln r_2' = -\frac{\Delta G_2^{\ddagger}}{R'T} + \text{const.} \qquad (F.6)$$

The splitting of eq. (F.4) into eqs. (F.5) and (F.6) is based on the assumption that the rate constant of the reaction depends only on the increase in free energy $\Delta G^{\#}$ going from the initial state (I) to the transition state (#), (see Figure F.1). Eqs. (F.5) and (F.6) can be written as

$$r' = \nu \exp\left(-\frac{\Delta G^{\#}}{R'T}\right) \qquad (F.7)$$

where ν is a constant.

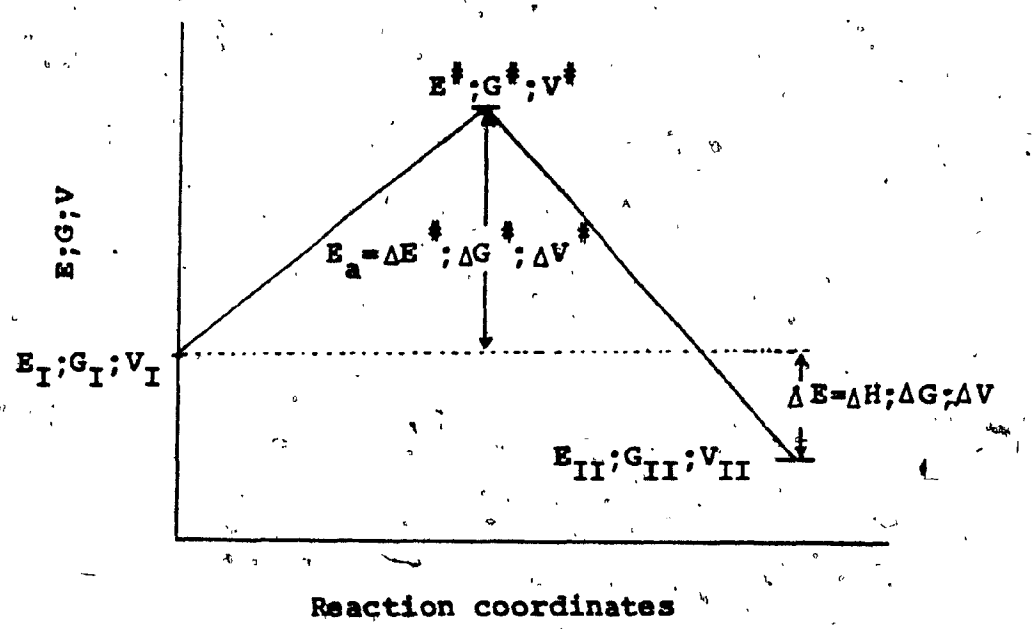

Figure F.1 : Schematic diagram for energy E, chemical potential G and volume V as a function of reaction coordinates for temperature and pressure induced reactions, showing in the same figure the variation of the Gibbs free energy (chemical potential) also.

Now, from transition state theory, one writes

$$\Delta G^{\#} = \Delta H^{\#} - T\Delta S^{\#} \qquad \text{(F.8)}$$

where $\Delta H^{\#}$ and $\Delta S^{\#}$ are the variations in enthalpy and entropy, respectively. Differentiating the free energy change, related to the transition state, with respect to pressure at constant temperature gives:

$$\left.\frac{\partial \Delta G^{\#}}{\partial P}\right|_T = \left.\frac{\partial \Delta H^{\#}}{\partial P}\right|_T - T \left.\frac{\partial \Delta S^{\#}}{\partial P}\right|_T \qquad \text{(F.9)}$$

The increase in enthalpy can be given as:

$$\Delta H^{\#} = \Delta E^{\#} + P\Delta v \qquad \text{(F.10)}$$

where $\Delta E^{\#}$ is the increase in the internal energy of the system, P is the pressure and Δv is the volume variation. Differentiating eq. (F.10), one obtains:

$$d\,\Delta H^{\#} = d\Delta E^{\#} + P\Delta d\,\Delta v + \Delta v\, dP \qquad \text{(F.11)}$$

From the laws of thermodynamics, one has:

$$d\,\Delta E^{\#} = T\, d\,\Delta S^{\#} - P\, d\,\Delta v \qquad \text{(F.12)}$$

Substituting eq. (F.12) into eq. (F.11), one gets:

$$d\,\Delta H^{\#} = T\, d\,\Delta S^{\#} + \Delta v\, dP \qquad \text{(F.13)}$$

Differentiating the last equation with respect to pressure at constant temperature, yields

$$\Delta v = \frac{\partial \Delta H^{\#}}{\partial P}\Big|_T - T\,\frac{\partial \Delta S^{\#}}{\partial P}\Big|_T \qquad (F.14)$$

Consequently, from eqs. (F.9) and (F.14), it follows that

$$\frac{\partial \Delta G^{\#}}{\partial P}\Big|_T = \Delta v \qquad (F.15)$$

Since $\Delta G^{\#}$ is the <u>increase</u> of free energy going from the initial (I) to the transition (#) states, for a forward reaction, the volume variation Δv given by its pressure derivative at constant temperature, can be identified with the activation volume $\Delta V^{\#}$, then :

$$\Delta V^{\#} = \Delta v = \frac{\partial \Delta G^{\#}}{\partial P}\Big|_T \qquad (F.16)$$

Thus, the volume of the activated complex or transition state $V^{\#}$ is greater than that of the initial V_I or final V_{II} states (see Fig. F.1) and the activation volume $\Delta V^{\#}$ is the difference in volumes between the initial and transition states, as defined by Evans and Polanyi [17]. Furthermore, these authors provided an expression for $\Delta V^{\#}$ related to the variation of the rate constant with respect to pressure as:

$$\frac{d \ln r}{dP} = -\frac{\Delta V^{\#}}{RT} \qquad (F.17)$$